Marcin Modrzejewski

New Density Functionals for Modeling Noncovalent Systems

A thesis submitted in partial fulfillment
of the requirements for the degree of
Doctor of Philosophy in Chemistry

Thesis supervisor Prof. Grzegorz Chałasiński

Warsaw
2016

Marcin Modrzejewski

Nowe funkcjonały gęstości elektronowej do modelowania układów związanych niekowalencyjnie

Praca doktorska wykonana w Pracowni Chemii Kwantowej
Wydziału Chemii Uniwersytetu Warszawskiego
pod kierunkiem prof. dr. hab. Grzegorza Chałasińskiego

Warszawa
2016

Acknowledgements

First and foremost I would like to thank my advisor Prof. Grzegorz Chałasiński for guidance and support during my studies.

Special thanks to Prof. Małgorzata Szczęśniak.

Contents

Chapter 1

Introduction

Modern density functional theory (DFT) is a pragmatic approach to modeling molecular electronic properties, which aims at the level of accuracy which is useful for real-world applications, but at the low cost of a single-determinantal method.

Decades before DFT become ubiquitous in chemistry, the theoretical foundations of this methodology were laid out by Hohenberg, Kohn, and Sham in the 1960s.[1,2] These mathematical theorems at the root of DFT are concerned with the existence of the universal density functional $E[\rho]$ but do not show a concrete way of its construction. Therefore, DFT is not as systematically improvable as wave-function theory is.

Only some features of the exact functional are known and only a fraction of the known features can be efficiently implemented in semilocal DFT approximations. The development of approximate DFT is carried out through testing and refining incremental additions to existing, well-established formulas for the exchange-correlation energy.

The hierarchy of semilocal DFT methods is established according to the type and amount of the variables which enter into the exchange-correlation energy density. A group of methods which depend on a common set of variables is called a rung.[3] The lowest rung, i.e., the local spin density approximation (LSDA), includes only the electron density and, in an infinitesimal volume element, models the exchange-correlation energy at the uniform electron gas level. The PW92 functional is an example of an accurate representation of the uniform electron gas energy,[4] which is embedded into other, higher-rung functionals, e.g., the PBE energy.[5] LSDA is rarely used in chemistry due to its systematic overestimation of binding energies and underestimation of bond lengths.[6]

An improvement upon LSDA is achieved by adding density gradient corrections which account for the inhomogeneity of the electron density of a real system.[6] In the earliest nonempirical gradient-corrected functionals of Perdew and coworkers,[6,7] the corrections beyond LSDA are applied by combining the second-order gradient expansion for the slowly varying electron gas and the exact conditions for the exchange-correlation hole which are valid for general systems.[6,7] Nonetheless, in most generalized-gradient approximations (GGAs), the holes are not used explicitly, and the derivations are based on direct modeling of the GGA formula for the exchange-correlation energy:

$$E_{\mathrm{XC}}^{\mathrm{GGA}} = \int \rho(\mathbf{r}_1)\epsilon_{\mathrm{XC}}^{\mathrm{GGA}}\left(\rho(\mathbf{r}_1), |\nabla\rho(\mathbf{r}_1)|\right) \mathrm{d}\mathbf{r}_1. \tag{1.0.1}$$

GGA reduces the LSDA overestimation of molecular binding energies,[6] but it is still far from the chemical accuracy for thermochemistry and kinetics.[8] The most advanced nonempirical GGA for chemistry is the PBE functional.[5]

A further addition of the kinetic energy density, which depends explicitly on the occupied KS orbitals, defines the meta-GGA rung. Optionally, as in the case of our LC-PBETPSS-D3 functional, the meta-GGA exchange-correlation energy may encompass the Laplacian of the density:

$$E_{\mathrm{XC}}^{\text{meta-GGA}} = \int \rho(\mathbf{r}_1)\epsilon_{\mathrm{XC}}^{\text{meta-GGA}}\left(\rho(\mathbf{r}_1), |\nabla\rho(\mathbf{r}_1)|, \tau(\mathbf{r}_1), \nabla^2\rho\right) \mathrm{d}\mathbf{r}_1. \tag{1.0.2}$$

Owing to their more sophisticated mathematical forms, nonempirical meta-GGAs, e.g., TPSS[9] and SCAN,[10] can obey a higher number of exact constraints than GGAs can satisfy. For example, the TPSS functional can accurately predict both thermochemistry of molecules and lattice parameters of solids, which is not achievable for GGAs.[11] The correlation part of TPSS is employed in the LC-PBETPSS-D3 functional presented in this work.

In addition to the three mentioned rungs of pure semilocal DFT, it is common to form hybrid (meta-)GGAs by supplying the pure semilocal energy with an admixture of the Hartree-Fock (HF) exchange. In chemical applications, various recommended amounts of the orbital exchange correlate with a good description of binding energies and barrier heights.[8] These properties can be well described by a pure (non-hybrid) meta-GGA, but at the expense of heavy empirical parametrization, as in M06-L of Zhao and Truhlar.[12]

Within the hybrid GGA and meta-GGA rungs, multiple mathematical forms and parametrizations are possible. Depending on the number of parameters adjusted to empirical or higher-level theoretical data, functionals are regarded as more or less empirical. As a result, a DFT user faces tens of methods available in software packages.[13] To guide a rational selection, functionals are tested on extensive sets of reference data representing the most frequent applications.

However, even if various benchmarks are taken into account, the choice of the optimal method is not clear-cut. The methods which are statistically top performers occasionally fail for unexpected yet important cases. For example, the M06-2X functional of Zhao and Truhlar,[14] which shows superb across-the-board performance for main-group thermochemistry and kinetics,[15] yields unusually large errors for proton-exchange barriers in hydrogen-bonded clusters.[16] The ωB97XD functional,[17] known as one of the best DFT methods for noncovalent interactions,[15,18] overbinds the fullerene C60 – catcher complex by 10 kcal/mol (35% of the reference E_{bind}, discussed further in the text). Also quite surprisingly, it has been discovered that most of density functionals fail to describe even at a qualitative level the energetic effect of successive alkylation of first row atoms.[19] The popular B3LYP functional,[20] despite its design for thermochemistry, gives wrong sign and is only marginally better than the HF method for the energy of isomerization between linear and branched octane.[19]

Although the errors of approximate DFT are to a certain degree unpredictable, the performance in two important domains, donor-acceptor systems and noncovalent complexes, can be explained by considering two systematic errors: the self-interaction error and the lack of the long-range dispersion energy. The self-interaction error is an excessive propensity to transfer electrons between donor and acceptor

groups, which in turn influences, e.g., noncovalent interaction energies, charge-transfer excitation energies, and (hyper)polarizabilities of conjugated polymers. It is partially avoided by using a range-separated exchange functional with the 100% HF exchange at long interelectron distances. The proper inclusion of the dispersion energy for noncovalent molecular systems is possible either via nonlocal correlation functionals, as in the double-hybrid class of functionals,[21] or with an explicit dispersion correction, e.g., the DFT-D3 forcefield-like method.[22]

If we limit ourselves to the relatively inexpensive DFT approaches which do not employ virtual orbitals, the highest rung available is range-separated hybrid meta-GGA. Until recently, only the highly empirical functionals of this kind achieved good overall performance, e.g., the M11 range-separated meta-GGA of Peverati and Truhlar,[23] which includes 40 empirical parameters. But the recent systematic search in a vast space of possible mathematical forms carried out by Mardirossian and Head-Gordon[24] have shown that the high amount of empiricism is not necessary and even not recommended if one pursues transferability beyond the training set; the ωB97M-V functional developed by these authors includes 12 fitted parameters.

In the most recent development, hitherto unutilized exact constraints were integrated into the SCAN meta-GGA functional.[10,25] Initial tests showed that the performance of this functional uniformly surpasses that of TPSS, which is a previous-generation nonempirical meta-GGA.[10] However, no hybrid range-separated variant of SCAN has been developed to date, therefore its usefulness in some important chemical applications, e.g., charge transfer systems, is currently limited. The LC-PBETPSS-D3 functional, which is the main focus of this work, is the first reliable range-separated meta-GGA hybrid that is based on a nonempirical model of the exchange-correlation energy (ref 26, Paper III).

This work is composed as follows. First, we summarize the basic definitions of DFT which are crucial for understanding how approximate functionals are derived. Next, we present the details of the functionals aimed solely at noncovalent systems and not for general properties: the correlation functional of ref 27 (Paper I) and the exchange-correlation functional of ref 28 (Paper II). Finally, we derive the most complete, general functional (LC-PBETPSS-D3) and compare it with existing approaches using numerical tests of noncovalent interaction energies, thermochemical energy differences, and excitation energies.

Chapter 2

Basic Definitions

2.1 Kohn-Sham theory

Our focus is on molecular systems described by a clamped-nuclei Hamiltonian,

$$H = T + V_{\text{ext}} + V_{\text{ee}}, \tag{2.1.1}$$

where $T = -1/2 \sum_i \nabla_i^2$ is the kinetic energy operator, $V_{\text{ext}} = -\sum_i \sum_A Z_A / r_{Ai}$ is the operator of the Coulombic attraction between electrons and nuclei, and $V_{\text{ee}} = \sum_{i>j} 1/r_{ij}$ represents the electron-electron repulsion. Atomic units are assumed in all formulas in this work. The exact ground-state energy is given by the variational formula

$$E_0 = \min_{\rho} \left[\int v_{\text{ext}}(\mathbf{r}_1) \rho(\mathbf{r}_1) \mathrm{d}^3\mathbf{r}_1 + F[\rho] \right], \tag{2.1.2}$$

$$F[\rho] = \min_{\Psi \to \rho} \left[\langle \Psi | T + V_{\text{ee}} | \Psi \rangle \right], \tag{2.1.3}$$

where $F[\rho]$ is the Hohenberg-Kohn universal density functional[1] defined in Levy's constrained-search formulation[29] of DFT.[1] The minimization in Eq. 2.1.3 is carried out in the space of N-electron functions Ψ which integrate to the given electron density ρ. Unfortunately, computing F directly from the formal definition is in general case an intractable task. The Kohn-Sham (KS) scheme[2] facilitates a practical evaluation of F by making reference to a fictitious ground-state system described by a single-determinantal function (the KS determinant Φ^{KS}), which nonetheless has the same electron density as the physical system. In the KS scheme, F is broken up into terms that explicitly depend on the density and the orbitals of the KS system:

$$F = T_{\text{S}} + U + E_{\text{XC}}. \tag{2.1.4}$$

$T_{\text{S}} = \left\langle \Phi^{\text{KS}} \middle| T \middle| \Phi^{\text{KS}} \right\rangle$ is the kinetic energy of the KS system. The Hartree energy U is the classical electrostatic energy of the electron density interacting with itself

$$U[\rho] = \frac{1}{2} \iint \frac{\rho(\mathbf{r}_1)\rho(\mathbf{r}_2)}{r_{12}} \mathrm{d}^3\mathbf{r}_1 \mathrm{d}^3\mathbf{r}_2. \tag{2.1.5}$$

Now, the only term of the Kohn-Sham scheme which needs to be approximated (except for the obvious approximations due to finite basis sets) is the exchange-correlation energy $E_{\text{XC}} = E_{\text{X}} + E_{\text{C}}$. In the majority of approximations the individual

exchange (E_X) and correlation (E_C) components are modeled separately because the exact constraints which guide the functional development are known separately for each of these terms.[30] The equations for the KS orbitals read

$$\left(-\frac{1}{2}\nabla^2 + v_\mathrm{ext}(\mathbf{r}_1) + v_\mathrm{U}(\mathbf{r}_1) + v_\mathrm{XC}(\mathbf{r}_1)\right)\phi_j(\mathbf{r}_1) = \epsilon_j\phi_j(\mathbf{r}_1). \tag{2.1.6}$$

The Coulomb potential generated by the electron density is $v_\mathrm{U}(\mathbf{r}_1) = \delta U/\delta\rho(\mathbf{r}_1)$. The exchange-correlation potential is given by the functional derivative $v_\mathrm{XC}(\mathbf{r}_1) = \delta E_\mathrm{XC}/\delta\rho(\mathbf{r}_1)$.[2]

2.2 Adiabatic connection

E_XC is usefully expressed through the adiabatic connection formula[31]

$$E_\mathrm{XC}[\rho] = \int_0^1 \left\langle \Psi_\rho^{\min,\lambda}\middle|V_\mathrm{ee}\middle|\Psi_\rho^{\min,\lambda}\right\rangle \mathrm{d}\lambda - U[\rho], \tag{2.2.1}$$

where $\Psi_\rho^{\min,\lambda}$ minimizes the expectation value of $T + \lambda V_\mathrm{ee}$ and yields the same electronic density ρ as the wavefunction of the real system at $\lambda = 1$. E_XC is further decomposed into the exchange energy

$$E_\mathrm{X} = \left\langle \Phi^\mathrm{KS}\middle|V_\mathrm{ee}\middle|\Phi^\mathrm{KS}\right\rangle - U[\rho] \tag{2.2.2}$$

and the correlation energy, which is expressed through the coupling-constant integral

$$E_\mathrm{C}[\rho] = \int_0^1 V_\mathrm{C}^\lambda[\rho]\,\mathrm{d}\lambda \tag{2.2.3}$$

$$V_\mathrm{C}^\lambda[\rho] = \left\langle \Psi_\rho^{\min,\lambda}\middle|V_\mathrm{ee}\middle|\Psi_\rho^{\min,\lambda}\right\rangle - \left\langle \Phi^\mathrm{KS}\middle|V_\mathrm{ee}\middle|\Phi^\mathrm{KS}\right\rangle. \tag{2.2.4}$$

While it is possible to approximate E_C directly without any attempt to model V_C^λ, our model of E_C employed in the MCS functional[28] requires V_C^λ at an intermediate stage (shown in section 3.3).

2.3 Exchange and correlation holes

A possible path towards new DFT approximations is through modeling of the exchange-correlation hole,[32–34] which is also the central concept employed in the derivations presented in this work. The exchange-correlation hole $h_\mathrm{XC}^{\sigma\sigma'}(\mathbf{r}_1,\mathbf{r}_2)$ is a distribution of charge which allows E_XC to be formulated in terms of the Coulombic interaction between $h_\mathrm{XC}^{\sigma\sigma'}(\mathbf{r}_1,\mathbf{r}_2)$ and the electron density:[32]

$$E_\mathrm{XC} = \frac{1}{2}\iint \frac{\rho_\sigma(\mathbf{r}_1)h_\mathrm{XC}^{\sigma\sigma'}(\mathbf{r}_1,\mathbf{r}_2)}{r_{12}}\mathrm{d}\mathbf{r}_1\mathrm{d}\mathbf{r}_2. \tag{2.3.1}$$

The hole plugged into Eq. 2.3.1 is an average of the holes at different values of the coupling strength λ

$$h_\mathrm{XC}^{\sigma\sigma'}(\mathbf{r}_1,\mathbf{r}_2) = \int_0^1 h_{\mathrm{XC}\lambda}^{\sigma\sigma'}(\mathbf{r}_1,\mathbf{r}_2)\mathrm{d}\lambda. \tag{2.3.2}$$

The hole at λ depends on the λ-dependent two-electron density matrix:

$$h_{\mathrm{XC}\lambda}^{\sigma\sigma'}(\mathbf{r}_1,\mathbf{r}_2)=\frac{P_{2\lambda}^{\sigma\sigma'}(\mathbf{r}_1,\mathbf{r}_2)}{\rho_\sigma(\mathbf{r}_1)}-\rho_{\sigma'}(\mathbf{r}_2), \tag{2.3.3}$$

where

$$\begin{aligned}P_{2\lambda}^{\sigma\sigma'}(\mathbf{r}_1,\mathbf{r}_2)&=N(N-1)\\&\times\sum_{\sigma_3\cdots\sigma_N}\int\Psi_\rho^{\min,\lambda*}(\mathbf{r}_1\sigma,\mathbf{r}_2\sigma',\ldots,\mathbf{r}_N\sigma_N)\\&\times\Psi_\rho^{\min,\lambda}(\mathbf{r}_1\sigma,\mathbf{r}_2\sigma',\ldots,\mathbf{r}_N\sigma_N)\\&\times\mathrm{d}^3\mathbf{r}_3\cdots\mathrm{d}^3\mathbf{r}_N.\end{aligned} \tag{2.3.4}$$

It is useful to split the total exchange-correlation hole into the exchange and correlation holes. Both contributions can be then approximated separately based on the knowledge of the exact conditions they fulfill. The exact exchange hole is expressed using the (spin)orbitals of the KS system and does not depend on λ:

$$h_{\mathrm{X}}^{\sigma\sigma'}(\mathbf{r}_1,\mathbf{r}_2)=-\delta_{\sigma\sigma'}\frac{\left|\sum_i^{N_\sigma}\psi_{i\sigma}^*(\mathbf{r}_1)\psi_{i\sigma}(\mathbf{r}_2)\right|^2}{\rho_\sigma(\mathbf{r}_1)}. \tag{2.3.5}$$

Now, at each λ, the correlation hole is simply the difference between $h_{\mathrm{XC}\lambda}^{\sigma\sigma'}$ and $h_{\mathrm{X}}^{\sigma\sigma'}$:

$$h_{\mathrm{C}\lambda}^{\sigma\sigma'}(\mathbf{r}_1,\mathbf{r}_2)=h_{\mathrm{XC}\lambda}^{\sigma\sigma'}(\mathbf{r}_1,\mathbf{r}_2)-h_{\mathrm{X}}^{\sigma\sigma'}(\mathbf{r}_1,\mathbf{r}_2). \tag{2.3.6}$$

Finally, the V_{C}^λ integrand in Eq. 2.2.3 can be expressed via the λ-dependent correlation hole

$$V_{\mathrm{C}}^\lambda=\frac{1}{2}\sum_{\sigma\sigma'}\iint\frac{\rho_\sigma(\mathbf{r}_1)h_{\mathrm{C}\lambda}^{\sigma\sigma'}(\mathbf{r}_1,\mathbf{r}_2)}{r_{12}}\mathrm{d}^3\mathbf{r}_1\mathrm{d}^3\mathbf{r}_2. \tag{2.3.7}$$

A semilocal model for V_{C}^λ (and $h_{\mathrm{C}\lambda}^{\sigma\sigma'}$) will be presented in Section 3.3.

2.4 Generalized Kohn-Sham scheme

In the case of semilocal functionals supplemented with a fraction of the Hartree-Fock exchange or functionals dependent on the KS kinetic energy density, E_{XC} depends explicitly on the occupied KS orbitals instead of the density only. As a result, the evaluation of $v_{\mathrm{XC}}=\delta E_{\mathrm{XC}}/\rho(\mathbf{r}_1)$ requires costly optimized effective potential methods.[35] Instead, the generalized Kohn-Sham (GKS) scheme[36–38] is applied in which v_{XC} is a nonlocal potential $v_{\mathrm{XC}}(\mathbf{r}_1,\mathbf{r}_2)=\delta E_{\mathrm{XC}}/\delta\rho_{\mathrm{S}}(\mathbf{r}_1,\mathbf{r}_2)$, where $\rho_{\mathrm{S}}(\mathbf{r}_1,\mathbf{r}_2)$ is the first-order KS density matrix.[38] An orbital-dependent exchange energy term contributes to the effective GKS Hamiltonian the exchange operator of the same form as in Hartree-Fock theory but expressed via the GKS orbitals.

In what follows, the GKS scheme will be applied in every case a functional includes a fraction of the Hartree-Fock exchange.

2.5 Range-separated hybrid exchange functionals

In range-separated exchange functionals, different models of the exchange energy are applied at long and short interelectron distances. The error function splits the electron-electron interaction operator,

$$\frac{1}{r_{12}} = \frac{\mathrm{erfc}(\omega r_{12})}{r_{12}} + \frac{\mathrm{erf}(\omega r_{12})}{r_{12}}, \tag{2.5.1}$$

according to the value of the range-separation parameter ω. The definitions of the short- and long-range components of the total exchange energy follow from Eq. 2.5.1:

$$E_{\mathrm{X}} = E_{\mathrm{X,approx}}^{\mathrm{SR}} + E_{\mathrm{X,exact}}^{\mathrm{LR}}, \tag{2.5.2}$$

$$E_{\mathrm{X,approx}}^{\mathrm{SR}} = \frac{1}{2}\sum_{\sigma}\iint \frac{\rho_\sigma(\mathbf{r}_1)h_{\mathrm{X,approx}}^{\sigma}(\mathbf{r}_1,\mathbf{r}_2)\mathrm{erfc}(\omega r_{12})}{r_{12}}\mathrm{d}^3\mathbf{r}_1\mathrm{d}^3\mathbf{r}_2, \tag{2.5.3}$$

$$E_{\mathrm{X,exact}}^{\mathrm{LR}} = \frac{1}{2}\sum_{\sigma}\iint \frac{\rho_\sigma(\mathbf{r}_1)h_{\mathrm{X,exact}}^{\sigma}(\mathbf{r}_1,\mathbf{r}_2)\mathrm{erf}(\omega r_{12})}{r_{12}}\mathrm{d}^3\mathbf{r}_1\mathrm{d}^3\mathbf{r}_2. \tag{2.5.4}$$

The long-range exchange energy $E_{\mathrm{X,exact}}^{\mathrm{LR}}$ is based on the exact, orbital-dependent HF exchange hole of Eq. 2.3.5. A semilocal DFT model of the exchange hole enters into the range-separated functional through $E_{\mathrm{X,approx}}^{\mathrm{SR}}$. Once an approximation to the exchange hole $h_{\mathrm{X,approx}}^{\sigma}$ and ω parameter are fixed, the range-separated exchange approximation is completely defined. We note that the local definition of an exchange hole is ambiguous.[34] The ambiguity disappears in the system average of the hole.[34]

Chapter 3

MCS Exchange-Correlation Functional

Modrzejewski et al.[28] have introduced the MCS-D3 functional aimed at noncovalent interactions, which combines the range-separated hybrid GGA exchange based on the PBEsol energy[11,39,40] and the meta-GGA correlation energy developed earlier by Modrzejewski et al.[27] (Paper I and Paper II). The hybrid semilocal part of E_{XC} is complemented by a correction for the long-range dispersion energy:

$$E_{\mathrm{XC}}(\text{MCS-D3}) = E_{\mathrm{C}} + E_{\mathrm{X}}(\omega\text{PBEsol}) + E_{\mathrm{disp}}(\text{D3}). \tag{3.0.1}$$

In ref 28, both the D3 model of Grimme et al.[22] and MBD-rsSCS of Ambrosetti et al.[41] are used for E_{disp}. However, in the numerical data provided in this work, we restrict ourselves to the D3 variant. This restriction does not change our conclusions on the performance of the MCS functional.

3.1 Exchange functional

The most unique feature of the MCS functionals is the base exchange model – PBEsol. It is rarely used in chemistry but proven to be accurate for solid state computations.[11] Nevertheless, PBEsol shows promising results for hydrocarbon thermochemistry.[39] Csonka et al.[39] and Johnson et al.[42] have demonstrated that the exact second-order gradient term in the PBEsol exchange leads to improved results for two longstanding problems of DFT for organic chemistry: the relative energies of the $(CH)_{12}$ isomers[19,39] and reaction energies of isodesmic n-alkane fragmentation.[42] Notwithstanding, PBEsol is rather poor for other problems relevant for chemistry, e.g., noncovalent interaction energies, barrier heights, and general cases of main-group thermochemistry.[15]

To probe the applicability of the PBEsol exchange beyond the mentioned cases of hydrocarbon thermochemistry, we apply it in the short-range part of the MCS functional[28] and supply with the 100% HF exchange at long range. The range-separated PBEsol exchange energy in Eq. 3.0.1 is derived by Henderson et al.[40,43] using the GGA exchange hole which integrates to the base PBEsol exchange energy density.

3.2 Dispersion correction

Range-separated functionals with a small number of empirical parameters, which are the main subject of this work, require a dispersion correction of larger magnitude than other types of functionals, e.g., the empirical meta-GGAs of Zhao and Truhlar,[14] where a part of the dispersion energy in the vicinity of equilibrium geometries is accounted for by empirical parametrization. Moreover, range-separated functionals, in most cases, do not overbind through the exchange contribution, which is a spurious effect that masks the need for a separate dispersion correction.[44–46]

The D3 dispersion energy reads[47]

$$E_{\text{disp}}(\text{D3}) = -\sum_{A>B}\sum_{n=6,8} s_n \frac{C_n^{AB}}{R_{AB}^n} f_{\text{damp}}^{(n)}\left(R_{AB}\right), \tag{3.2.1}$$

$$f_{\text{damp}}^{(n)}\left(R_{AB}\right) = \frac{1}{1+6(R_{AB}/(r_n R_0^{AB}))^{-\alpha_n}}, \tag{3.2.2}$$

where $f_{\text{damp}}^{(n)}$ is a damping function which vanishes at $R_{AB}=0$, and s_8 and r_6 are empirical, functional-dependent parameters.[22] The C_6^{AB} coefficients are common to all functionals. Effective coordination numbers are used for the interpolation of C_6^{AB} to account for the effect of the molecular environment. The interpolation is between C_6^{AB} values obtained for hydrides with zero charge.[22] A 3-body term can be added for large systems to model the Axilrod-Teller-Muto contribution to the dispersion energy:[47]

$$E_{\text{disp}}^{\text{3-body}}(\text{D3}) = -\sum_{A>B>C} C_9^{ABC} \frac{(3\cos\theta_a\cos\theta_b\cos\theta_c+1)}{(R_{AB}R_{BC}R_{CA})^3} f_{\text{damp}}^{(9)}\left(\overline{R}_{\text{ABC}}\right), \tag{3.2.3}$$

where θ_a, θ_b, and θ_c are angles between the three interacting atoms, $\overline{R}_{\text{ABC}}$ is the geometric mean of the interatomic distances, and the C_9^{ABC} is approximated as

$$C_9^{ABC} \approx -\sqrt{C_6^{AB}C_6^{AC}C_6^{BC}}. \tag{3.2.4}$$

The nonadditive 3-body term is nonnegligible for large supramolecular systems.[48]

3.3 Correlation functional

The E_{C} term in Eq. 3.0.1 is based on the meta-GGA correlation model of Modrzejewski et al.[27] The derivation of this model is based on a meta-GGA correlation hole, which is then plugged into Eqs. 2.3.7 and 2.2.3. The model correlation hole has a simple mathematical form, which is forced to recover the short-range behavior of the pair correlation function of the uniform electron gas[49] and to satisfy formal constraints, e.g., the normalization integral.[27] On top of that, E_{C} includes a single empirical parameter which enables empirical optimization of the total dispersion-corrected exchange-correlation functional on a set of noncovalent interaction energies.

Owing to the spherical symmetry of the $1/r_{12}$ operator, only the spherical average

of the correlation hole enters explicitly into the formula for $V_{\mathrm{C}}^{\sigma\sigma',\lambda}$:

$$\begin{aligned} V_{\mathrm{C}}^{\sigma\sigma',\lambda} &= \frac{1}{2}\iint \frac{\rho_\sigma(\mathbf{r}_1)h_{\mathrm{C}\lambda}^{\sigma\sigma'}(\mathbf{r}_1,\mathbf{r}_2)}{r_{12}}\mathrm{d}^3\mathbf{r}_1\mathrm{d}^3\mathbf{r}_2 \\ &= \frac{1}{2}\int \mathrm{d}^3\mathbf{r}_1 \int_0^\infty \frac{\rho_\sigma(\mathbf{r}_1)h_{\mathrm{C}\lambda}^{\sigma\sigma'}(\mathbf{r}_1,r_{12})}{r_{12}}4\pi r_{12}^2\mathrm{d}r_{12}, \end{aligned} \tag{3.3.1}$$

where the spherical average of the correlation hole is

$$h_{\mathrm{C}\lambda}^{\sigma\sigma'}(\mathbf{r}_1,r_{12}) = \frac{1}{4\pi}\int_0^{2\pi}\mathrm{d}\phi_{\mathbf{r}_{12}}\int_0^\pi h_{\mathrm{C}\lambda}^{\sigma\sigma'}(\mathbf{r}_1,\mathbf{r}_1+\mathbf{r}_{12})\sin\theta_{\mathbf{r}_{12}}\mathrm{d}\theta_{\mathbf{r}_{12}}. \tag{3.3.2}$$

Thus, the correlation energy model requires only a spherically-symmetric model of $h_{\mathrm{C}\lambda}^{\sigma\sigma'}$.

The correlation hole which underlies the correlation energy of Modrzejewski et al.[27] comprises parallel- and opposite-spin components

$$h_{\mathrm{C}\lambda}^{\alpha\beta}(\mathbf{r}_1,r_{12}) = (a_{\alpha\beta}+b_{\alpha\beta}r_{12}+c_{\alpha\beta}r_{12}^2)\exp(-d_{\alpha\beta}r_{12}), \tag{3.3.3}$$

$$h_{\mathrm{C}\lambda}^{\alpha\alpha}(\mathbf{r}_1,r_{12}) = r_{12}^2(a_{\alpha\alpha}+b_{\alpha\alpha}r_{12}+c_{\alpha\alpha}r_{12}^2)\exp(-d_{\alpha\alpha}r_{12}). \tag{3.3.4}$$

The functions $a_{\sigma\sigma'}$, $b_{\sigma\sigma'}$, and $c_{\sigma\sigma'}$ depend on the density, density gradient, and the kinetic energy density at each point of space:

$$a_{\alpha\beta} = B_{\alpha\beta} - \rho_\beta, \tag{3.3.5}$$

$$b_{\alpha\beta} = \lambda B_{\alpha\beta} + d_{\alpha\beta}a_{\alpha\beta}. \tag{3.3.6}$$

$$c_{\alpha\beta} = -\frac{1}{12}(a_{\alpha\beta}d_{\alpha\beta}^2 + 3b_{\alpha\beta}d_{\alpha\beta}) \tag{3.3.7}$$

$$a_{\alpha\alpha} = B_{\alpha\alpha} - \frac{D_\alpha}{3}, \tag{3.3.8}$$

$$b_{\alpha\alpha} = \frac{\lambda}{2}B_{\alpha\alpha} + a_{\alpha\alpha}d_{\alpha\alpha}, \tag{3.3.9}$$

$$c_{\alpha\alpha} = -\frac{1}{30}(a_{\alpha\alpha}d_{\alpha\alpha}^2 + 5b_{\alpha\alpha}d_{\alpha\alpha}), \tag{3.3.10}$$

where the functions $B_{\alpha\beta}$ and $B_{\alpha\alpha}$ are chosen to recover the first terms of the short-range pair correlation function of the uniform electron gas proposed by Gori-Giorgi and Perdew:[49]

$$\begin{aligned} B_{\alpha\beta}(\rho_\alpha,\rho_\beta,\lambda) = \rho_\beta \Big(1 &+ 0.0207\lambda r_{\mathrm{s}}^{\alpha\beta} + 0.08193(\lambda r_{\mathrm{s}}^{\alpha\beta})^2 \\ &- 0.01277(\lambda r_{\mathrm{s}}^{\alpha\beta})^3 + 0.001859(\lambda r_{\mathrm{s}}^{\alpha\beta})^4\Big)\exp(-0.7524\lambda r_{\mathrm{s}}^{\alpha\beta}), \end{aligned} \tag{3.3.11}$$

$$\begin{aligned} B_{\alpha\alpha}(\rho_\alpha,|\nabla\rho_\alpha|,\tau_\alpha,\lambda) = \frac{D_\alpha}{3}&\left(1 - 0.01624\lambda r_{\mathrm{s}}^{\alpha\alpha} + 0.00264(\lambda r_{\mathrm{s}}^{\alpha\alpha})^2\right) \\ &\times \exp(-0.5566\lambda r_{\mathrm{s}}^{\alpha\alpha}), \end{aligned} \tag{3.3.12}$$

where $r_{\mathrm{s}}^{\alpha\beta}$, and r_{s} depend on the electron (spin)-densities

$$r_{\mathrm{s}}^{\alpha\alpha} = \frac{(3/\pi)^{1/3}}{2\rho_\alpha^{1/3}}, \tag{3.3.13}$$

$$r_{\mathrm{s}}^{\alpha\beta} = \frac{(3/\pi)^{1/3}}{\rho_\alpha^{1/3}+\rho_\beta^{1/3}}, \tag{3.3.14}$$

$$r_{\mathrm{s}} = \left(\frac{3}{4\pi\rho}\right)^{1/3}. \tag{3.3.15}$$

Table 3.1: ***Ab Initio*** **Numerical Constants Appearing in Eqs. 3.3.24–3.3.27.**

k	P_k	Q_k	R_k	S_k
0	1.696	3.356	1.775	3.205
1	−0.2763	−2.525	0.01213	−1.784
2	−0.09359	−0.4500	-4.743×10^{-3}	3.613×10^{-3}
3	3.837×10^{-3}	−0.1060	0.5566	-4.743×10^{-3}
4	-2.471×10^{-3}	5.532×10^{-4}		0.5566
5	0.7524	-2.471×10^{-3}		
6		0.7524		

The dependence on the kinetic energy density τ_α is introduced into the parallel-spin hole via the variable D_α, which is always non-negative and vanishes for single-orbital densities:

$$D_\alpha = \tau_\alpha - \frac{|\nabla\rho_\alpha|^2}{4\rho_\alpha}. \tag{3.3.16}$$

Consequently, the parallel-spin hole vanishes for single orbital densities, where the parallel-spin correlation should be zero.[27]

The numerical parameters of the correlation holes $h_{\mathrm{C}\lambda}^{\alpha\beta}$ and $h_{\mathrm{C}\lambda}^{\alpha\alpha}$ are derived from the uniform electron gas with the exception of the empirical parameter G, which enters in the gradient term of the exponential damping factor:

$$d_{\alpha\beta} = \frac{2.1070}{r_{\mathrm{s}}^{\alpha\beta}} + d_{\mathrm{grad}}, \tag{3.3.17}$$

$$d_{\alpha\alpha} = \frac{2.6422}{r_{\mathrm{s}}^{\alpha\alpha}} + d_{\mathrm{grad}}, \tag{3.3.18}$$

$$d_{\mathrm{grad}} = \frac{G}{r_{\mathrm{s}}} \frac{\nabla\rho\cdot\nabla\rho}{\rho^{8/3}}, \tag{3.3.19}$$

where G is fitted together with other parameters of the MCS functionals to match the reference interaction energies on the S22 set.[50,51] While the parameter G is adjusted to reference data, the physical constraints imposed onto $h_{\mathrm{C}\lambda}^{\alpha\alpha}$ and $h_{\mathrm{C}\lambda}^{\alpha\beta}$ stay untouched, in particular the short-range expansion of the correlation hole, which is known to be reliable at the semilocal DFT level.[52]

The total correlation energy is a sum of spin-parallel and spin-opposite components

$$E_{\mathrm{C}} = E_{\mathrm{C}}^{\alpha\beta} + E_{\mathrm{C}}^{\beta\alpha} + E_{\mathrm{C}}^{\alpha\alpha} + E_{\mathrm{C}}^{\beta\beta}, \tag{3.3.20}$$

where the components $E_{\mathrm{C}}^{\sigma\sigma'}$ originate from the adiabatic-connection integral of $V_{\mathrm{C}\lambda}^{\sigma\sigma'}$

$$E_{\mathrm{C}}^{\sigma\sigma'} = \int_0^1 V_{\mathrm{C}\lambda}^{\sigma\sigma'}\,\mathrm{d}\lambda. \tag{3.3.21}$$

The explicit, implementation-ready expressions for $E_{\mathrm{C}}^{\sigma\sigma'}$ are

$$E_{\mathrm{C}}^{\alpha\beta} = \frac{1}{2}\int \mathrm{d}^3\mathbf{r}_1 \int_0^1 \mathrm{d}\lambda \int_0^\infty \frac{\rho_\alpha(\mathbf{r}_1) h_{\mathrm{C}\lambda}^{\alpha\beta}(\mathbf{r}_1, r_{12})}{r_{12}} 4\pi r_{12}^2 \mathrm{d}r_{12}$$
$$= \int \mathrm{d}^3\mathbf{r}_1 \rho_\alpha \pi \frac{\mathcal{B}_{\alpha\beta} + \mathcal{A}_{\alpha\beta} d_{\alpha\beta}}{d_{\alpha\beta}^3}, \tag{3.3.22}$$

$$E_{\mathrm{C}}^{\alpha\alpha} = \frac{1}{2}\int \mathrm{d}^3\mathbf{r}_1 \int_0^1 \mathrm{d}\lambda \int_0^\infty \frac{\rho_\alpha(\mathbf{r}_1) h_{\mathrm{C}\lambda}^{\alpha\alpha}(\mathbf{r}_1, r_{12})}{r_{12}} 4\pi r_{12}^2 \mathrm{d}r_{12}$$
$$= \int \mathrm{d}^3\mathbf{r}_1 \rho_\alpha \pi \frac{8\mathcal{B}_{\alpha\alpha} + 4\mathcal{A}_{\alpha\alpha} d_{\alpha\alpha}}{d_{\alpha\alpha}^5}. \tag{3.3.23}$$

The integral over the coupling constant λ is computed analytically. $\mathcal{A}_{\alpha\beta}$, $\mathcal{B}_{\alpha\beta}$, $\mathcal{A}_{\alpha\alpha}$, $\mathcal{B}_{\alpha\alpha}$, $d_{\alpha\beta}$, and $d_{\alpha\alpha}$ are functions evaluated at each grid point,

$$\mathcal{A}_{\alpha\beta} = \frac{\rho_\beta}{r_{\mathrm{s}}^{\alpha\beta}} \left[\left(-P_0 + \sum_{k=1}^{4} P_k (r_{\mathrm{s}}^{\alpha\beta})^k \right) \exp\left(-P_5 r_{\mathrm{s}}^{\alpha\beta} \right) + P_0 \right] - \rho_\beta, \tag{3.3.24}$$

$$\mathcal{B}_{\alpha\beta} = \frac{\rho_\beta}{(r_{\mathrm{s}}^{\alpha\beta})^2} \left[\left(-Q_0 + \sum_{k=1}^{5} Q_k (r_{\mathrm{s}}^{\alpha\beta})^k \right) \exp\left(-Q_6 r_{\mathrm{s}}^{\alpha\beta} \right) + Q_0 \right] + d_{\alpha\beta}\mathcal{A}_{\alpha\beta}, \tag{3.3.25}$$

$$\mathcal{A}_{\alpha\alpha} = \frac{D_\alpha}{3 r_{\mathrm{s}}^{\alpha\alpha}} \left[\left(-R_0 + \sum_{k=1}^{2} R_k (r_{\mathrm{s}}^{\alpha\alpha})^k \right) \exp\left(-R_3 r_{\mathrm{s}}^{\alpha\alpha} \right) + R_0 \right] - \frac{D_\alpha}{3}, \tag{3.3.26}$$

$$\mathcal{B}_{\alpha\alpha} = \frac{D_\alpha}{6(r_{\mathrm{s}}^{\alpha\alpha})^2} \left[\left(-S_0 + \sum_{k=1}^{3} S_k (r_{\mathrm{s}}^{\alpha\alpha})^k \right) \exp\left(-S_4 r_{\mathrm{s}}^{\alpha\alpha} \right) + S_0 \right] + d_{\alpha\alpha}\mathcal{A}_{\alpha\alpha}. \tag{3.3.27}$$

The nonempirical parameters in Eqs. 3.3.24-3.3.27 are derived from a short-range model of the correlation hole in the homogeneous electron gas.[27] Their values are provided in Table 3.1.

Chapter 4

LC-PBETPSS-D3 Exchange-Correlation Functional

The LC-PBETPSS-D3 functional is a dispersion-corrected range-separated meta-GGA (ref 26, Paper III). In contrast to the MCS functionals, which were developed primarily for noncovalent interaction energies, LC-PBETPSS-D3 is designed and tested for general purposes: main-group thermochemistry, barrier heights, and excitation energies. The exchange-correlation model combines the (unmodified) TPSS correlation,[9] the range-separated PBE exchange of Modrzejewski et al.,[26] and the D3 dispersion correction:

$$E_{\mathrm{XC}}(\text{LC-PBETPSS-D3}) = E_{\mathrm{C}}(\text{TPSS}) + E_{\mathrm{X}}(\text{range-separated PBE}) + E_{\mathrm{disp}}(\text{D3}). \tag{4.0.1}$$

It may look somewhat surprising that the functional has a meta-GGA correlation and a PBE-based exchange, but the short-range part of E_{X} is in fact promoted to the meta-GGA rung. Here, the exchange hole model, which is required to construct the short-range functional according to Eq. 2.5.3, has the correct coefficient of the r_{12}^2 term in the short-range expansion around the reference electron. This coefficient depends on the kinetic energy density and the Laplacian, therefore the resulting short-range exchange energy is a meta-GGA even though the base functional is a lower-rung functional. The derivation of E_{X} will be presented in detail in the next section.

4.1 General scheme for range-separated exchange meta-GGAs

4.1.1 Existing approaches

The differences between existing approaches to the range-separated exchange energy boil down to different models of the approximate exchange hole in the short-range exchange energy formula of Eq. 2.5.3.

In what follows, we consider the exchange energy of a closed-shell system with $\rho_\alpha = \rho_\beta = \rho/2$. The formulas derived below can be applied to open-shell systems by using the exact relation[53]

$$E_{\mathrm{X}}[\rho_\alpha, \rho_\beta] = \frac{1}{2} E_{\mathrm{X}}[2\rho_\alpha] + \frac{1}{2} E_{\mathrm{X}}[2\rho_\beta]. \tag{4.1.1}$$

For clarity, hereafter we skip the spin index in the exchange hole symbol.

The most widely employed model of the exchange hole is that of Iikura, Tsuenda, Yanai, and Hirao (ITYH).[54] It is a general model which can be applied in an automated manner for arbitrary exchange energy approximations (but with varying degrees success). The important examples of its usage are LC-BLYP, LC-BOP, LC-PBEOP, and CAM-B3LYP.[55–57]

The ITYH exchange hole is directly based on a modified LDA exchange hole,[54] which limits the set of exact constraints that it can satisfy. It has the correct value at $r_{12} = 0$,

$$h_{\mathrm{X,ITYH}}(\mathbf{r}_1, r_{12} = 0) = h_{\mathrm{X,exact}}(\mathbf{r}_1, r_{12} = 0) = -\frac{\rho(\mathbf{r}_1)}{2}, \tag{4.1.2}$$

and satisfies the energy integral

$$\frac{1}{2}\int \frac{h_{\mathrm{X,ITYH}}(\mathbf{r}_1, r_{12})}{r_{12}} 4\pi r_{12}^2 \mathrm{d}r_{12} = \epsilon_{\mathrm{X,approx}}(\mathbf{r}_1), \tag{4.1.3}$$

where $\epsilon_{\mathrm{X,approx}}$ is the exchange energy density of a given base functional. But the ITYH hole fails to fulfill two other exact conditions: the hole normalization[40]

$$\int h_{\mathrm{X,exact}}(\mathbf{r}_1, r_{12}) 4\pi r_{12}^2 \mathrm{d}r_{12} = -1 \tag{4.1.4}$$

and the correct second-order short-range expansion of the spherically-averaged exchange hole at zero current density,[32,58,59]

$$h_{\mathrm{X,exact}}(\mathbf{r}_1, r_{12}) = -\frac{\rho}{2} - Q r_{12}^2 + \ldots, \tag{4.1.5}$$

$$Q = \frac{1}{12}\nabla^2\rho - \frac{1}{6}\tau + \frac{1}{24}\frac{(\nabla\rho)^2}{\rho}, \tag{4.1.6}$$

where τ is the kinetic energy density of a closed-shell system

$$\tau = 2\sum_i |\nabla\psi_i|^2. \tag{4.1.7}$$

The exact coefficient Q of Eq. 4.1.6 includes meta-GGA ingredients, therefore it cannot be included in the model at a GGA level.

More advanced models of the exchange hole which satisfy more conditions than $h_{\mathrm{X,ITYH}}$ have been employed in the range-separated PBE functionals of Henderson et al.[40] and of Vydrov et al.[60] These expressions satisfy Eq. 4.1.2, Eq. 4.1.3, Eq. 4.1.4, but only approximately Eq. 4.1.6.

The nonempirical range-separated meta-GGA TPSS functional has been tried before but, quite remarkably, it failed to benefit in general from using the long-range HF exchange component.[61]

The exchange hole of Modrzejewski et al.[26] which is employed in E_{X} of Eq. 4.0.1 goes beyond the most popular GGA approaches. Owing to the use of the meta-GGA ingredients, τ and $\nabla^2\rho$, it has the correct coefficient Q defined in Eq. 4.1.6. The improved exchange allows for employing a more advanced correlation, e.g., the range-separated meta-GGA exchange based on PBE is paired with the TPSS correlation energy.

The presentation of the range-separated exchange of Modrzejewski et al.[26] is divided into two parts. First, we establish a Becke-Roussel-type exchange hole which integrates to a given exchange energy density. Second, we employ this model in Eq. 2.5.3 to derive analytic expressions for the short-range PBE exchange, which is then employed with the 100% HF exchange at long range.

4.1.2 Exchange hole model

The range-separated energy E_{X} of the LC-PBETPSS-D3 functional includes the short-range DFT exchange component, which is build up on a model for the exchange hole. The exchange hole, when integrated with the full-range operator $1/r_{12}$, yields the base PBE exchange energy density. We will present a general $h_{\mathrm{X,approx}}$ which can be adjusted, in a black box manner like the ITYH method,[54] to recover an arbitrary semilocal exchange energy density. So far we have found good numerical performance for the range-separated exchange energy derived from the base PBE exchange, but our search space has been limited only to the nonempirical PBE and TPSS models.[26] It is certainly possible to employ the equations derived below for an empirical functional, i.e., in an optimization procedure similar to that of Mardirossian and Head-Gordon.[24]

Our exchange energy is based on the generalized Becke-Roussel (BR) exchange hole proposed by Becke[62]

$$h_{\mathrm{X,BR}}(a,b,\mathcal{N};r_{12}) = -\mathcal{N}\frac{a}{16\pi b r_{12}}\Big[(a|b-r_{12}|+1)e^{-a|b-r_{12}|} - (a|b+r_{12}|+1)e^{-a|b+r_{12}|}\Big], \quad (4.1.8)$$

where the three free parameters, $a > 0$, $b > 0$, and $\mathcal{N} > 0$, will be defined later so that the second-order short-range expansion of $h_{\mathrm{X,BR}}$ matches Eq. 4.1.5, and the energy integral of $h_{\mathrm{X,BR}}$ recovers a given base exchange energy $\epsilon_{\mathrm{X,approx}}$:

$$\frac{1}{2}\int_0^\infty \frac{h_{\mathrm{X,BR}}(a,b,\mathcal{N};r_{12})}{r_{12}} 4\pi r_{12}^2 \mathrm{d}r_{12} = \epsilon_{\mathrm{X,approx}}. \quad (4.1.9)$$

The price paid for satisfying these conditions is the violation of the normalization integral

$$\int h_{\mathrm{X,BR}}(a,b,\mathcal{N};r_{12}) 4\pi r_{12}^2 \mathrm{d}r_{12} = -\mathcal{N}, \quad (4.1.10)$$

where $\mathcal{N}$ is no longer guaranteed to be 1, as in the original BR model derived from the exact exchange hole for the hydrogen atom.[33]

The generalized BR hole which integrates to a given exchange energy density has been already employed by Becke[62] and Precechtelova et al.[63] The equations derived by these authors are recast below using the notation assumed in this work.

To get $h_{\mathrm{X,BR}}$ at each point of space, a nonlinear equation for an auxiliary variable $x = ab$ is solved first, and then the individual values of a, b, and $\mathcal{N}$ are computed using x and the electron density. The equation for x is

$$\frac{x-2}{x^2}\left(e^x - 1 - \frac{x}{2}\right) = -\frac{6Q}{\pi\rho^2}\epsilon_{\mathrm{X,approx}}, \quad (4.1.11)$$

where the solution is sought for with, e.g., the bijection method. For any physically allowed right-hand side, a unique $x > 0$ solves Eq. 4.1.11. The computation of $h_{\mathrm{X,BR}}$ is completed by specifying a, b, and $\mathcal{N}$:

$$a = \sqrt{\pi\rho\frac{(2-2e^x+x)}{x\epsilon_{\mathrm{X,approx}}}}, \quad (4.1.12)$$

$$b = x/a, \quad (4.1.13)$$

$$\mathcal{N} = 4\pi\rho e^x/a^3. \quad (4.1.14)$$

To recapitulate the properties of $h_{\mathrm{X,BR}}$ defined via Eqs. 4.1.11–4.1.14: it integrates to the given $\epsilon_{\mathrm{X,approx}}$ (Eq. 4.1.9), has the exact value at the origin (Eq. 4.1.2), and recovers the exact coefficient of r_{12}^2 (Eq. 4.1.6). Nonetheless, its normalization integral differs in general from the exact value of -1.

4.1.3 Short-range exchange energy

We now employ the exchange hole derived in the previous section to derive the analytic expression for the short-range exchange energy component of the base exchange energy. The short-range exchange energy density $\epsilon^{\mathrm{SR}}_{\mathrm{X,approx}}$ is the difference

$$\epsilon^{\mathrm{SR}}_{\mathrm{X,approx}} = \epsilon_{\mathrm{X,approx}} - \epsilon^{\mathrm{LR}}_{\mathrm{X,approx}}, \tag{4.1.15}$$

where the long-range component $\epsilon^{\mathrm{LR}}_{\mathrm{X,approx}}$ is

$$\epsilon^{\mathrm{LR}}_{\mathrm{X,approx}} = \frac{1}{2}\int_0^\infty \frac{h_{\mathrm{X,BR}}(r_{12})\mathrm{erf}(\omega r_{12})}{r_{12}} 4\pi r_{12}^2 \mathrm{d}r_{12} = \frac{1}{2} U^{\mathrm{LR}}_{\mathrm{X,approx}}, \tag{4.1.16}$$

$$\begin{aligned} U^{\mathrm{LR}}_{\mathrm{X,approx}} = &-\frac{\mathcal{N}\omega}{\nu}\mathrm{erf}\left(\nu\right) + \frac{\mathcal{N}\omega}{2\nu}\left(1-\mu^2+\mu\nu\right)\mathrm{erfc}\left(\mu-\nu\right)\exp\left(\mu^2-2\mu\nu\right) \\ &+ \frac{\mathcal{N}\omega}{2\nu}\left(-1+\mu^2+\mu\nu\right)\mathrm{erfc}\left(\mu+\nu\right)\exp\left(\mu^2+2\mu\nu\right), \end{aligned} \tag{4.1.17}$$

$$\mu = \frac{a}{2\omega}, \tag{4.1.18}$$

$$\nu = b\omega. \tag{4.1.19}$$

For small values of ν, the right-hand side of Eq. 4.1.17 should be evaluated using the Taylor expansion to avoid numerical errors. The final short-range exchange energy is evaluated using a numerical quadrature over the whole space

$$E^{\mathrm{SR}}_{\mathrm{X,approx}} = \int \epsilon^{\mathrm{SR}}_{\mathrm{X,approx}}(\mathbf{r}_1)\rho(\mathbf{r}_1)\mathrm{d}\mathbf{r}_1. \tag{4.1.20}$$

The complete range-separated exchange energy E_{X} of Eq. 4.0.1 includes the long-range HF exchange (Eq. 2.5.4),

$$E_{\mathrm{X,approx}} = E^{\mathrm{SR}}_{\mathrm{X,approx}} + E^{\mathrm{LR}}_{\mathrm{X,exact}}, \tag{4.1.21}$$

which completes the construction of the range-separated exchange energy in the scheme of Modrzejewski et al.[26] We stress that at this point the scheme is general, and one can employ it to derive a range-separated exchange energy from any given semilocal approximation. However, because of the possible presence of error cancellations, it is not guaranteed that the resulting exchange energy will work well with a given correlation part. Therefore, although the range-separation scheme is simple in itself, numerical tests and possibly refitting of some parameters are required to construct a practical exchange-correlation model.

4.2 One-electron self-interaction error

The range-separated exchange functional constructed using the scheme of Modrzejewski et al.[26] differs substantially from existing range-separated GGAs, even in

cases where these functionals stem from the same base semilocal exchange. To compare the new approach with the existing ones, we compute a series of short-range DFT exchange energies for the ground state of the hydrogen atom and compare against the HF short-range exchange computed with the same basis set.

In the limit of the hydrogenic density, $E_{\mathrm{X}}[\rho]$ should exactly cancel $U[\rho]$. A deviation from the perfect cancellation between these terms is the one-electron self-interaction error.[33,64] The self-interaction error arises in GGAs, which use only the variables $\rho(\mathbf{r}_1)$ and $\nabla\rho(\mathbf{r}_1)$, but lack the dependence on $\tau(\mathbf{r}_1)$ which is needed to recognize that the electron density comes from a single orbital. One of the advantages of meta-GGAs is the ability to recognize one-electron densities.[65]

The large-ω behavior of the exact short-range exchange energy $E^{\mathrm{SR}}_{\mathrm{X,exact}}(\omega)$ of the hydrogen atom is given by the expansion[66]

$$E^{\mathrm{SR}}_{\mathrm{X,exact}}(\omega \to \infty) = -\frac{1}{16\omega^2} + \frac{1}{32\omega^4} + \ldots \tag{4.2.1}$$

Eq. 4.2.1 assumes the exact density. Gill et al.[66] have shown that the first term on the right-hand side is recovered already by the local density approximation, but the term of order $1/\omega^4$ requires $h_{\mathrm{X,approx}}$ with the correct second-order expansion for small r_{12}.[66] Indeed, the short-range meta-GGA functionals derived in this work, which satisfy Eq. 4.1.6, approach $E^{\mathrm{SR}}_{\mathrm{X,exact}}(\omega \to \infty)$ visibly faster than the existing GGAs (Figure 4.1). The reduction of errors for large ω is seen for all tested base functionals: PBE,[5] B88,[67] and TPSS.[9]

Another contribution to the self-interaction error is in the correlation energy. Clearly, the correlation energy should vanish for the hydrogen atom, but it does not at the GGA level. The pure PBE exchange-correlation functional yields $E_{\mathrm{C}} = -0.006$ a.u. (-3.8 kcal/mol). This error can be eliminated only at the meta-GGA level by using, e.g., the TPSS correlation.[9,68] In the next section it will be shown that the TPSS correlation is the best choice to be combined with the range-separated exchange energy of Modrzejewski et al.[26]

4.3 Pairing approximate exchange with approximate correlation

We now proceed to employ the range-separation scheme of Modrzejewski et al.[26] in a complete exchange-correlation functional, and to show that the combination of the PBE-based exchange and the TPSS correlation is the preferred choice of the base semilocal models. We restrict ourselves to the nonempirical functionals, PBE and TPSS, and apply them in three candidate combinations labeled LC-PBETPSS, LC-PBEPBE, and LC-TPSSTPSS. (LC-XY denotes a range-separated functional where X is the base model for exchange, $\epsilon_{\mathrm{X,approx}}$ in Eq. 4.1.11, and Y is the accompanying correlation.) The candidate functionals are applied on the AE6 set of atomization energies[70] and BH6 set of barrier heights.[70] For each functional we search for the optimal value of the range-separation parameter ω. Otherwise there are no adjustable parameters. The AE6 and BH6 benchmarks are representative of 109 atomization energies and 44 barrier heights, respectively, in the Database/3 collection.[70]

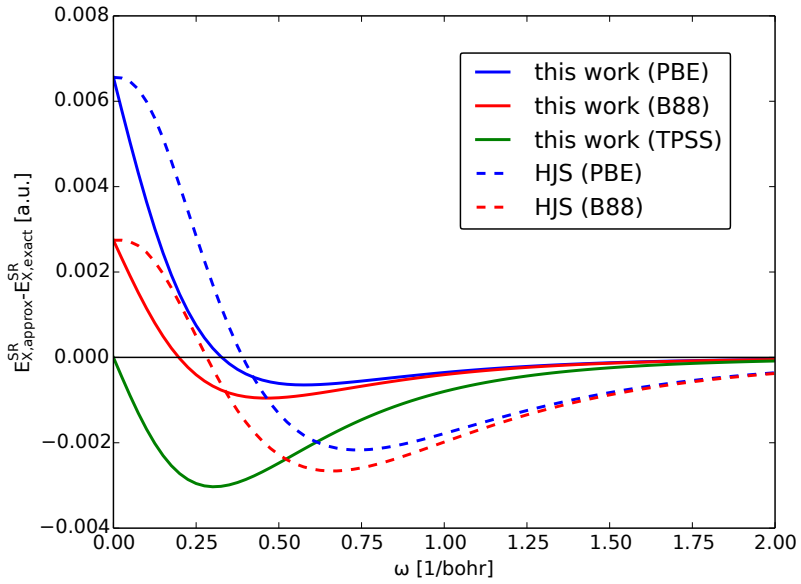

Figure 4.1: Differences between approximate and exact short-range exchange energies of the ground state of the hydrogen atom. All computations employ the aug-cc-pV5Z basis set[69] and HF orbitals. The short-range GGA models of Henderson et al.[40,43] are denoted as HJS. Correlation energies are not included.

Consistently with the results of other authors,[61] the range-separated hybrid based entirely on the TPSS exchange-correlation, LC-TPSSTPSS, fails to yield better atomization energies than the pure TPSS functional. The optimal value of ω for atomization energies of the AE6 set is zero, i.e., no exact long-range exchange. In contrast to AE6, the errors on the BH6 set are minimized for $\omega = 0.35$. No single value of ω makes LC-TPSSTPSS applicable for both atomization energies and barrier heights. The numerical data for LC-TPSSTPSS are available in the Supporting Information for ref 26.

Among all candidates, LC-PBETPSS achieves the best overall accuracy (Figure 4.2). The optimal range-separation parameter for this functional is in the interval $0.30 \leq \omega \leq 0.35$, depending on the relative weight of the barrier heights (BH6). The absolute percentage errors for the BH6 set are much larger than for AE6, therefore a value at the upper end of this interval seems more appropriate.

We use the value of $\omega = 0.35$ as the range-separation parameter of the LC-PBETPSS functional. This approximately coincides with ω that makes the self-interaction error for the hydrogen atom vanish, which can be viewed as an alternative theoretical justification for this choice (Figure 4.1). (The latter is important because a number of nonempirical functionals have been designed to recover the exact energy in the limit of the hydrogen atom.[9,65])

The candidate which is fully based on the PBE functional, LC-PBEPBE, show a strong dependence of the atomization energies on the range-separation parameter. The error curve for AE6 is steep and precludes the choice of a single value of ω which is good enough for both AE6 and BH6. For example, at $\omega = 0.30$, the average error in the barrier heights is only 1.6 kcal/mol, which is acceptable, but at the same time the error for the atomization energies is as high as 10.5 kcal/mol, which is large compared to the existing range-separated functionals.[40] Thus, LC-PBETPSS is the only functional which we discuss further and employ in the full suite of test sets.

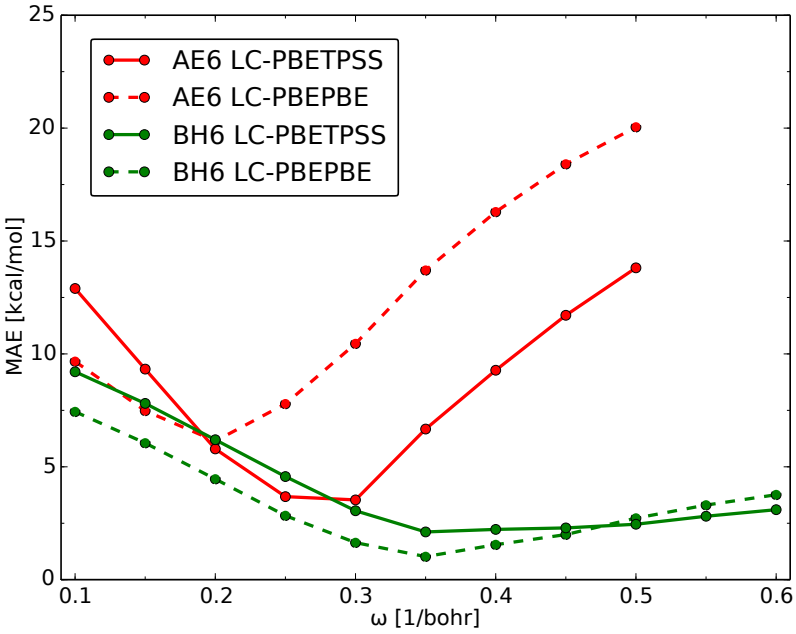

Figure 4.2: Mean absolute errors on the AE6 and BH6 sets.[70] All DFT computations employ the def2-QZVPP basis set.[69,71] The reference values are taken from ref 13 (AE6) and ref 72 (BH6).

Alternatively, it is possible to employ existing schemes to build a range-separated functional based on the PBE exchange and the TPSS correlation. For example, it is possible in the Gaussian program using the simpler ITYH exchange hole.[54] The alternative functional, denoted as LC-PBETPSS*, minimizes the errors on AE6 and BH6 at $\omega = 0.7$. The resulting errors (MAE=14.7 kcal/mol for AE6 and MAE=2.6 kcal/mol for BH6) are larger than for LC-PBETPSS. For $0.20 \leq \omega \leq 0.35$, where LC-PBETPSS performs well for AE6, LC-PBETPSS* yields MAE $>$ 30 kcal/mol, which is an extremely large error. The numerical data for LC-PBETPSS* are available in the Supporting Information of ref 26.

4.4 Dispersion correction

We combine the LC-PBETPSS functional with the D3 dispersion correction of Grimme et al.[22] (see Eq. 3.2.1). The minimization of the MAE for LC-PBETPSS-D3 on the S22 set of noncovalent systems[50,51] yields $r_6 = 0.88971$. We include only the $1/R^6$ contribution because adding the $1/R^8$ term does not decrease the MAE for the training set. Therefore, we limit the number of empirical, functional-dependent parameters in the dispersion energy to only one. We employ the original damping function $f_n(R_{AB})$,[22] which vanishes for $R_{AB} \to 0$, instead of the newer Becke-Johnson damping[73] to avoid double counting of the interaction energy at short range. The instances where we add the nonadditive three-body term are indicated by an appropriate label.

Chapter 5

Results and Discussion

5.1 Electronic-structure methods

In most tests described in this work, we add the D3 dispersion correction to the DFT energy. The labels of the dispersion-corrected methods are supplemented with the "-D3" suffix.

The functionals developed by Modrzejewski et al.[26,28] are denoted as MCS-D3 and LC-PBETPSS-D3. The empirical parameters included in MCS-D3 are $G = 0.075$, $\omega = 0.3$, $r_6 = 1.1822$, and $s_8 = 0.7740$. Our main focus is on the LC-PBETPSS-D3 functional, which is, in contrast to MCS-D3, a general-purpose method designed for properties beyond noncovalent interactions energies. The tests of the MCS-D3 functional are carried out only on a subset of the full test set. The MCS-D3 functional is implemented in our in-house code.

The LC-PBETPSS-D3 functional includes the meta-GGA short-range PBE exchange and the 100% HF exchange at long range. The range-separation parameter of the exchange is fixed at $\omega = 0.35$. The TPSS model is used for the correlation term. The LC-PBETPSS functional is applied with the D3 dispersion correction (LC-PBETPSS-D3) and for some systems without the dispersion term (LC-PBETPSS). The LC-PBETPSS functional is implemented in the Molpro program.[74]

A wide set of existing methods is gathered and employed in our test calculations. The comparison with the LC-ωPBE-D3 functional of Vydrov and Scuseria[60] probes the combined influence of upgrading the PBE-based short-range component of the exchange functional to a meta-GGA and using the meta-GGA TPSS correlation instead of PBE. The M06-2X empirical meta-GGA functional of Zhao and Truhlar[14] is currently one of the most popular methods employed in computational chemistry. While it accounts for a part of the dispersion energy via empirical parametrization, it only does so in the vicinity of equilibrium separations. In most cases, we use it in a dispersion-corrected form (M06-2X-D3), which is thoroughly tested by Goerigk and Grimme.[15] ωB97XD is an empirical, dispersion-corrected, range-separated GGA functional of Chai and Head-Gordon.[17] It is designed for thermochemistry, kinetics, and energies of noncovalent systems. ωB97X[75] is a predecessor of ωB97XD, which is not optimized for use with a dispersion correction. It is known to perform well for spectroscopic properties.[76] We employ ωB97X in the part of our tests devoted to excitation energies. M06-L is an empirical, pure meta-GGA functional without the HF exchange.[14] Finally, B3LYP-D3 is employed to show the progress that has been made with respect to the functionals developed in the 1990s.[20]

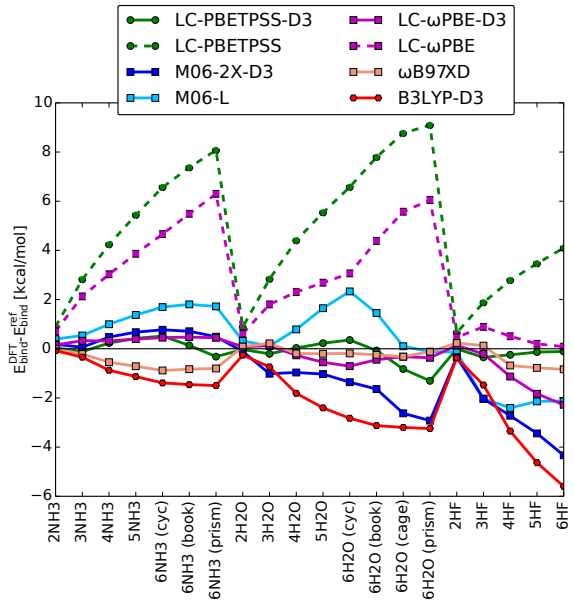

Figure 5.1: Errors for the binding energies of the CEPX33 set. The computational details are provided in Table 5.1.

For $(CH)_{12}$ isomers, we employ the DLPNO-CCSD(T) method to get the reference energies,[77] with the numerical thresholds set at the "tight" level defined in Table 1 of ref 78. The DLPNO-CCSD(T) computations are performed with the ORCA 3.0.3 program.[79]

5.2 Range-separated functionals for noncovalent complexes

A dispersion-corrected range-separated exchange corrects some of the problems that traditional functionals have for noncovalent systems. The interaction energy curves computed with range-separated functionals no longer critically depend on the behavior of the enhancement factor for large reduced density gradients.[44–46] Range-separated functionals improve on the description of the exchange repulsion, which is otherwise systematically overestimated or underestimated. In pure functionals, the systematic errors for noncovalent systems are extremely sensitive to the behavior of the approximate exchange in the low-density regions where the density gradient changes substantially upon bond formation.[45,80] In this context, the crucial feature of an exchange functional is the limit of the exchange enhancement factor for large reduced density gradients: either it explodes to infinity, as in the B88 exchange, or approaches a constant, as in PBE. The functionals based on the B88 exchange, e.g., BLYP, tend to predict a much more pronounced repulsion than the HF method.[44] In dispersion-corrected approaches, this error in the exchange energy has to be compensated by a strongly attractive dispersion term. At the other end of the spectrum, the functionals based on the PBE exchange tend to give, somewhat confusingly, binding exchange-only interaction energy curves for noble gases due to an artificial exchange component.[44] Applying the long-range HF term makes the underlying semilocal model of the exchange energy much less critical. It has been demonstrated

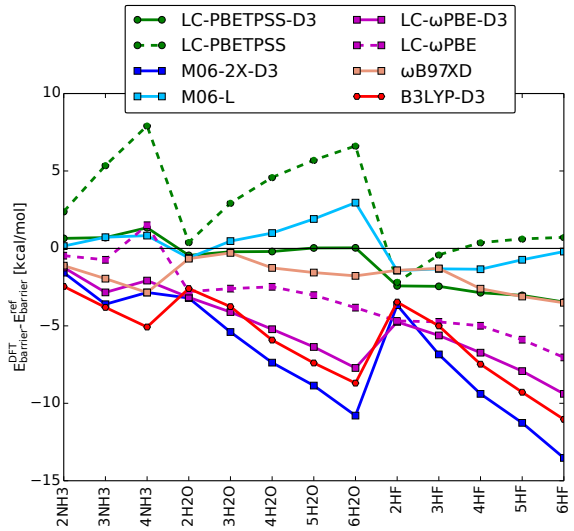

Figure 5.2: Errors for the proton-exchange barriers of the CEPX33 set. The computational details are provided in Table 5.1.

by Kamiya et al. for noble gas dimers that range-separated functionals derived from different base exchange models converge to give repulsive curves.[46]

The most apparent advantage of range-separated functionals is for donor-acceptor noncovalent complexes. Nearly all pure and global hybrid methods developed in the 1990s, with the notable exception of Becke's half-and-half functional,[81] overestimate the charge transfer in these systems and, as a result, dramatically overestimate the interaction energy and predict too short equilibrium separations.[82,83] This issue is corrected in range-separated functionals. Owing to the 100% exact exchange at long range, the partial charge transfer is controlled by more realistic frontier orbital energy differences. The long-range correction limits the spurious delocalization of electrons around the equilibrium and prevents the formation of unphysical partial charges at the dissociated constituents of a donor-acceptor dimer.[84] The improved electron density in charge-transfer dimers implies more realistic binding energies, provided that a necessary dispersion correction is supplied.[84]

5.3 Hydrogen-bonded systems

Hydrogen-bonded dimers belong to apparently a simple type of systems to be described by semilocal DFT models, but larger hydrogen-bonded clusters remain challenging. For example, the DFT methods tested by Chan et al.[16] on the CEPX33 set (the clusters of NH_3, H_2O, and HF) struggle to achieve good accuracy simultaneously or both binding energies and proton-exchange barriers. Our numerical tests demonstrate excellent performance of the LC-PBETPSS-D3 method (Figures 5.1 and 5.2, Table 5.1). It is the best tested method for binding energies and the second best method for proton-exchange barriers, after the empirical M06-L functional. The D3 dispersion correction added to LC-PBETPSS uniformly improves the results for both types of properties (Table 5.1). This is not the case for LC-ωPBE, which gives less accurate barrier heights upon addition of the dispersion correction.

LC-PBETPSS-D3 is accurate for the absolute binding energies of the water 16-mers studied by Yoo et al.[85] but does not capture the minuscule energy differences

Table 5.1: Mean Absolute Errors (kcal/mol) for the Binding Energies (BE) and Proton-Exchange Barriers (PX) of the CEPX33 Set[a]

method	BE	PX
LC-PBETPSS-D3	0.28	1.37
LC-PBETPSS	4.71	3.09
MCS-D3	0.77	12.65
M06-L	1.21	1.05
ωB97XD	0.41	1.80
M06-2X-D3	1.40	6.79
LC-ωPBE	2.74	3.44
LC-ωPBE-D3	0.55	5.16
B3LYP-D3	1.99	5.84

[a] DFT energies are computed with the aug-cc-pVQZ basis,[69] except for MCS-D3, which employs the def2-TZVPPD basis. The geometries and reference energies are taken from ref 86.

between different kinds of clusters (Figure 5.3). The structures of kind I (4444-a and 4444-b) include eight water molecules connected through hydrogen bonds to four nearest neighbors, whereas the structures of kind II (antiboat, boat-a, and boat-b) include four such water molecules.[85] LC-PBETPSS-D3 predicts that the clusters of kind I are slightly too stable relative to the clusters of kind II. A similar, yet more pronounced errors in the relative energies are present for the M06-type functionals: M06-L and M06-2X-D3. LC-ωPBE-D3 predicts better relative energy differences than LC-PBETPSS-D3, but it is not as accurate for the absolute energies.

The MCS-D3 functional performs well for the binding energies of hydrogen-bonded clusters but fails to accurately predict barrier heights; it captures the subtle energy differences between the water 16-mers but is by far the worst method for proton exchange barrier heights (Table 5.1 and Figure 5.3). A plausible reason for this poor performance is connected to the base exchange energy from which the range-separated exchange of MCS-D3 stems: the PBEsol functional. The PBEsol exchange energy is designed primarily for the properties of solid-state systems, e.g., lattice constants.[11] But a GGA cannot perform well for both the properties of solids and for atomization energies of molecules. Indeed, while PBEsol gives smaller errors for equilibrium lattice constants than PBE and TPSS,[11] it is one of the worst performing methods for thermochemistry and noncovalent interactions on the GMTKN30 set of Goerigk and Grimme.[15] Our own numerical results show that applying the PBEsol exchange energy in the MCS functional yields a robust method for noncovalent interaction energies, but mirrors the deficiencies of the base PBEsol energy for the properties of covalent systems.

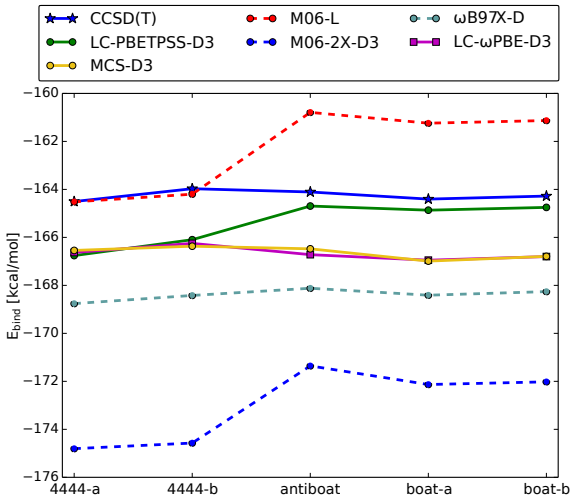

Figure 5.3: Binding energies of water 16-mers. The def2-TZVPPD basis[69,71] is employed for LC-PBETPSS-D3. The basis-set extrapolated CCSD(T) energies are taken from ref 28. The energies for the existing DFT methods are taken from ref 87.

5.4 Noncovalent charge-transfer dimers

The notorious self-interaction error of approximate DFT has a strong effect on the interaction energy curve of the NH_3...ClF dimer. The traditional global hybrid functional B3LYP (supplemented with a dispersion correction) and the pure M06-L functional are two outliers with the most excessive binding (Figure 5.4). The artificial binding is corrected only with a high fraction of the HF exchange, as in M06-2X-D3, or with the long-range HF exchange in range-separated functionals.

The curve belonging to LC-PBETPSS-D3 is close to the reference curve in the vicinity of the equilibrium geometry of the NH_3...ClF dimer. For the smallest separation, at $R = 0.8R_{eq}$, LC-PBETPSS-D3 is excessively repulsive; however, other tested methods are not repulsive enough or even predict binding, as in the case of LC-ωPBE-D3 and M06-L. The MCS-D3 functional overbinds to a much larger extent than the other range-separated functionals, but it is still more accurate than B3LYP-D3 and M06-L.

While the NH_3...ClF dimer represents strong donor-acceptor binding, similar advantages of range-separated functionals are clearly seen also for the weaker-bound dimers of the CT9 set (Figure 5.5, Table 5.2). The MAEs for the CT9 set are similar for all range-separated functionals and M06-2X-D3, but the range-separated hybrids tend to underbind, while M06-2X-D3 predicts excessive binding. Both LC-PBETPSS and LC-ωPBE benefit from the D3 dispersion correction.

5.5 Buckyball-catcher complex

If proven accurate, DFT methods could be a prime choice of methodology for modeling supramolecular systems; because of the typical system size, wave-function computations with large basis sets are currently formidable. However, the reliability of approximate DFT remains an issue.

Some authors suggest that dispersion-corrected range-separated functionals pre-

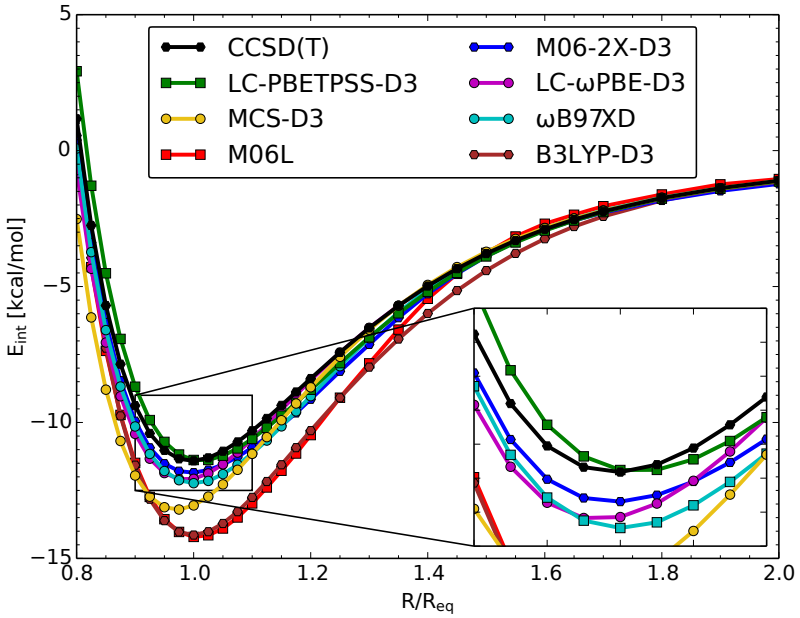

Figure 5.4: Interaction energy curves for the NH_3...ClF dimer.

dict excessive binding for supramolecular systems. Otero-de-la-Roza and Johnson[88] have concluded that *a functional that provides uniformly good across-the-board performance for all types of noncovalent interactions presently is not available.* Their tests of the LC-ωPBE functional, supplemented with the XDM dispersion correction,[89,90] have shown severe overbinding on the S12L set of Grimme,[48,91] with the energies over 40% too low for the dispersion-bound buckyball-catcher complexes 4a and 4b.[88]

In contrast, the pure PBE functional has been reported to yield nearly perfect energy for the complex 4a (reference E_{bind}=-27.5 kcal/mol) when combined with D3[91] (-26.6 kcal/mol), MBD[92] (-28.3 kcal/mol), and XDM[88] (-26.3 kcal/mol) dispersion energies. But a pure functional cannot be general – we already know that pure functionals overshot the binding energies for donor-acceptor complexes. Therefore, it may seem that no PBE-based functional is capable of describing the full gamut of noncovalent systems.

To establish if the excessive binding is also present for LC-PBETPSS-D3, we focus on the paradigmatic dispersion-bound buckyball (C_{60})-catcher complex (labeled 4a in ref 48). Comparing LC-PBETPSS with and without the dispersion part, we find that the attraction between the host and guest is predicted solely due to the dispersion term, which in this case is not merely a correction but a principal contribution (Table 5.3). While the final binding energy (E_{bind}=-30.1 kcal/mol) is within the expected error bounds, we arrive at this value by including the three-body correction to the atom-pairwise D3 energy ($E_{\text{disp}}^{\text{3-body}}$=+3.18 kcal/mol), which is less important for smaller systems. The counterpoise correction for the basis set is E_{BSSE}=+2.05 kcal/mol. The resulting binding energy for LC-PBETPSS-D3 is as accurate as the energies provided by M06-2X-D3 and DFT-SAPT.[93]

Contrary to the conclusions of ref 88, we find that the LC-ωPBE functional supplied with the D3 correction does not overbind as severely as when applied with the XDM dispersion energy (Table 5.3). After addition of the three-body dispersion term, which has not been accounted for in ref 88, the binding energy is in line with

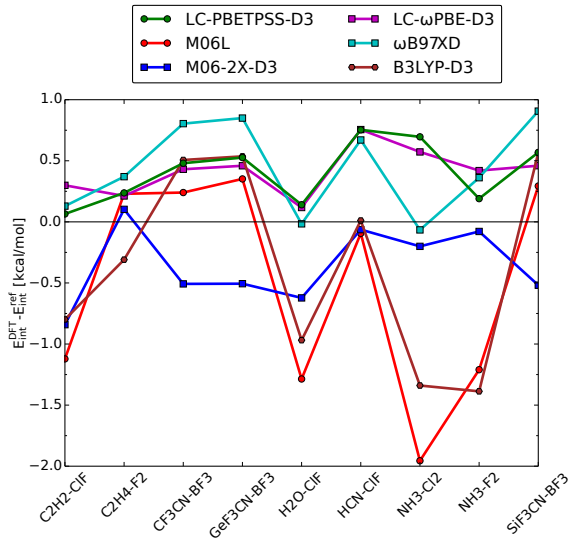

Figure 5.5: Errors for the interaction energies of the CT9 set of charge-transfer dimers.

the results of LC-PBETPSS-D3 and M06-2X-D3. Therefore, our computations do not confirm that the findings of Otero-de-la-Roza and Johnson[88] can be generalized to dispersion models other than XDM.

Surprisingly, we have found that the ωB97XD functional, which is designed for noncovalent systems, overestimates the binding energy of the buckyball–catcher complex by over 10 kcal/mol. This error may be caused by the dispersion model (DFT-D) employed in this approach, which is older and simpler than Grimme's DFT-D3.[17] Owing to their empirical optimization, all tested Minnesota-type functionals (M06-L, M06-2X, and M11) account for the dispersion contribution at equilibrium bond lengths. However, for the buckyball–catcher complex, we find that these functionals are prone to underestimation of the binding energy if the dispersion correction is not supplied.

5.6 Thermochemistry of hydrocarbons

Most approximate DFT functionals struggle to yield even a qualitative picture in certain, apparently simple, cases of hydrocarbon thermochemistry, e.g., for relative stability of linear vs. branched alkanes. In 2006, a series of computational studies was published, including the works of Schreiner et al.,[94] Woodrich et al.,[95] Zhao and Truhlar,[96] and Grimme[19], where the authors pointed out both severe and unexpected failures of traditional DFT approximations, most notably B3LYP. Approximate exchange-correlation models were reported to fail to account for the energetic effects which were otherwise simple enough to be predicted with great fidelity by the (SCS-)MP2 method. With some exceptions, the size of the errors made some of the authors question the applicability of the currently available DFT methods to polymer science and studies of alkane combustion.[19,96]

Our test set for hydrocarbon thermochemistry spans the model cases which were proven in the literature to be extremely difficult for the functionals developed in the 1990s, and for which modern methods yield rather mixed results: (i) The energy difference between *n*-octane and 2,2,3,3-tetramethylbutane represents the well-studied

Table 5.2: Mean Absolute Errors (kcal/mol) for the Interaction Energies of the CT9 Set of Charge-Transfer Dimers[a]

method	MAE
M06-2X-D3	0.37
LC-PBETPSS-D3	0.39
LC-PBETPSS	1.44
LC-ωPBE-D3	0.41
LC-ωPBE	1.14
ωB97XD	0.41
B3LYP-D3	0.73
M06-L	0.81

[a] DFT computations are performed with the def2-QZVPP basis. The reference energies at the CCSD(T) level are extrapolated to the basis-set limit (aug-cc-pVTZ $\rightarrow$ aug-cc-pVQZ) with the automated extrapolation scheme available in ORCA.[79] The same computational procedure is employed for the interaction energy curves of the NH_3...ClF dimer.

problem of predicting the relative energies of branched and linear alkanes[19] (Table 5.4). (ii) The energy differences between the $(CH)_{12}$ isomers are known examples that reveal the difficulties of approximate DFT for large hydrocarbons, possibly with bicyclic structures[94] (Figure 5.7, Table 5.5). (iii) The energy of isodesmic n-alkane fragmentation

$$CH_3(CH_2)_mCH_3 + mCH_4 \longrightarrow (m+1)C_2H_6 \tag{5.6.1}$$

is a model problem where most functionals fail to properly account for the noncovalent interactions between contiguous CH_2 units;[28,42,97–99] as a result, the errors in the reaction energies accumulate dramatically as the length of the n-alkane increases. (iv) The reaction energies of the IDISP test set of Goerigk and Grimme[15] probe the ability of an approximate functional to account for the intramolecular dispersion energy (Figure 5.9, Table 5.6). (v) The DARC subset of the GMTKN30 database[15] comprises fourteen Diels-Alder reaction energies in which the reactants containing multiple conjugated bonds react to form cyclic and bicyclic products (Figure 5.6, Table 5.6); good results for this subset are expected for the functionals which reduce the self-interaction error.[100]

Using the SCS-MP2 method with localized molecular orbitals, Grimme[19] has demonstrated that the main correlation contributions to the energy differences be-

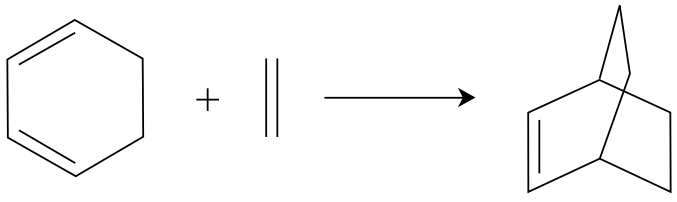

Figure 5.6: Example of a reaction included in the DARC set.

Table 5.3: Binding Energy (kcal/mol) of the Fullerene C_{60}–Catcher complex.[a]

method	E_{bind}
ref[b]	-28.4
LC-PBETPSS-D3[c]	-30.11
LC-PBETPSS	+12.09
LC-ωPBE-D3[c]	-30.71
LC-ωPBE	+7.53
DFT-SAPT[d]	-30.72
M06-L	-21.32
M06-2X-D3[c]	-30.82
M06-2X	-25.19
B3LYP-D3[c]	-25.75
ωB97XD	-38.29
MCSh-D3[c]	-32.89
M11	-23.74
LC-ωPBE-XDM[e]	-40.0

[a] Geometry of the complex is taken from ref 48. All DFT computations are counterpoise corrected and employ the def2-TZVPP basis set.
[b] Ref 47. [c] D3 dispersion energies are supplied with the 3-body term which is common for all functionals (+3.18 kcal/mol).
[d] Ref 93. The deformation energy is accounted for at the SCS-MP2 level. [e] LC-ωPBE supplied with the XDM dispersion correction, ref 88.

tween branched and linear alkanes come from orbital pairs with the charge centers separated on the length scale of atomic 1,3-interactions.[19] Upon addition of a branching point to a linear alkane, two atomic H-C-C interactions are replaced by H-C-H and C-C-C.[101] Therefore, the difference between the energy of the H-C-C interaction and the other two determines the relative stability of the linear vs branched forms of alkanes.[19] Inability to predict these differences has general consequences for the whole class of molecules.

While Grimme hypothesized that this middle-range correlation effect might be too difficult for semilocal correlation functionals,[19] Zhao and Truhlar have shown that the empirical M05-2X functional is able to predict the energy differences between hydrocarbon isomers with quantitative accuracy.[96] Our numerical results given in Table 5.4 demonstrate that both LC-PBETPSS-D3 and a more recent functional from Truhlar's group, M06-2X-D3, predict the energy differences between the octane isomers within the error bounds of the reference energy. The performance of B3LYP-D3 is representative for the functionals developed in the 1990s, which yield qualitatively wrong energetic effects of adding a branching point to an alkane. Surprisingly, the ωB97XD functional, which generally performs well for thermochemistry, also fails to predict the correct sign.

The middle-range correlation, which, as Grimme argues, underlies alkane thermochemistry,[19,97,98] does not explain the performance of the approximate DFT methods for which the error varies from one case to another. For example, LC-ωPBE-D3

Table 5.4: Energy Differences (kcal/mol) Between *n*-Octane (3b) and 2,2,3,3-Tetramethylbutane (3a).[a]

method	$E(3b) - E(3a)$
reference[b]	1.9 ± 0.5
LC-PBETPSS-D3[c]	1.57
M06-L[d]	0.37
M06-2X-D3[d]	1.63
LC-ωPBE-D3[d]	0.54
B3LYP-D3[d]	-2.79
ωB97XD[d]	-0.73

[a] Geometries are obtained from the companion website of ref 15. [b] Ref 19. [c] Computed with the def2-QZVP basis. [d] Ref 15.

is among the best methods for the isodesmic fragmentation of *n*-alkanes (Figure 5.8). and is also qualitatively correct for the octane isomers (Table 5.4). However, it dramatically fails for the $(CH)_{12}$ isomers (Figure 5.7, Table 5.5). Its most catastrophic prediction is for the energy difference $E(4b) - E(4a)$, where the overestimation is as large as 20 kcal/mol (150% of the reference energy). The error of the MCS-D3 functional is similarly large. Thus, the inferior description of bicyclic structures containing small rings, discussed by Schreiner et al.,[94] is not resolved by range separation of the exchange energy. In fact, LC-ωPBE-D3 performs much worse than the global hybrid PBE0. The ωB97XD functional yields nearly perfect results for the (CH)12 isomers but predicts wrong energetic order of linear and branched octane (Table 5.4). Of the range-separated functionals, the only method which performs consistently well for all tested cases is LC-PBETSS-D3.

The performance of range-separated functionals for hydrocarbon thermochemistry is uneven, but the reaction of *n*-alkane fragmentation is an exception (Figure 5.8). Here, all tested dispersion-corrected range-separated functionals, including LC-PBETPSS-D3 and MCS-D3, are bunched together among the top performers. This is explained by Johnson et al.,[42] who argue that the errors of approximate DFT for *n*-alkane fragmentation have their roots in a bad description of the regions of density between interacting CH_2 groups. The energetic contributions originating from the noncovalent interaction regions[42] between contiguous methylene or methyl groups are critically dependent on the reduced-gradient dependence of the exchange functional. Therefore, for example, the PBEsol exchange energy[39] – which obeys

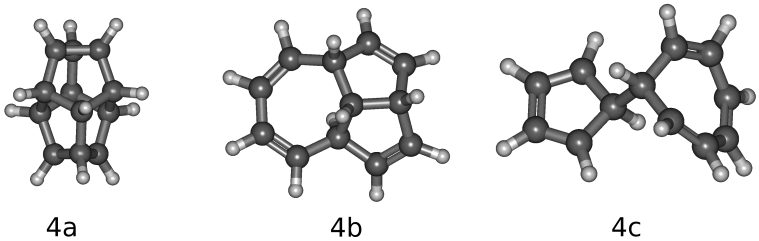

Figure 5.7: Isomers of $(CH)_{12}$. The naming convention is the same as in ref 39.

Table 5.5: Energy Differences (kcal/mol) Between $(CH)_{12}$ Isomers.[a]

method	$E(4c) - E(4b)$	$E(4b) - E(4a)$
DLPNO-CCSD(T)[b]	8.90	14.15
LC-PBETPSS-D3	9.23	18.46
LC-PBETPSS	8.19	18.55
MCS-D3	15.22	47.20
M06-L	3.10	16.12
M06-2X-D3	6.73	15.32
LC-ωPBE-D3	14.85	36.63
LC-ωPBE	14.34	37.40
B3LYP-D3	2.55	-2.72
ωB97XD	7.98	15.55
PBE0	8.55	22.80
TPSS	2.85	11.17

[a] The structures are depicted in Figure 5.7. The geometries are taken from Zhao and Truhlar.[96] All DFT computations except for MCS-D3 employ the def2-QZVPP basis set. The MCS-D3 energies are computed with the def2-TZVPP basis set.
[b] The DLPNO-CCSD(T) method is employed with the "tight" set of parameters defined in Table 1 of ref 78. The energies are extrapolated (cc-pVTZ→cc-pVQZ) to the basis set limit using the default algorithm available in ORCA 3.0.3.

the exact second-order expansion for small density gradients – works better than the functionals which employ stronger reduced-gradient dependence, e.g., PBE.[39,42] Owing to the long-range HF exchange, range-separated functionals are less dependent on the reduced-gradient term in the base functional and, as a result, perform better for the isodesmic reaction provided that the long-range dispersion energy is properly supplied (Figure 5.8).[28,99]

The DARC subset of the GMTKN30 database[15] comprises fourteen Diels-Alder reaction energies in which the reactants containing multiple conjugated bonds react to form cyclic and bicyclic products (see Figure 1 in ref 100). Most of the existing DFT approximations underestimate the reaction energies in this set.[100] The reasons for that have general implications for the application of approximate DFT for main group thermochemistry. Johnson et al.[100] have argued that the reactants of the Diels-Alder reaction have delocalized electron density, therefore these structures are artificially stabilized due to the self-interaction (delocalization) error. On the products side, the bicyclic molecules have bridgehead carbons whose noncovalent repulsion tends to be overestimated by approximate DFT.[100] Because of these two systematic effects, the energetic gain of going from the reactants to the products is underestimated.

LC-PBETPSS-D3 achieves the lowest mean absolute error of all functionals tested on the DARC set (Table 5.6). The addition of the dispersion correction to LC-PBETPSS reduces the MAE by a factor of four. In contrast, supplying the D3 term to LC-ωPBE increases the MAE from 6.3 kcal/mol to 10 kcal/mol. The effect of the three-body dispersion term included in LC-PBETPSS-D3+3body is

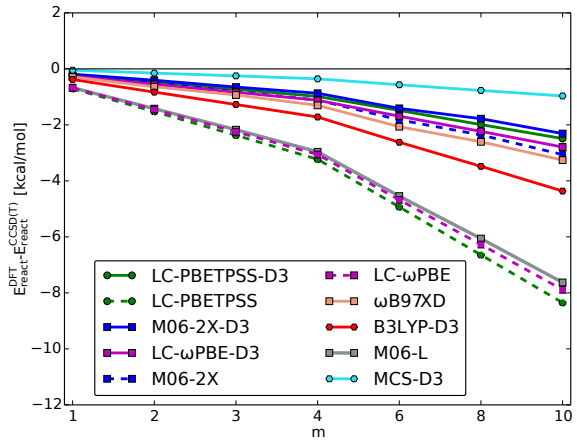

Figure 5.8: Errors in isodesmic reaction energies of n-alkane fragmentation. The geometries and reference energies at the CCSD(T) level are taken from ref 97. The def2-QZVP basis is employed for DFT computations.

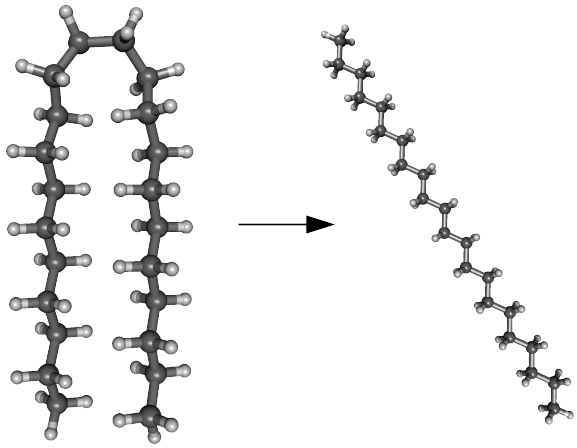

Figure 5.9: Example of a reaction included in the test set for intramolecular dispersion interactions (IDISP).[15]

negligible due to the small size of the systems.

The IDISP subset of the GMTKN30 database is composed of six reaction energies in which alkanes undergo transformations between structures with different amounts of the intramolecular dispersion energy.[15] A typical reaction included in IDISP is presented in Figure 5.9. LC-PBETPSS-D3, M06-2X-D3, and ωB97XD are the best methods tested on this set (Table 5.6). The D3 correction is important and beneficial for both LC-PBETPSS and LC-ωPBE. The addition of the three-body D3 term has a perceivable beneficial effect on the reaction energies predicted by LC-PBETPSS-D3+3body.

To sum up our results, LC-PBETPSS-D3 is the only range-separated functional in our tests which rivals M06-2X-D3 for hydrocarbon thermochemistry. It is as good as the other range-separated functionals for isodesmic fragmentation of n-alkanes but avoids the inconsistent performance for alkane branching and isomerization of larger hydrocarbons, e.g., $(CH)_{12}$. Remarkably, LC-PBETPSS-D3 accurately describes the energy differences between the $(CH)_{12}$ isomers, whereas LC-ωPBE-D3–which is based on the same base exchange functional–yields catastrophic results in the cases involving the bicyclic structure 4a.

Table 5.6: Mean Absolute Errors (kcal/mol) for the Reaction Energies of the IDISP and DARC Sets[a]

method	IDISP	DARC
LC-PBETPSS-D3	2.35[b]	1.38[c]
LC-PBETPSS-D3+3body	2.27[b]	1.37[c]
LC-PBETPSS	11.38[b]	6.07[c]
M06-L[d]	6.55	8.04
M06-2X-D3[d]	1.71	2.28
LC-ωPBE-D3[d]	4.13	10.04
LC-ωPBE[d]	8.03	6.30
B3LYP-D3[d]	6.63	10.23
ωB97XD[d]	2.63	1.98

[a] Reference energies and geometries are obtained from the companion website of ref 15.
[b] Computed with the def2-QZVP basis.
[c] Computed with the def2-QZVPP basis. [d] Ref 15.

5.7 Excitation energies

To further establish versatility of the LC-PBETPSS functional, we apply it to compute valence and Rydberg excitation energies of small molecules (CO, N_2, H_2CO, C_2H_4, and C_4H_6) and the lowest charge-transfer excitation energies of aromatic donor-tetracyanoetylene noncovalent complexes (Ar-TCNE). Traditional pure and global hybrid functionals do not treat these transitions with the same accuracy. While valence excitations are usually described at a fairly good level, frequently with MAEs $\leq$ 0.3 eV, Rydberg and charge-transfer states are predicted to lie too low.[102]

This systematic error is corrected in range-separated functionals.[55,57] Indeed, LC-PBETPSS achieves about the same level of accuracy for all types of excitations (Tables 5.7 and 5.8). Clearly, the best performer for the charge-transfer transitions is ωB97X,[75] but only a small number of systems of this type is tested due to the technical difficulties associated with carrying out real-time TDDFT propagation. There are only insignificant differences among the three best functionals for valence and Rydberg excitations: ωB97X, LC-PBETPSS, and LC-ωPBE.

5.8 Symmetry-adapted perturbation theory

The LC-PBETPSS functional, like any other range-separated hybrid, can be employed to compute the interaction energy contributions defined in symmetry-adapted perturbation theory[111] (SAPT), but its range-separated parameter must be adjusted to satisfy[112]

$$\epsilon_{\mathrm{HOMO}}(\omega) = -\mathrm{IP}(\omega). \tag{5.8.1}$$

Satisfying Eq. 5.8.1 enforces Koopmans' theorem and, therefore, provides a realistic description of the density tail. For global hybrids and pure functionals, one achieves the same goal by using asymptotic corrections of the exchange-correlation potential.[113]

Table 5.7: Energies (eV) of Valence and Rydberg Transitions in CO, N_2, Formaldehyde, Ethylene, and trans-1,3-Butadiene

transition	ref	B3LYP	M06-L	M06-2X	ωB97X[g]	LC-ωPBE	LC-PBETPSS
CO[a]							
$\sigma \rightarrow \pi^*$	8.51[d]	8.40	8.58	8.22	8.53	8.55	8.66
$\sigma \rightarrow 3s$	10.78[d]	9.83	9.35	10.86	10.77	10.84	10.76
$\sigma \rightarrow 3p\sigma$	11.40[d]	10.21	9.61	10.86	11.22	11.34	11.15
$\sigma \rightarrow 3p\pi$	11.53[d]	10.27	9.87	10.90	11.31	11.42	11.28
N_2[a]							
$\sigma_g \rightarrow 3p\pi_u$	12.90[d]	11.78	10.85	12.47	12.57	12.68	12.50
$\sigma_g \rightarrow 3p\sigma_u$	12.98[d]	11.62	10.53	12.53	12.59	12.70	12.52
$\pi_u \rightarrow 3s\sigma_g$	13.24[f]	12.04	11.76	12.49	12.88	13.01	12.86
H_2CO[a]							
$n \rightarrow 3sa_1$	7.09[d]	6.43	6.14	7.09	7.28	7.26	7.11
$n \rightarrow 3pb_2$	7.97[d]	7.15	6.49	7.90	8.12	8.11	7.98
$n \rightarrow 3pa_1$	8.12[d]	7.16	6.57	7.78	8.00	8.00	7.84
$\sigma \rightarrow \pi^*$	8.68[d]	9.01	7.01	8.81	8.99	9.11	8.92
C_2H_4[b]							
$\pi \rightarrow 3s$	7.11[e]	6.56	6.60	6.85	7.38	7.52	7.44
$\pi \rightarrow \pi^*$	7.96[c]	7.32	7.18	7.47	7.57	7.63	7.69
$\pi \rightarrow 3d\delta$	8.90[e]	7.61	7.22	8.42	8.98	9.23	9.13
$\pi \rightarrow 3d\delta$	9.08[e]	7.77	7.47	8.52	9.08	9.33	9.21
$\pi \rightarrow 3d\pi$	9.33[e]	7.69	7.52	8.58	9.09	9.38	9.28
$\pi \rightarrow 3d\pi$	9.51[e]	8.09	7.92	8.82	9.46	9.79	9.68
C_4H_6[b]							
$\pi \rightarrow \pi^*$	6.32[c]	5.54	5.62	5.76	5.88	5.97	5.98
Ryd ($2A_u$)	6.66[e]	5.88	5.87	6.15	6.84	6.94	6.86
Ryd ($2B_u$)	7.07[e]	6.36	6.09	6.75	7.29	7.40	7.29
Ryd ($3B_u$)	8.00[e]	6.74	6.39	7.46	8.04	8.30	8.18
MAE		0.97	1.36	0.42	0.20	0.23	0.22

[a] Energies are computed with the augmented Sadlej basis.[103] [b] Energies are computed with the 6-311(3+,3+)G** basis.[104] [c] Theoretical energy at the FCIQMC level, ref 105.
[d] Experimental energy, ref 55. [e] Experimental energy, ref 106. [f] Experimental energy, ref 107.
[g] Ref 75.

Table 5.8: Energies (eV) of the Lowest CT Transitions in Gas-Phase Ar-TCNE Complexes[a]

Ar	benzene	toluene	o-xylene
ref[108]	3.59	3.36	3.15
ωB97X[75]	3.67	3.34	3.37
LC-ωPBE	4.00	3.65	3.68
LC-PBETPSS	3.87	3.50	3.49
B3LYP	2.06	1.81	1.88
M06-L	1.65	1.46	1.56
M06-2X	3.03	2.93	2.78

[a] DFT calculations employ the cc-pVDZ basis set.[69] The excitation energies for this functional are obtained using real-time time-dependent DFT (RT-TDDFT) instead of the usual linear response equations.[109,110] Technical details are provided in ref 26.

We test the performance of LC-PBETPSS against the range-separated PBE functional of Henderson et al.[40] (HJS-ωPBE) and the global hybrid functional PBE0[114] supplemented with the asymptotic correction of Gruning et al.[113] (denoted as PBE0AC) on the A24 set of small noncovalent dimers.[115] The improvement of LC-PBETPSS upon enforcing Eq. 5.8.1 is clear, with over threefold reduction of the MAE for the total interaction energies (Table 5.9). A similar effect is seen for HJS-ωPBE. The LC-PBETPSS variant with the adjusted ω achieves slightly better accuracy than PBE0AC. Detailed numerical data are provided in the Supporting Information for ref 26.

Table 5.9: Mean Absolute Errors (kcal/mol) for the Total SAPT Interaction Energies of the A24 Set[a]

method	MAE
HJS-ωPBE(ω=0.40)	0.19
HJS-ωPBE(ω=$*$)[b]	0.07
LC-PBETPSS(ω=0.35)	0.30
LC-PBETPSS(ω=$*$)[b]	0.09
PBE0AC	0.12

[a] SAPT calculations employ the aug-cc-pVTZ basis set. The total interaction energy is a sum of the first- and second-order SAPT contributions plus a so-called delta-HF term. Each DFT method is used to compute the orbitals and orbital energies, but the exchange-correlation kernel is in every case at the LDA level.
[b] Range-separation parameters are adjusted to satisfy Eq. 5.8.1.

Chapter 6

Summary and Conclusions

We have presented two approximate exchange-correlation density functionals developed by Modrzejewski et al. in a series of works since 2012,[26–28] both belonging to the rung of dispersion-corrected range-separated hybrid meta-GGAs. Numerical evidence demonstrates clear progress of the methodology: the newest functional, LC-PBETPSS-D3,[26] is generally as good as the earlier one, MCS-D3,[28] for noncovalent systems, but it is qualitatively better for thermochemistry.

The MCS-D3 functional employs a range-separated hybrid variant of the PBEsol exchange,[11] the D3 dispersion correction,[22] and the meta-GGA correlation of ref 28 with one empirical parameter adjusted to match the other components of the functional. While the base PBEsol exchange is designed primarily for solids, we have shown that, when included in a range-separated exchange, it works well for noncovalent interactions of molecular systems, e.g., for water 16-mers, where MCS-D3 correctly predicts the tiny energy differences between the isomers. Still, we have found some problematic cases: MCS-D3 overestimates the interaction energy of the model charge-transfer NH_3−ClF dimer and binds too strongly the dispersion-dominated buckyball-catcher complex. MCS-D3 accurately describes the reaction energies of n-alkane fragmentation owing to the exact second-order gradient expansion of the PBEsol exchange energy. Nonetheless, its good performance is not transferable to other problems of hydrocarbon thermochemistry which are difficult for approximate DFT. In particular, the energy differences of the $(CH)_{12}$ isomers come out unexpectedly poor, similarly as for LC-ωPBE-D3.

In contrast to MCS-D3, the LC-PBETPSS-D3 functional embodies a more elaborate exchange component based on the meta-GGA short-range functional of Modrzejewski et al.,[26] with the dependence on both the kinetic energy density and the density Laplacian. The unaltered TPSS energy accounts for the correlation part.[9,68] The included D3 dispersion correction is limited to the $1/R^6$ contribution. The only purely empirical parameter is in the damping function of the dispersion energy. The range-separation parameter is estimated both theoretically, by minimization of the self-interaction error for the hydrogen atom, and empirically to be $\omega = 0.35$. Compared to other currently available range-separated hybrid meta-GGAs, LC-PBETPSS-D3 reduces the amount of empirical parameters by an order of magnitude.

LC-PBETPSS-D3 approaches, and in some important cases surpasses, the accuracy of top-of-the-line empirical DFT methods (Figure 6.1). The accuracy of LC-PBETPSS-D3 is remarkably consistent across the whole range of tests employed in

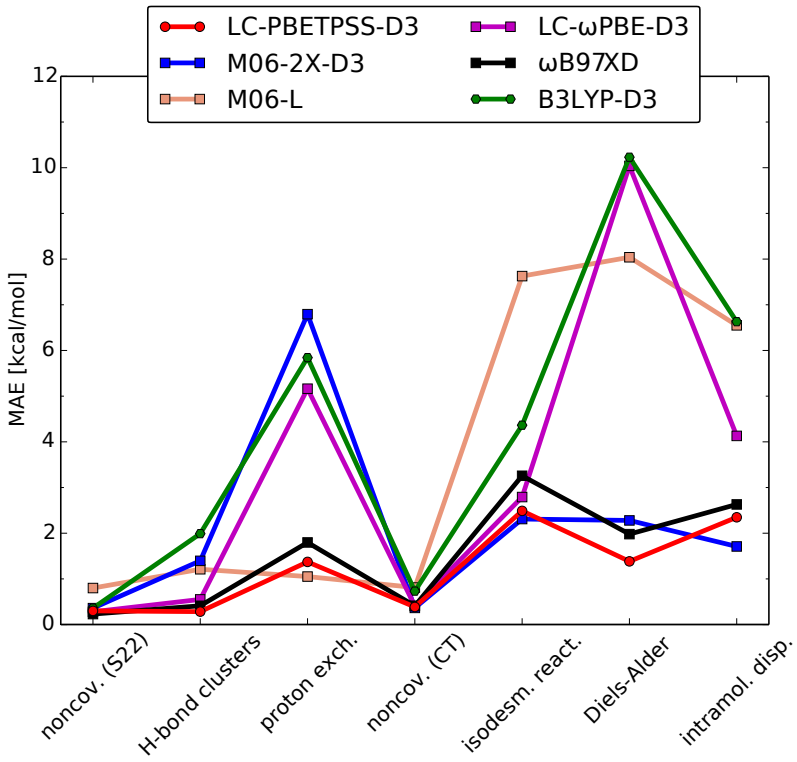

Figure 6.1: General view of the performance of DFT methods on the benchmark sets considered in this work.

this work, including noncovalent interaction energies, thermochemistry, and excitation energies.

While LC-PBETPSS-D3 is better than M06-2X-D3 for noncovalent systems, especially for clusters of hydrogen-bonded molecules, it is as good as this well-established empirical functional for hydrocarbon thermochemistry. The ωB97XD GGA hybrid affords a similar degree of consistent accuracy as LC-PBETPSS-D3 for small noncovalent dimers and for the major part of the tested thermochemistry, but it is much less accurate for the binding energy of the buckyball catcher complex and predicts a wrong sign for the energy difference of linear vs. branched octane. Compared to LC-ωPBE-D3, another range-separated hybrid derived from the nonempirical PBE energy, LC-PBETPSS-D3 performs similarly for noncovalent systems but better for hydrocarbon thermochemistry. In some cases, e.g., for the $(CH)_{12}$ isomers and Diels-Alder reactions, the functional of Vydrov and Scuseria yields extraordinarily poor energies, whereas the approach presented in this work stays robust.

When applied to excited states of small model systems, LC-PBETPSS describes charge-transfer and Rydberg excitations at a similar level of accuracy as valence excitations.

To summarize, we have derived and tested two minimally-empirical range-separated hybrid meta-GGAs: MCS-D3 and LC-PBETPSS-D3. The latter method supersedes the former and is recommended for noncovalent interaction energies, hydrocarbon thermochemistry, and excitation energies. Our LC-PBETPSS-D3 functional is a part of the most recent wave of meta-GGA functionals with reduced empiricism and extended transferability,[10,24] yet it fills a unique place in it–it is the only range-

separated hybrid built from a nonempirical meta-GGA exchange-correlation energy. The available data in the test set demonstrate that LC-PBETPSS-D3 is competitive against or even better than the best empirical functionals, but still more work has to be done to establish its predictive power for general thermochemistry and systems including transition metals.

Bibliography

[1] P. Hohenberg and W. Kohn, "Inhomogeneous Electron Gas," Phys. Rev. **136**, B864 (1964).

[2] W. Kohn and L. J. Sham, "Self-Consistent Equations Including Exchange and Correlation Effects," Phys. Rev. **140**, A1133 (1965).

[3] J. P. Perdew, A. Ruzsinszky, L. A. Constantin, J. Sun, and G. I. Csonka, "Some Fundamental Issues in Ground-State Density Functional Theory: A Guide for the Perplexed," J. Chem. Theory Comput. **5**, 902 (2009).

[4] J. P. Perdew and Y. Wang, "Accurate and simple analytic representation of the electron-gas correlation energy," Phys. Rev. B **45**, 13244 (1992).

[5] J. Perdew, K. Burke, and M. Ernzerhof, "Generalized Gradient Approximation Made Simple," Phys. Rev. Lett. **77**, 3865 (1996).

[6] K. Burke, J. P. Perdew, and Y. Wang, "Derivation of a generalized gradient approximation: The PW91 density functional," in *Electronic Density Functional Theory* (Springer, 1998) pp. 81–111.

[7] J. P. Perdew, "Accurate Density Functional for the Energy: Real-Space Cutoff of the Gradient Expansion for the Exchange Hole," Phys. Rev. Lett. **55**, 1665 (1985).

[8] B. G. Janesko, "Density Functional Theory Beyond the Generalized Gradient Approximation for Surface Chemistry," in *Density Functionals: Thermochemistry*, edited by R. E. Johnson (Springer International Publishing, 2015) pp. 25–51.

[9] J. Tao, J. P. Perdew, V. N. Staroverov, and G. E. Scuseria, "Climbing the Density Functional Ladder: Nonempirical meta-Generalized Gradient Approximation Designed for Molecules and Solids," Phys. Rev. Lett. **91**, 146401 (2003).

[10] J. Sun, A. Ruzsinszky, and J. P. Perdew, "Strongly Constrained and Appropriately Normed Semilocal Density Functional," Phys. Rev. Lett. **115**, 036402 (2015).

[11] J. P. Perdew, A. Ruzsinszky, G. I. Csonka, O. A. Vydrov, G. E. Scuseria, L. A. Constantin, X. Zhou, and K. Burke, "Restoring the Density-Gradient Expansion for Exchange in Solids and Surfaces," Phys. Rev. Lett. **100**, 136406 (2008).

[12] Y. Zhao and D. G. Truhlar, "A new local density functional for main-group thermochemistry, transition metal bonding, thermochemical kinetics, and noncovalent interactions," J. Chem. Phys. **125**, 194101 (2006).

[13] R. Peverati and D. G. Truhlar, "Quest for a universal density functional: the accuracy of density functionals across a broad spectrum of databases in chemistry and physics," Phil. Trans. R. Soc. A **372**, 20120476 (2014).

[14] Y. Zhao and D. Truhlar, "The M06 suite of density functionals for main group thermochemistry, thermochemical kinetics, noncovalent interactions, excited states, and transition elements: two new functionals and systematic testing of four M06-class functionals and 12 other functionals," Theor. Chem. Acc. **120**, 215 (2008).

[15] L. Goerigk and S. Grimme, "A thorough benchmark of density functional methods for general main group thermochemistry, kinetics, and noncovalent interactions," Phys. Chem. Chem. Phys. **13**, 6670 (2011).

[16] B. Chan, A. T. Gilbert, P. M. Gill, and L. Radom, "Performance of Density Functional Theory Procedures for the Calculation of Proton-Exchange Barriers: Unusual Behavior of M06-Type Functionals," J. Chem. Theory Comput. **10**, 3777 (2014).

[17] J.-D. Chai and M. Head-Gordon, "Long-range corrected hybrid density functionals with damped atom–atom dispersion corrections," Phys. Chem. Chem. Phys. **10**, 6615 (2008).

[18] N. Mardirossian and M. Head-Gordon, "Mapping the genome of meta-generalized gradient approximation density functionals: The search for B97M-V," J. Chem. Phys. **142**, 074111 (2015).

[19] S. Grimme, "Seemingly Simple Stereoelectronic Effects in Alkane Isomers and the Implications for Kohn–Sham Density Functional Theory," Angew. Chem. Int. Ed. **45**, 4460 (2006).

[20] P. J. Stephens, F. J. Devlin, C. F. Chabalowski, and M. J. Frisch, "Ab initio calculation of vibrational absorption and circular dichroism spectra using density functional force fields," J. Phys. Chem. **98**, 11623 (1994).

[21] L. Goerigk and S. Grimme, "Efficient and Accurate Double-Hybrid-Meta-GGA Density Functionals–Evaluation with the Extended GMTKN30 Database for General Main Group Thermochemistry, Kinetics, and Noncovalent Interactions," J. Chem. Theory Comput. **7**, 291 (2010).

[22] S. Grimme, J. Antony, S. Ehrlich, and H. Krieg, "A consistent and accurate ab initio parametrization of density functional dispersion correction (DFT-D) for the 94 elements H-Pu," J. Chem. Phys. **132**, 154104 (2010).

[23] R. Peverati and D. G. Truhlar, "Improving the Accuracy of Hybrid meta-GGA Density Functionals by Range Separation," J. Phys. Chem. Lett. **2**, 2810 (2011).

[24] N. Mardirossian and M. Head-Gordon, "ωB97M-V: A combinatorially optimized, range-separated hybrid, meta-GGA density functional with VV10 nonlocal correlation," J. Chem. Phys. **144**, 214110 (2016).

[25] J. Sun, R. C. Remsing, Y. Zhang, Z. Sun, A. Ruzsinszky, H. Peng, Z. Yang, A. Paul, U. Waghmare, X. Wu, M. L. Klein, and J. P. Perdew, "Accurate first-principles structures and energies of diversely bonded systems from an efficient density functional," Nat. Chem. **8**, 831 (2016).

[26] M. Modrzejewski, M. Hapka, G. Chalasinski, and M. M. Szczesniak, "Employing Range Separation on the meta-GGA Rung: New Functional Suitable for Both Covalent and Noncovalent Interactions," J. Chem. Theory Comput. **12**, 3662 (2016).

[27] M. Modrzejewski, M. Lesiuk, L. Rajchel, M. M. Szczesniak, and G. Chalasinski, "A first-principles-based correlation functional for harmonious connection of short-range correlation and long-range dispersion," J. Chem. Phys. **137**, 204121 (2012).

[28] M. Modrzejewski, G. Chalasinski, and M. M. Szczesniak, "Range-Separated meta-GGA Functional Designed for Noncovalent Interactions," J. Chem. Theory Comput. **10**, 4297 (2014).

[29] M. Levy, "Universal variational functionals of electron densities, first-order density matrices, and natural spin-orbitals and solution of the v-representability problem," Proc. Natl. Acad. Sci. U. S. A. **76**, 6062 (1979).

[30] M. Levy and J. Perdew, "Hellmann-Feynman, virial, and scaling requisites for the exact universal density functionals. Shape of the correlation potential and diamagnetic susceptibility for atoms," Phys. Rev. A **32**, 2010 (1985).

[31] M. Levy, "Elementary concepts in density functional theory," in *Theoretical and Computational Chemistry*, Vol. 4, edited by J. Seminario (Elsevier, 1996).

[32] A. Becke, "Correlation energy of an inhomogeneous electron gas: A coordinate-space model," J. Chem. Phys. **88**, 1053 (1988).

[33] A. Becke and M. Roussel, "Exchange holes in inhomogeneous systems: A coordinate-space model," Phys. Rev. A **39**, 3761 (1989).

[34] M. Ernzerhof and J. P. Perdew, "Generalized gradient approximation to the angle- and system-averaged exchange hole," J. Chem. Phys. **109**, 3313 (1998).

[35] J. Krieger, Y. Li, and G. Iafrate, "Systematic approximations to the optimized effective potential: Application to orbital-density-functional theory," Phys. Rev. A **46**, 5453 (1992).

[36] A. Seidl, A. Goerling, P. Vogl, J. A. Majewski, and M. Levy, "Generalized Kohn-Sham schemes and the band-gap problem," Phys. Rev. B **53**, 3764 (1996).

[37] R. Baer, E. Livshits, and U. Salzner, "Tuned Range-Separated Hybrids in Density Functional Theory," Annu. Rev. Phys. Chem. **61**, 85 (2010).

[38] W. Yang, A. J. Cohen, and P. Mori-Sánchez, "Derivative discontinuity, bandgap and lowest unoccupied molecular orbital in density functional theory," J. Chem. Phys. **136**, 204111 (2012).

[39] G. I. Csonka, A. Ruzsinszky, J. P. Perdew, and S. Grimme, "Improved Description of Stereoelectronic Effects in Hydrocarbons Using Semilocal Density Functional Theory," J. Chem. Theory Comput. **4**, 888 (2008).

[40] T. M. Henderson, B. G. Janesko, and G. E. Scuseria, "Generalized gradient approximation model exchange holes for range-separated hybrids," J. Chem. Phys. **128**, 194105 (2008).

[41] A. Ambrosetti, A. M. Reilly, R. A. DiStasio Jr, and A. Tkatchenko, "Long-range correlation energy calculated from coupled atomic response functions," J. Chem. Phys. **140**, 18A508 (2014).

[42] E. R. Johnson, J. Contreras-García, and W. Yang, "Density-Functional Errors in Alkanes: A Real-Space Perspective," J. Chem. Theory Comput. **8**, 2676 (2012).

[43] E. Weintraub, T. M. Henderson, and G. E. Scuseria, "Long-Range-Corrected Hybrids Based on a New Model Exchange Hole," J. Chem. Theory Comput. **5**, 754 (2009).

[44] F. O. Kannemann and A. D. Becke, "Van der Waals Interactions in Density-Functional Theory: Rare-Gas Diatomics," J. Chem. Theory Comput. **5**, 719 (2009).

[45] E. D. Murray, K. Lee, and D. C. Langreth, "Investigation of Exchange Energy Density Functional Accuracy for Interacting Molecules," J. Chem. Theory Comput. **5**, 2754 (2009).

[46] M. Kamiya, T. Tsuneda, and K. Hirao, "A density functional study of van der Waals interactions," J. Chem. Phys. **117**, 6010 (2002).

[47] S. Grimme, A. Hansen, J. G. Brandenburg, and C. Bannwarth, "Dispersion-Corrected Mean-Field Electronic Structure Methods," Chem. Rev. **116**, 5105 (2016).

[48] S. Grimme, "Supramolecular Binding Thermodynamics by Dispersion-Corrected Density Functional Theory," Chem. Eur. J. **18**, 9955 (2012).

[49] P. Gori-Giorgi and J. Perdew, "Short-range correlation in the uniform electron gas: Extended Overhauser model," Phys. Rev. B **64**, 155102 (2001).

[50] P. Jurecka, J. Sponer, J. Cerny, and P. Hobza, "Benchmark database of accurate (MP2 and CCSD(T) complete basis set limit) interaction energies of small model complexes, DNA base pairs, and amino acid pairs," Phys. Chem. Chem. Phys. **8**, 1985 (2006).

[51] R. Podeszwa, K. Patkowski, and K. Szalewicz, "Improved interaction energy benchmarks for dimers of biological relevance," Phys. Chem. Chem. Phys. **12**, 5974 (2010).

[52] K. Burke, J. Perdew, and M. Ernzerhof, "Why semilocal functionals work: Accuracy of the on-top pair density and importance of system averaging," J. Chem. Phys. **109**, 3760 (1998).

[53] G. Oliver and J. Perdew, "Spin-density gradient expansion for the kinetic energy," Phys. Rev. A **20**, 397 (1979).

[54] H. Iikura, T. Tsuneda, T. Yanai, and K. Hirao, "A long-range correction scheme for generalized-gradient-approximation exchange functionals," J. Chem. Phys. **115**, 3540 (2001).

[55] Y. Tawada, T. Tsuneda, S. Yanagisawa, T. Yanai, and K. Hirao, "A long-range-corrected time-dependent density functional theory," J. Chem. Phys. **120**, 8425 (2004).

[56] J.-W. Song, T. Hirosawa, T. Tsuneda, and K. Hirao, "Long-range corrected density functional calculations of chemical reactions: Redetermination of parameter," J. Chem. Phys. **126**, 154105 (2007).

[57] T. Yanai, D. P. Tew, and N. C. Handy, "A new hybrid exchange-correlation functional using the Coulomb-attenuating method (CAM-B3LYP)," Chem. Phys. Lett. **393**, 51 (2004).

[58] A. Becke, "Current-density dependent exchange-correlation functionals," Can. J. Chem. **74**, 995 (1996).

[59] C. Lee and R. Parr, "Gaussian and other approximations to the first-order density matrix of electronic systems, and the derivation of various local-density-functional theories," Phys. Rev. A **35**, 2377 (1987).

[60] O. A. Vydrov and G. E. Scuseria, "Assessment of a long-range corrected hybrid functional," J. Chem. Phys. **125**, 234109 (2006).

[61] O. A. Vydrov, J. Heyd, A. V. Krukau, and G. E. Scuseria, "Importance of short-range versus long-range Hartree-Fock exchange for the performance of hybrid density functionals," J. Chem. Phys. **125**, 074106 (2006).

[62] A. D. Becke, "A real-space model of nondynamical correlation," J. Chem. Phys. **119**, 2972 (2003).

[63] J. P. Precechtelova, H. Bahmann, M. Kaupp, and M. Ernzerhof, "Design of exchange-correlation functionals through the correlation factor approach," J. Chem. Phys. **143**, 144102 (2015).

[64] J. P. Perdew and A. Zunger, "Self-interaction correction to density-functional approximations for many-electron systems," Phys. Rev. B **23**, 5048 (1981).

[65] J. Sun, J. P. Perdew, and A. Ruzsinszky, "Semilocal density functional obeying a strongly tightened bound for exchange," Proc. Natl. Acad. Sci. U. S. A. **112**, 685 (2015).

[66] P. M. Gill, R. D. Adamson, and J. A. Pople, "Coulomb-attenuated exchange energy density functionals," Mol. Phys. **88**, 1005 (1996).

[67] A. D. Becke, "Density-functional exchange-energy approximation with correct asymptotic behavior," Phys. Rev. A **38**, 3098 (1988).

[68] J. P. Perdew, J. Tao, V. N. Staroverov, and G. E. Scuseria, "Meta-generalized gradient approximation: Explanation of a realistic nonempirical density functional," J. Chem. Phys. **120**, 6898 (2004).

[69] K. L. Schuchardt, B. T. Didier, T. Elsethagen, L. Sun, V. Gurumoorthi, J. Chase, J. Li, and T. L. Windus, "Basis Set Exchange: A Community Database for Computational Sciences," J. Chem. Inf. Model. **47**, 1045 (2007).

[70] B. J. Lynch and D. G. Truhlar, "Small Representative Benchmarks for Thermochemical Calculations," J. Phys. Chem. A **107**, 8996 (2003).

[71] F. Weigend and R. Ahlrichs, "Balanced basis sets of split valence, triple zeta valence and quadruple zeta valence quality for H to Rn: Design and assessment of accuracy," Phys. Chem. Chem. Phys. **7**, 3297 (2005).

[72] A. Karton, A. Tarnopolsky, J.-F. Lamere, G. C. Schatz, and J. M. Martin, "Highly Accurate First-Principles Benchmark Data Sets for the Parametrization and Validation of Density Functional and Other Approximate Methods. Derivation of a Robust, Generally Applicable, Double-Hybrid Functional for Thermochemistry and Thermochemical Kinetics," J. Phys. Chem. A **112**, 12868 (2008).

[73] S. Grimme and S. Ehrlich, "Effect of the damping function in dispersion corrected density functional theory," J. Comput. Chem. **32**, 1456 (2011).

[74] H.-J. Werner, P. J. Knowles, G. Knizia, F. R. Manby, and M. Schütz, "Molpro: a general-purpose quantum chemistry program package," WIREs Comput. Mol. Sci. **2**, 242 (2012).

[75] J. Chai and M. Head-Gordon, "Systematic optimization of long-range corrected hybrid density functionals," J. Chem. Phys. **128**, 084106 (2008).

[76] C.-W. Tsai, Y.-C. Su, and J.-D. Chai, "Assessment of density functional methods with correct asymptotic behavior," Phys. Chem. Chem. Phys. **15**, 8352 (2013).

[77] C. Riplinger, B. Sandhoefer, A. Hansen, and F. Neese, "Natural triple excitations in local coupled cluster calculations with pair natural orbitals," J. Chem. Phys. **139**, 134101 (2013).

[78] D. G. Liakos, M. Sparta, M. K. Kesharwani, J. M. Martin, and F. Neese, "Exploring the Accuracy Limits of Local Pair Natural Orbital Coupled-Cluster Theory," J. Chem. Theory Comput. **11**, 1525 (2015).

[79] F. Neese, "The ORCA program system," WIREs Comput. Mol. Sci. **2**, 73 (2012).

[80] D. J. Lacks and R. G. Gordon, "Pair interactions of rare-gas atoms as a test of exchange-energy-density functionals in regions of large density gradients," Phys. Rev. A **47**, 4681 (1993).

[81] A. D. Becke, "A new mixing of Hartree–Fock and local density-functional theories," J. Chem. Phys. **98**, 1372 (1993).

[82] E. Ruiz, D. R. Salahub, and A. Vela, "Defining the Domain of Density Functionals: Charge-Transfer Complexes," J. Am. Chem. Soc. **117**, 1141 (1995).

[83] E. Ruiz, D. R. Salahub, and A. Vela, "Charge-Transfer Complexes: Stringent Tests for Widely Used Density Functionals," J. Phys. Chem. **100**, 12265 (1996).

[84] S. N. Steinmann and C. Corminboeuf, "Exploring the Limits of Density Functional Approximations for Interaction Energies of Molecular Precursors to Organic Electronics," J. Chem. Theory Comput. **8**, 4305 (2012).

[85] S. Yoo, E. Apra, X. C. Zeng, and S. S. Xantheas, "High-Level Ab Initio Electronic Structure Calculations of Water Clusters $(H2O)_{16}$ and $(H2O)_{17}$: A New Global Minimum for $(H2O)_{16}$," J. Phys. Chem. Lett. **1**, 3122 (2010).

[86] A. Karton, R. J. O'Reilly, B. Chan, and L. Radom, "Determination of Barrier Heights for Proton Exchange in Small Water, Ammonia, and Hydrogen Fluoride Clusters with G4(MP2)-Type, MPn, and SCS-MPn Procedures–A Caveat," J. Chem. Theory Comput. **8**, 3128 (2012).

[87] H. R. Leverentz, H. W. Qi, and D. G. Truhlar, "Assessing the Accuracy of Density Functional and Semiempirical Wave Function Methods for Water Nanoparticles: Comparing Binding and Relative Energies of $(H2O)_{16}$ and $(H2O)_{17}$ to CCSD (T) Results," J. Chem. Theory Comput. **9**, 995 (2013).

[88] A. Otero-De-La-Roza and E. R. Johnson, "Predicting Energetics of Supramolecular Systems Using the XDM Dispersion Model," J. Chem. Theory Comput. **11**, 4033 (2015).

[89] E. R. Johnson, I. D. Mackie, and G. A. DiLabio, "Dispersion interactions in density-functional theory," J. Phys. Org. Chem. **22**, 1127 (2009).

[90] A. Becke and E. Johnson, "Exchange-hole dipole moment and the dispersion interaction," J. Chem. Phys. **122**, 154104 (2005).

[91] T. Risthaus and S. Grimme, "Benchmarking of London Dispersion-Accounting Density Functional Theory Methods on Very Large Molecular Complexes," J. Chem. Theory Comput. **9**, 1580 (2013).

[92] A. Ambrosetti, D. Alfe, R. A. DiStasio Jr, and A. Tkatchenko, "Hard Numbers for Large Molecules: Toward Exact Energetics for Supramolecular Systems," J. Phys. Chem. Lett. **5**, 849 (2014).

[93] A. Hesselmann and T. Korona, "Intermolecular symmetry-adapted perturbation theory study of large organic complexes," J. Chem. Phys. **141**, 094107 (2014).

[94] P. R. Schreiner, A. A. Fokin, R. A. Pascal, and A. de Meijere, "Many Density Functional Theory Approaches Fail to Give Reliable Large Hydrocarbon Isomer Energy Differences," Org. Lett. **8**, 3635 (2006).

[95] M. D. Wodrich, C. Corminboeuf, and P. v. R. Schleyer, "Systematic Errors in Computed Alkane Energies Using B3LYP and Other Popular DFT Functionals," Org. Lett. **8**, 3631 (2006).

[96] Y. Zhao and D. G. Truhlar, "A Density Functional That Accounts for Medium-Range Correlation Energies in Organic Chemistry," Org. Lett. **8**, 5753 (2006).

[97] S. Grimme, "n-Alkane Isodesmic Reaction Energy Errors in Density Functional Theory Are Due to Electron Correlation Effects," Org. Lett. **12**, 4670 (2010).

[98] W. C. McKee and P. v. R. Schleyer, "Correlation Effects on the Relative Stabilities of Alkanes," J. Am. Chem. Soc. **135**, 13008 (2013).

[99] J.-W. Song, T. Tsuneda, T. Sato, and K. Hirao, "Calculations of Alkane Energies Using Long-Range Corrected DFT Combined with Intramolecular van der Waals Correlation," Org. Lett. **12**, 1440 (2010).

[100] E. R. Johnson, P. Mori-Sanchez, A. J. Cohen, and W. Yang, "Delocalization errors in density functionals and implications for main-group thermochemistry," J. Chem. Phys. **129**, 204112 (2008).

[101] S. Gronert, "An Alternative Interpretation of the CH Bond Strengths of Alkanes," J. Org. Chem. **71**, 1209 (2006).

[102] M. Isegawa, R. Peverati, and D. G. Truhlar, "Performance of recent and high-performance approximate density functionals for time-dependent density functional theory calculations of valence and rydberg electronic transition energies," J. Chem. Phys. **137**, 244104 (2012).

[103] M. E. Casida, C. Jamorski, K. C. Casida, and D. R. Salahub, "Molecular excitation energies to high-lying bound states from time-dependent density-functional response theory: Characterization and correction of the time-dependent local density approximation ionization threshold," J. Chem. Phys. **108**, 4439 (1998).

[104] M. Caricato, G. W. Trucks, M. J. Frisch, and K. B. Wiberg, "Oscillator Strength: How Does TDDFT Compare to EOM-CCSD?" J. Chem. Theory Comput. **7**, 456 (2011).

[105] C. Daday, S. Smart, G. H. Booth, A. Alavi, and C. Filippi, "Full Configuration Interaction Excitations of Ethene and Butadiene: Resolution of an Ancient Question," J. Chem. Theory Comput. **8**, 4441 (2012).

[106] M. Caricato, G. W. Trucks, M. J. Frisch, and K. B. Wiberg, "Electronic Transition Energies: A Study of the Performance of a Large Range of Single Reference Density Functional and Wave Function Methods on Valence and Rydberg States Compared to Experiment," J. Chem. Theory Comput. **6**, 370 (2010).

[107] Y. Zhao and D. G. Truhlar, "Density Functional for Spectroscopy: No Long-Range Self-Interaction Error, Good Performance for Rydberg and Charge-Transfer States, and Better Performance on Average than B3LYP for Ground States," J. Phys. Chem. A **110**, 13126 (2006).

[108] I. Hanazaki, "Vapor-phase electron donor-acceptor complexes of tetracyanoethylene and of sulfur dioxide," J. Phys. Chem. **76**, 1982 (1972).

[109] K. Lopata and N. Govind, "Modeling Fast Electron Dynamics with Real-Time Time-Dependent Density Functional Theory: Application to Small Molecules and Chromophores," J. Chem. Theory Comput. **7**, 1344 (2011).

[110] H. Eshuis, G. G. Balint-Kurti, and F. R. Manby, "Dynamics of molecules in strong oscillating electric fields using time-dependent Hartree–Fock theory," J. Chem. Phys. **128**, 114113 (2008).

[111] A. Misquitta, R. Podeszwa, B. Jeziorski, and K. Szalewicz, "Intermolecular potentials based on symmetry-adapted perturbation theory with dispersion energies from time-dependent density-functional calculations," J. Chem. Phys. **123**, 214103 (2005).

[112] M. Hapka, L. Rajchel, M. Modrzejewski, G. Chalasinski, and M. M. Szczesniak, "Tuned range-separated hybrid functionals in the symmetry-adapted perturbation theory," J. Chem. Phys. **141**, 134120 (2014).

[113] M. Gruning, O. V. Gritsenko, S. J. A. van Gisbergen, and E. J. Baerends, "Shape corrections to exchange-correlation potentials by gradient-regulated seamless connection of model potentials for inner and outer region," J. Chem. Phys. **114**, 652 (2001).

[114] C. Adamo and V. Barone, "Toward reliable density functional methods without adjustable parameters: The PBE0 model," J. Chem. Phys. **110**, 6158 (1999).

[115] J. Rezac and P. Hobza, "Describing Noncovalent Interactions beyond the Common Approximations: How Accurate Is the "Gold Standard," CCSD(T) at the Complete Basis Set Limit?" J. Chem. Theory Comput. **9**, 2151 (2013).

Appendices

Appendix A

Paper I: J. Chem. Phys. 137, 204121 (2012)

A first-principles-based correlation functional for harmonious connection of short-range correlation and long-range dispersion

Marcin Modrzejewski,[1,a)] Michał Lesiuk,[1] Łukasz Rajchel,[2] Małgorzata M. Szczęśniak,[3] and Grzegorz Chałasiński[1]
[1]*Faculty of Chemistry, University of Warsaw, 02-093 Warsaw, Pasteura 1, Poland*
[2]*Interdisciplinary Centre for Mathematical and Computational Modelling, University of Warsaw, 02-093 Warsaw, Pawińskiego 5a, Poland*
[3]*Department of Chemistry, Oakland University, Rochester, Michigan 48309-4477, USA*

(Received 25 September 2012; accepted 6 November 2012; published online 29 November 2012)

We present a physically motivated correlation functional belonging to the meta-generalized gradient approximation (meta-GGA) rung, which can be supplemented with long-range dispersion corrections without introducing double-counting of correlation contributions. The functional is derived by the method of constraint satisfaction, starting from an analytical expression for a real-space spin-resolved correlation hole. The model contains a position-dependent function that controls the range of the interelectronic correlations described by the semilocal functional. With minimal empiricism, this function may be adjusted so that the correlation model blends with a specific dispersion correction describing long-range contributions. For a preliminary assessment, our functional has been combined with an atom-pairwise dispersion correction and full Hartree-Fock (HF)-like exchange. Despite the HF-exchange approximation, its predictions compare favorably with reference interaction energies in an extensive set of non-covalently bound dimers. © *2012 American Institute of Physics*. [http://dx.doi.org/10.1063/1.4768228]

I. INTRODUCTION

Inclusion of the dispersion interactions into the set of phenomena accounted for by density functional theory (DFT) models is recognized as one of the challenges in the development of new density functional approximations (DFAs).[1–4] Several ways have been proposed to correct the currently available semilocal (SL) DFAs for the lacking nonlocal (NL) correlation contribution responsible for the dispersion interactions.[1,3] Hereafter, global hybrid and range-separated hybrid functionals will be called SL DFAs. Although the exchange parts of such functionals are nonlocal, our focus will be on the correlation contributions, which in this case depend on variables calculated at a single point of space. The examples of such dispersion-corrected methods are: (i) the exchange-hole dipole method (XDM),[5–9] (ii) the atom pairwise additive schemes of Goerigk and Grimme, DFT-D3,[10] and Tkatchenko-Scheffler approach,[11] (iii) seamless van der Waals density functionals.[4,12–17] It is clear that the accuracy of these methods depends not only on a faithful representation of long-range electronic correlations, but also on a consistent matching of a dispersion correction and the chosen SL complement.

Several groups have studied the conditions under which a SL functional can be incorporated into a dispersion-corrected method.[18–21] It has been concluded that the improper behavior of a GGA exchange functional in the density tail (large reduced gradient regime) is responsible for artificial exchange binding (as for the PBE[22] exchange) or overly repulsive interaction (as for the B88[23] exchange).[20,21] Such systematic errors may cause the NL correction to worsen the results compared to the bare SL functional. The following exchange functionals: PW86,[24] refitted PW86,[21] and range-separated hybrids[16,20] were found to be free from artificial binding, thus being consistent with NL dispersion correction. Similarly, combining exact exchange with NL correlation performs satisfactorily.[25]

It has been observed that a failure to satisfy the condition of vanishing correlation for a rapidly varying density by SL correlation functionals[22] leads to a systematic overbinding of non-covalent complexes.[20] The *ad hoc* cure is to cancel the error of the correlation by the opposite-sign error of an exchange component.[20] However, this does not resolve the problem of the double counting of SL and NL correlation. Several remedies have been proposed. For atom pairwise schemes, multiple damping functions have been devised.[26] For VV09[15] and VV10[16] density functionals the problem is avoided by demanding the NL constituent to vanish in the homogeneous electron gas (HEG) limit, because the SL constituent is able to describe the whole range of the electronic interactions in this limit. Finally, Pernal *et al.*[18] devised a procedure to reoptimize an existing SL exchange-correlation functional so as to recover the dispersionless interaction energy.[18] The rationale of such an approach is to let the SL functional contribute only the terms that it can describe reliably.

At this point we would like to shed light on the dispersion problem[27] in DFT. It has been well established that SL functionals fail to recover the long-range multipole-expanded dispersion energy. In fact, nearly all dispersion-corrected DFT approaches aim at recovering only long-range dispersion,

a)Electronic mail: modrzej@tiger.chem.uw.edu.pl.

roughly determined by the leading terms of the multipole expansion: C_6, and possibly C_8. The exceptions are the approaches of Pernal *et al.*[18] and Rajchel *et al.*[19] which supplement a SL functional with total non-expanded dispersion from symmetry-adapted perturbation theory (SAPT). It is often overlooked that the long-range contribution, however, does not constitute the whole dispersion energy at near-equilibrium distances. Setting aside the exchange-dispersion part, the dispersion energy, defined as SAPT,[28,29] has a complex nature, and includes both long- and short-range contributions. This has first been observed by Koide[30] who quantified the short-distance behavior of the dispersion energy as $A + BR^2$, with R being the intermonomer separation. The importance of the short-range correlation is also unambiguously, though indirectly, supported by the significance of bond functions and explicitly correlated Gaussian geminals in the dispersion energy calculations.[31] A more direct argument points to the existence of short-range terms in the exact angular expansion of the dispersion energy. In the case of atomic interactions, the latter involves the interaction between S states of monomers,[30] which give no contribution to the multipole expansion. Numerical results show that near the equilibrium bond length these terms, decaying exponentially with the overlap density, can be comparable in magnitude to the multipole expansion terms.[32] As demonstrated by Dobson *et al.*[27] with the aid of simple models, SL functionals cannot recover the multipole expansion of the dispersion energy. However, there is a good reason to believe that SL functionals are capable of describing the terms that depend on overlap density.[27] Our model is intended to capture this contribution.

Recent thorough assessments of DFT-D, XDM, and VV10 approaches have clearly shown that a combination of a SL functional specifically designed for a dispersion-corrected treatment with a dispersion correction improves both the description of noncovalent interactions[33–37] and general molecular properties.[34,35] Among the functionals that use atom-pairwise DFT-D correction, B97-D,[38] B97-D3,[34] and ω-B97X-D[39,40] are characterized by one of the smallest magnitude and spread of errors in interaction energies[33] while performing well in thermochemistry and reaction kinetics. The methods utilizing unaltered conventional SL functional suffer from systematic errors. For example, PBE0-D2, PBE-D3, and B3LYP-D3 tend to underbind dispersion-bound complexes and overbind hydrogen-bonded systems.[33] The systematic overbinding of charge-transfer complexes within DFT is more pronounced for the dispersion-corrected approaches than for the pure DFAs.[41,42] See Ref. 42 and Table II in Ref. 43, where numerical examples of huge overbinding by ω-B97X-D and B97-D functionals applied to charge-transfer complexes are given.

Although much attention has been devoted to the development of the proper exchange contribution,[20,21,44] the theoretical effort to derive a dispersion-consistent SL correlation functional thus far has been reduced to reoptimizing known expressions. It has also been observed[38,40] that fitting to empirical data coupled with addition of higher-order terms in the B97 expansion[45] does not systematically improve the performance as the saturation is approached. Clearly, there is a demand for the theoretical effort to overcome the problem.

The aim of this work is to develop a SL correlation functional that can be matched with an arbitrary long-range dispersion correction by optimizing a single parameter that has a simple physical meaning. As a demonstration of this approach, we will combine our approximation with DFT-D3 dispersion correction,[10] which contributes damped $C_6/R^6 + C_8/R^8$ terms, with no short-range contributions. To avoid the systematic error of spurious exchange attraction, full HF exchange will be used. To match SL and NL constituents, a function which controls the spatial extent of our SL correlation hole will be adjusted by minimization of errors in a relevant set of molecules.

II. THEORY

We consider an electronic ground state of a finite molecular system described by an electronic Hamiltonian of the form

$$\hat{H} = \hat{T} + \sum_i \hat{v}_{\text{ext}}(\mathbf{r}_i) + \hat{V}_{\text{ee}}, \tag{1}$$

where $\hat{T}$ is the kinetic energy operator, the multiplicative external potential $\hat{v}_{\text{ext}}$ is taken to be the Coulomb potential of nuclear attraction, and $\hat{V}_{\text{ee}}$ is the interelectronic repulsion. Atomic units are assumed throughout this work. In constrained-search formulation[46] of DFT[47] the ground state energy of electronic system can be expressed as

$$E_0 = \min_\rho \left[\int \hat{v}_{\text{ext}}(\mathbf{r}_1)\rho(\mathbf{r}_1)\mathrm{d}^3\mathbf{r}_1 + \left\langle \Psi_\rho^{\min} \middle| \hat{T} + \hat{V}_{\text{ee}} \middle| \Psi_\rho^{\min} \right\rangle \right], \tag{2}$$

where $\Psi_\rho^{\min}$ denotes an N-body wavefunction that yields electronic density ρ and simultaneously minimizes expectation value of $\hat{T} + \hat{V}_{\text{ee}}$. In Kohn-Sham scheme[48] the second term on the right-hand side of Eq. (2) is decomposed into noninteracting kinetic, Hartree, and exchange-correlation energies, respectively,

$$\left\langle \Psi_\rho^{\min} \middle| \hat{T} + \hat{V}_{\text{ee}} \middle| \Psi_\rho^{\min} \right\rangle = T_{\text{s}}[\rho] + U[\rho] + E_{\text{XC}}[\rho]. \tag{3}$$

Noninteracting kinetic energy T_{s} is known explicitly in terms of the wavefunction of the KS system, denoted here as $\Phi_\rho^{\min}$, which merely minimizes the expectation value of $\hat{T}$:

$$T_{\text{s}}[\rho] = \left\langle \Phi_\rho^{\min} \middle| \hat{T} \middle| \Phi_\rho^{\min} \right\rangle. \tag{4}$$

Hartree energy is given by a classical formula

$$U[\rho] = \frac{1}{2} \iint \frac{\rho(\mathbf{r}_1)\rho(\mathbf{r}_2)}{r_{12}} \mathrm{d}^3\mathbf{r}_1 \mathrm{d}^3\mathbf{r}_2. \tag{5}$$

Exchange-correlation energy can be formally expressed through adiabatic connection formula[49]

$$E_{\text{XC}}[\rho] = \int_0^1 \left\langle \Psi_\rho^{\min,\lambda} \middle| \hat{V}_{\text{ee}} \middle| \Psi_\rho^{\min,\lambda} \right\rangle \mathrm{d}\lambda - U[\rho], \tag{6}$$

where $\Psi_\rho^{\min,\lambda}$ minimizes the expectation value of $\hat{T} + \lambda \hat{V}_{\text{ee}}$ and yields the same electronic density as wavefunction at $\lambda = 1$. Eq. (6) can be further decomposed so that the correlation energy is separately expressed through coupling-constant

integral

$$E_{\mathrm{C}}[\rho] = \int_0^1 V_{\mathrm{C}}^{\lambda}[\rho]\mathrm{d}\lambda \tag{7}$$

where

$$V_{\mathrm{C}}^{\lambda}[\rho] = \left\langle \Psi_{\rho}^{\min,\lambda} \middle| \hat{V}_{\mathrm{ee}} \middle| \Psi_{\rho}^{\min,\lambda} \right\rangle - \left\langle \Phi_{\rho}^{\min} \middle| \hat{V}_{\mathrm{ee}} \middle| \Phi_{\rho}^{\min} \right\rangle. \tag{8}$$

Approximating V_{C}^{λ} is the primary objective of this work. Let us begin by expressing V_{C}^{λ} in terms of a λ-dependent correlation hole

$$V_{\mathrm{C}}^{\lambda} = \frac{1}{2}\sum_{\sigma\sigma'}\iint \frac{\rho_{\sigma}(\mathbf{r}_1)h_{\mathrm{C}\lambda}^{\sigma\sigma'}(\mathbf{r}_1,\mathbf{r}_2)}{r_{12}}\mathrm{d}^3\mathbf{r}_1\mathrm{d}^3\mathbf{r}_2, \tag{9}$$

where σ denotes a spin variable,

$$h_{\mathrm{C}\lambda}^{\sigma\sigma'}(\mathbf{r}_1,\mathbf{r}_2) = h_{\mathrm{XC}\lambda}^{\sigma\sigma'}(\mathbf{r}_1,\mathbf{r}_2) - h_{\mathrm{X}}^{\sigma\sigma'}(\mathbf{r}_1,\mathbf{r}_2) \tag{10}$$

and

$$h_{\mathrm{XC}\lambda}^{\sigma\sigma'}(\mathbf{r}_1,\mathbf{r}_2) = \frac{P_{2\lambda}^{\sigma\sigma'}(\mathbf{r}_1,\mathbf{r}_2)}{\rho_{\sigma}(\mathbf{r}_1)} - \rho_{\sigma'}(\mathbf{r}_2), \tag{11}$$

$$h_{\mathrm{X}}^{\sigma\sigma'}(\mathbf{r}_1,\mathbf{r}_2) = -\delta_{\sigma\sigma'}\frac{\left|\sum_i^{N_\sigma}\psi_{i\sigma}^{*}(\mathbf{r}_1)\psi_{i\sigma}(\mathbf{r}_2)\right|^2}{\rho_{\sigma}(\mathbf{r}_1)}. \tag{12}$$

N_σ is a number of σ-spin electrons and pair probability density, $P_{2\lambda}^{\sigma\sigma'}(\mathbf{r}_1,\mathbf{r}_2)$, is defined as

$$\begin{aligned} P_{2\lambda}^{\sigma\sigma'}(\mathbf{r}_1,\mathbf{r}_2) = N(N-1) & \\ \times \sum_{\sigma_3\cdots\sigma_N}\int \Psi_{\rho}^{\min,\lambda *}(\mathbf{r}_1\sigma,\mathbf{r}_2\sigma',\ldots,\mathbf{r}_N\sigma_N) & \\ \times \Psi_{\rho}^{\min,\lambda}(\mathbf{r}_1\sigma,\mathbf{r}_2\sigma',\ldots,\mathbf{r}_N\sigma_N) & \\ \times \mathrm{d}^3\mathbf{r}_3\cdots\mathrm{d}^3\mathbf{r}_N. & \end{aligned} \tag{13}$$

Note that, due to the symmetry of r_{ij}^{-1} operator, it is the spherical average of exchange-correlation hole around the reference electron that enters the energy expression:

$$\begin{aligned} V_{\mathrm{C}}^{\sigma\sigma',\lambda} &= \frac{1}{2}\iint \frac{\rho_{\sigma}(\mathbf{r}_1)h_{\mathrm{C}\lambda}^{\sigma\sigma'}(\mathbf{r}_1,\mathbf{r}_2)}{r_{12}}\mathrm{d}^3\mathbf{r}_1\mathrm{d}^3\mathbf{r}_2 \\ &= \frac{1}{2}\int \mathrm{d}^3\mathbf{r}_1\int_0^{\infty}\frac{\rho_{\sigma}(\mathbf{r}_1)h_{\mathrm{C}\lambda}^{\sigma\sigma'}(\mathbf{r}_1,s)}{s}4\pi s^2\mathrm{d}s, \end{aligned} \tag{14}$$

where the spherical average is implied by scalar argument s,

$$h_{\mathrm{C}\lambda}^{\sigma\sigma'}(\mathbf{r}_1,s) = \frac{1}{4\pi}\int_0^{2\pi}\mathrm{d}\phi_{\mathbf{s}}\int_0^{\pi}h_{\mathrm{C}\lambda}^{\sigma\sigma'}(\mathbf{r}_1,\mathbf{r}_1+\mathbf{s})\sin\theta_{\mathbf{s}}\mathrm{d}\theta_{\mathbf{s}}. \tag{15}$$

Equation (14) means that without loss of generality we can focus our attention on approximating isotropic quantity defined in Eq. (15).

We postulate the following form of opposite-spin and same-spin correlation holes:

$$h_{\mathrm{C}\lambda}^{\alpha\beta}(\mathbf{r}_1,s) = (a_{\alpha\beta} + b_{\alpha\beta}s + c_{\alpha\beta}s^2)\exp(-d_{\alpha\beta}s), \tag{16}$$

$$h_{\mathrm{C}\lambda}^{\alpha\alpha}(\mathbf{r}_1,s) = s^2(a_{\alpha\alpha} + b_{\alpha\alpha}s + c_{\alpha\alpha}s^2)\exp(-d_{\alpha\alpha}s). \tag{17}$$

Unknown parameters appearing above are actually functions of $\rho(\mathbf{r}_1)$, but we will not write that explicitly for the sake of brevity. Quadratic behavior of $h_{\mathrm{C}\lambda}^{\alpha\alpha}$ near the reference point

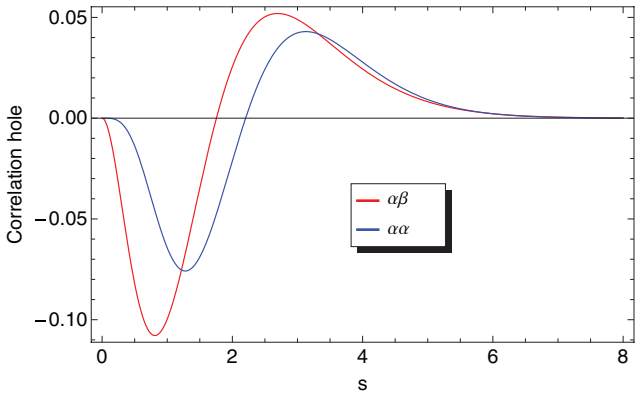

FIG. 1. Shape of the approximate correlation holes defined in Eqs. (16) and (17). The functions illustrated on the graph are $h_{\mathrm{C}}^{\alpha\beta,1}$ and $h_{\mathrm{C}}^{\alpha\alpha,1}$ multiplied by $4\pi s^2$. The functions are evaluated at $r_{\mathrm{s}} = 1$ in the spin-compensated HEG limit. Atomic units are used.

results from the Pauli exclusion principle and the cusp condition discussed further below. The model of Eqs. (16) and (17) cannot recover radial dependence of the true hole at each point, however, its simple form leads to reasonable shape of the system-averaged correlation hole. We thus assume that the wealth of features of the exact hole[50] is averaged out, and use system-averaged function of shape similar to Eqs. (16) and (17) in the energy expression. The argument involving system average was originally put forward by Burke *et al.*[51] in their discussion of the success of the local-density approximation (LDA).

The shape of the correlation holes corresponding to Eqs. (16) and (17) is illustrated in Fig. 1 (the details of parametrization are discussed below). For any spin density the qualitative picture is similar: both same-spin and opposite-spin holes are removing electrons in the vicinity of the origin, then cross the abscissa exactly once, and decay exponentially. The fact that both model correlation holes (16) and (17) change sign exactly once can be readily proven.

The form of correlation holes given in Eqs. (16) and (17) has been derived from observation of system-averaged correlation holes (correlation intracules) in simple systems dominated by dynamical correlation. Qualitatively, the shape of our model correlation hole is similar to correlation intracules in He,[52] Ne,[52] and H_2 (Ref. 53) near the equilibrium bond length. We note that there is a qualitative discrepancy between our approximate correlation hole and the accurate one for systems like Li (Ref. 52) or Be.[52] These systems are characterized by a significant contribution of static correlation. However, there is a substantial cancellation between exchange and correlation holes in systems of this type.

The cusp conditions for same-spin and opposite-spin exchange-correlation holes[54] considerably restrict the short-range expansion[55] of $h_{\mathrm{XC}\lambda}^{\alpha\beta}$ and $h_{\mathrm{XC}\lambda}^{\alpha\alpha}$:

$$h_{\mathrm{XC}\lambda}^{\alpha\beta}(\mathbf{r}_1,s) = (B_{\alpha\beta} - \rho_{\beta}) + \lambda B_{\alpha\beta}s + \ldots, \tag{18}$$

$$h_{\mathrm{XC}\lambda}^{\alpha\alpha}(\mathbf{r}_1,s) = -\rho_{\alpha} + \left(B_{\alpha\alpha} - \frac{1}{6}\nabla^2\rho_{\alpha}\right)s^2 + \frac{\lambda}{2}B_{\alpha\alpha}s^3 + \ldots. \tag{19}$$

Equation (10) together with Eqs. (18) and (19), and the expansion of spherically averaged exact exchange hole valid at zero current density,[55–57]

$$h_{\mathrm{X}}^{\alpha\alpha}(\mathbf{r}_1, s) = -\rho_\alpha - \frac{1}{6}\left[\nabla^2\rho_\alpha - 2\tau_\alpha + \frac{1}{2}\frac{(\nabla\rho_\alpha)^2}{\rho_\alpha}\right]s^2 + \ldots, \tag{20}$$

yields short-range expansions of correlation holes:[55]

$$h_{\mathrm{C}\lambda}^{\alpha\beta}(\mathbf{r}_1, s) = (B_{\alpha\beta} - \rho_\beta) + \lambda B_{\alpha\beta} s + \ldots, \tag{21}$$

$$h_{\mathrm{C}\lambda}^{\alpha\alpha}(\mathbf{r}_1, s) = \left(B_{\alpha\alpha} - \frac{1}{3}D_\alpha\right)s^2 + \frac{\lambda}{2}B_{\alpha\alpha}s^3 + \ldots. \tag{22}$$

D_α is always non-negative and vanishes for single orbital densities,

$$D_\alpha = \tau_\alpha - \frac{|\nabla\rho_\alpha|^2}{4\rho_\alpha}, \tag{23}$$

where τ_α is essentially the density of noninteracting kinetic energy

$$\tau_\alpha = \sum_i^{N_\alpha} |\nabla\psi_{i\alpha}|^2. \tag{24}$$

We will adjust the unknown functions $B_{\alpha\beta}$ and $B_{\alpha\alpha}$ in Eqs. (18) and (19) to recover short range expansion of spin-resolved pair distribution function of the HEG developed by Gori-Giorgi and Perdew.[58] The pair distribution function represents the solution of the Overhauser model.[59] $B_{\alpha\alpha}$ will be further modified to eliminate self-interaction error of the correlation functional. We leave the on-top value of the correlation hole (determined solely by $B_{\alpha\beta}$) unchanged by inhomogeneity corrections because it is well-transferable from the HEG to real systems.[51] For the discussion of the quality of the HEG on-top hole density see the work of Burke, Perdew, and Ernzerhof.[51]

Comparison of homogeneous density limit of Eqs. (18) and (19) with short-range expansions of the spin-resolved HEG pair distribution function[58] yields

$$\begin{aligned} B_{\alpha\beta}(\rho_\alpha, \rho_\beta, \lambda) = \rho_\beta\big(&1 + 0.0207\lambda r_{\mathrm{s}}^{\alpha\beta} + 0.08193\big(\lambda r_{\mathrm{s}}^{\alpha\beta}\big)^2 \\ &- 0.01277\big(\lambda r_{\mathrm{s}}^{\alpha\beta}\big)^3 + 0.001859\big(\lambda r_{\mathrm{s}}^{\alpha\beta}\big)^4\big) \\ &\times \exp\big(-0.7524\lambda r_{\mathrm{s}}^{\alpha\beta}\big), \end{aligned} \tag{25}$$

$$\begin{aligned} B_{\alpha\alpha}^{\mathrm{HEG}}(\rho_\alpha, \lambda) = \frac{D_\alpha^{\mathrm{HEG}}}{3}\big(&1 - 0.01624\lambda r_{\mathrm{s}}^{\alpha\alpha} + 0.00264\big(\lambda r_{\mathrm{s}}^{\alpha\alpha}\big)^2\big) \\ &\times \exp\big(-0.5566\lambda r_{\mathrm{s}}^{\alpha\alpha}\big), \end{aligned} \tag{26}$$

where $r_{\mathrm{s}}^{\alpha\alpha}$ and $r_{\mathrm{s}}^{\alpha\beta}$ introduce the dependence on electronic spin densities,

$$r_{\mathrm{s}}^{\alpha\alpha} = \frac{(3/\pi)^{1/3}}{2\rho_\alpha^{1/3}}, \tag{27}$$

$$r_{\mathrm{s}}^{\alpha\beta} = \frac{(3/\pi)^{1/3}}{\rho_\alpha^{1/3} + \rho_\beta^{1/3}}, \tag{28}$$

and each of them reduces to the Seitz radius

$$r_{\mathrm{s}} = \left(\frac{3}{4\pi\rho}\right)^{1/3}, \tag{29}$$

for spin-compensated systems. The formulae (25) and (26) respect the exact high-density expansion derived by Rassolov, Pople, and Ratner.[60] The HEG limit of parameter (23) in (26) reads[55]

$$D_\alpha^{\mathrm{HEG}} = \frac{3}{5}(6\pi^2)^{2/3}\rho_\alpha^{5/3}. \tag{30}$$

We substitute D_α^{HEG} in Eq. (26) for D_α of Eq. (23) to get $B_{\alpha\alpha}$:

$$\begin{aligned} &B_{\alpha\alpha}(\rho_\alpha, |\nabla\rho_\alpha|, \tau_\alpha, \lambda) \\ &\quad= \frac{D_\alpha}{3}\big(1 - 0.01624\lambda r_{\mathrm{s}}^{\alpha\alpha} + 0.00264\big(\lambda r_{\mathrm{s}}^{\alpha\alpha}\big)^2\big) \\ &\qquad\times \exp\big(-0.5566\lambda r_{\mathrm{s}}^{\alpha\alpha}\big). \end{aligned} \tag{31}$$

Such choice of the $B_{\alpha\alpha}$ function leads to vanishing parallel spin correlation contribution for single orbital densities. In that sense no correlation self-interaction error is present.

Restricting undetermined coefficients in Eqs. (16) and (17) to yield short-range expansions of Eqs. (21) and (22), respectively, gives

$$a_{\alpha\beta} = B_{\alpha\beta} - \rho_\beta, \tag{32}$$

$$b_{\alpha\beta} = \lambda B_{\alpha\beta} + d_{\alpha\beta}a_{\alpha\beta}. \tag{33}$$

Correct shape of $h_{\mathrm{C}\lambda}^{\alpha\beta}$ can be ensured requiring that the function satisfies the appropriate sum rule,

$$4\pi\int_0^\infty h_{\mathrm{C}\lambda}^{\alpha\beta}(\mathbf{r}_1, s)s^2\mathrm{d}s = 0. \tag{34}$$

Consequently, coefficient $c_{\alpha\beta}$ is fixed for Eq. (34) to hold for all densities:

$$c_{\alpha\beta} = -\frac{1}{12}\big(a_{\alpha\beta}d_{\alpha\beta}^2 + 3b_{\alpha\beta}d_{\alpha\beta}\big). \tag{35}$$

Analogously,

$$a_{\alpha\alpha} = B_{\alpha\alpha} - \frac{D_\alpha}{3}, \tag{36}$$

$$b_{\alpha\alpha} = \frac{\lambda}{2}B_{\alpha\alpha} + a_{\alpha\alpha}d_{\alpha\alpha}, \tag{37}$$

$$c_{\alpha\alpha} = -\frac{1}{30}\big(a_{\alpha\alpha}d_{\alpha\alpha}^2 + 5b_{\alpha\alpha}d_{\alpha\alpha}\big). \tag{38}$$

With all but $d_{\alpha\beta}$ and $d_{\alpha\alpha}$ coefficients determined, spin resolved contributions to V_{C}^{λ},

$$V_{\mathrm{C}}^{\sigma\sigma',\lambda} = \frac{1}{2}\int \mathrm{d}^3\mathbf{r}_1 \int_0^\infty \frac{\rho_\sigma h_{\mathrm{C}\lambda}^{\sigma\sigma'}(\mathbf{r}_1, s)}{s}4\pi s^2\mathrm{d}s, \tag{39}$$

can now be given as

$$V_{\mathrm{C}}^{\alpha\beta,\lambda} = \int \mathrm{d}^3\mathbf{r}_1\rho_\alpha\pi\frac{b_{\alpha\beta} + a_{\alpha\beta}d_{\alpha\beta}}{d_{\alpha\beta}^3}, \tag{40}$$

$$V_{\mathrm{C}}^{\alpha\alpha,\lambda} = \int \mathrm{d}^3\mathbf{r}_1\rho_\alpha\pi\frac{8b_{\alpha\alpha} + 4a_{\alpha\alpha}d_{\alpha\alpha}}{d_{\alpha\alpha}^5}. \tag{41}$$

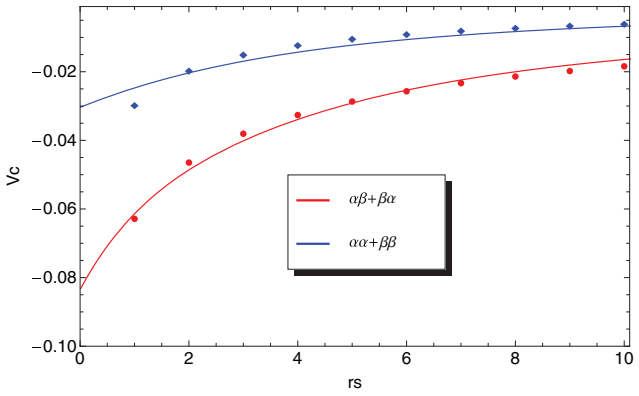

FIG. 2. Comparison of the approximate $V_C^{\sigma\sigma',\lambda=1}$ energies in the HEG limit with reference Monte Carlo data.[63] Solid lines refer to Eqs. (40) and (41). Circles and diamonds represent reference values. The cause of discrepancy at low r_s (high densities) is discussed in the main text. Atomic units are used.

Several requisites for the exact exchange-correlation functional were derived using uniform coordinate scaling technique,[61,62] i.e., by applying uniformly scaled density

$$\rho_\kappa(\mathbf{r}_1) = \kappa^3 \rho(\kappa \mathbf{r}_1). \tag{42}$$

These relations are particularly valuable because they hold for arbitrary N-electron densities. A density-scaling identity proved by Levy,[61]

$$h_{C\lambda}^{\sigma\sigma'}(\rho; \mathbf{r}_1, s) = \lambda^3 h_{C\lambda'=1}^{\sigma\sigma'}(\rho_{1/\lambda}; \lambda \mathbf{r}_1, \lambda s), \tag{43}$$

constrains the set of admissible forms of $d_{\alpha\beta}$ and $d_{\alpha\alpha}$. Eq. (43) implies that

$$d_{\sigma\sigma'}(\rho, |\nabla\rho|, \lambda) = \lambda d_{\sigma\sigma'}\left(\frac{\rho}{\lambda^3}, \frac{|\nabla\rho|}{\lambda^4}, 1\right). \tag{44}$$

We propose the following simple function which satisfies the scaling condition:

$$d_{\sigma\sigma'} = \frac{F_{\sigma\sigma'}}{r_s^{\sigma\sigma'}} + \frac{G}{r_s} \frac{\nabla\rho \cdot \nabla\rho}{\rho^{8/3}}. \tag{45}$$

As Eq. (45) is independent of λ, the coupling-constant integration of Eq. (7) can be done analytically. The values of $F_{\alpha\beta}$ and $F_{\alpha\alpha}$ were determined by least-squares fit of the HEG limit of $V_C^{\alpha\beta,\lambda=1}$ and $V_C^{\alpha\alpha,\lambda=1}$ to the reference values.[63] Opposite-spin and parallel-spin components were fit independently. Reference values of $V_C^{\sigma\sigma',\lambda=1}$ for the HEG were obtained by Gori-Giorgi *et al.*[63] by integrating pair correlation functions from quantum Monte Carlo simulation.[64] Our estimates of $V_C^{\alpha\beta,\lambda=1}$ and $V_C^{\alpha\alpha,\lambda=1}$ were optimized to recover the reference values for spin-compensated system at metallic densities ($r_s = 1, 2, 3, \ldots, 10$). The resulting parameters are $F_{\alpha\beta} = 2.1070$ and $F_{\alpha\alpha} = 2.6422$. The corresponding mean absolute percentage errors (MAPE) of opposite-spin and parallel-spin components are 5.0% and 12.0%, respectively. The MAPE of total $V_C^{\lambda=1}$ is equal to 4.6%. See Fig. 2 for comparison of our fit to the reference values. At high densities ($r_s < 1$) our model does not reduce to the accurate correlation functional for the HEG as it does not account for the logarithmic divergence of the correlation energy density for $r_s \to 0$.[65] This is, however, a peculiarity of the HEG that is not present in finite molecular systems.

We supply our SL correlation functional with the DFT-D3 dispersion correction of Grimme *et al.*,[10] which contributes damped terms of the multipole expansion of the dispersion energy. The adjustment of the SL part to harmonize with the NL correction is accomplished by optimization of the G parameter, see Eq. (45). The G parameter can be adjusted freely, without interfering with any of the above-mentioned physical and formal constraints. In particular, it does not alter the first two terms in the short-range spatial Taylor expansion of the correlation holes. The value of G can be chosen so that the correlation contributions described by SL and NL parts do not overlap. As $G \to 0$, our SL correlation model reduces to the correlation of the HEG with self-interaction removed from parallel-spin part. Our numerical results show that this leads to a systematic overestimation of intermolecular interactions. On the other hand, when $G \to \infty$, the SL correlation vanishes, and the SL functional reduces to an exchange-only approximation (without adding the dispersion correction). Provided that the exchange functional is free from artificial binding, the interaction energies should be underestimated in this limit. Between these two limits lays the optimal G, which corresponds to an interaction curve slightly shallower than the real one, for the addition of the negative dispersion term should move the interaction energy towards the accurate value.

The G parameter of Eq. (45) and the two empirical parameters present in DFT-D3 dispersion correction, $s_{r,6}$ and s_8, (see Eqs. (3) and (4) in Ref. 10) were chosen to optimize mean absolute percentage error of binding energies in S22 set of non-covalently bound complexes.[66] The numerical optimization has been carried out with the constraint that the dispersion-free energy cannot fall below the reference total interaction energy. During the optimization process, self-consistent KS calculations in aug-cc-pVTZ basis set were performed using the molecular structures published in Ref. 66. Reference interaction energies were taken from Ref. 67. The resulting optimal values are $G = 0.096240$, $s_{r,6} = 1.1882$, and $s_8 = 0.65228$. The interaction energies in S22 set are presented in Table II.

III. IMPLEMENTATION

The expression for the correlation energy is obtained after inserting Eqs. (40) and (41) into Eq. (7) and integrating with respect to λ. Below we present E_C in a form convenient for implementation,

$$E_C = E_C^{\alpha\beta} + E_C^{\beta\alpha} + E_C^{\alpha\alpha} + E_C^{\beta\beta}, \tag{46}$$

$$E_C^{\alpha\beta} = \int_0^1 V_C^{\alpha\beta,\lambda} d\lambda = \int d^3\mathbf{r}_1 \rho_\alpha \pi \frac{\mathcal{B}_{\alpha\beta} + \mathcal{A}_{\alpha\beta} d_{\alpha\beta}}{d_{\alpha\beta}^3}, \tag{47}$$

$$E_{\mathrm{C}}^{\alpha\alpha} = \int_0^1 V_{\mathrm{C}}^{\alpha\alpha,\lambda} \mathrm{d}\lambda = \int \mathrm{d}^3\mathbf{r}_1 \rho_\alpha \pi \frac{8\mathcal{B}_{\alpha\alpha} + 4\mathcal{A}_{\alpha\alpha} d_{\alpha\alpha}}{d_{\alpha\alpha}^5}, \tag{48}$$

$$\mathcal{A}_{\alpha\beta} = \frac{\rho_\beta}{r_{\mathrm{s}}^{\alpha\beta}} \left[\left(-P_0 + \sum_{k=1}^{4} P_k \left(r_{\mathrm{s}}^{\alpha\beta} \right)^k \right) \exp\left(-P_5 r_{\mathrm{s}}^{\alpha\beta} \right) + P_0 \right] - \rho_\beta, \tag{49}$$

$$\mathcal{B}_{\alpha\beta} = \frac{\rho_\beta}{\left(r_{\mathrm{s}}^{\alpha\beta} \right)^2} \left[\left(-Q_0 + \sum_{k=1}^{5} Q_k \left(r_{\mathrm{s}}^{\alpha\beta} \right)^k \right) \exp\left(- Q_6 r_{\mathrm{s}}^{\alpha\beta} \right) + Q_0 \right] + d_{\alpha\beta} \mathcal{A}_{\alpha\beta}, \tag{50}$$

$$\mathcal{A}_{\alpha\alpha} = \frac{D_\alpha}{3 r_{\mathrm{s}}^{\alpha\alpha}} \left[\left(-R_0 + \sum_{k=1}^{2} R_k \left(r_{\mathrm{s}}^{\alpha\alpha} \right)^k \right) \exp\left(-R_3 r_{\mathrm{s}}^{\alpha\alpha} \right) + R_0 \right] - \frac{D_\alpha}{3}, \tag{51}$$

$$\mathcal{B}_{\alpha\alpha} = \frac{D_\alpha}{6\left(r_{\mathrm{s}}^{\alpha\alpha} \right)^2} \left[\left(-S_0 + \sum_{k=1}^{3} S_k \left(r_{\mathrm{s}}^{\alpha\alpha} \right)^k \right) \exp\left(-S_4 r_{\mathrm{s}}^{\alpha\alpha} \right) + S_0 \right] + d_{\alpha\alpha} \mathcal{A}_{\alpha\alpha}. \tag{52}$$

Note that $E_{\mathrm{C}}^{\alpha\beta} = E_{\mathrm{C}}^{\beta\alpha}$. The formula for $E_{\mathrm{C}}^{\beta\beta}$ can be obtained by substitution of spin indices in $E_{\mathrm{C}}^{\alpha\alpha}$. The values of the numerical constants appearing in Eqs. (49)–(52) are listed in Table I. The following functions: D_α, $r_{\mathrm{s}}^{\alpha\alpha}$, and $r_{\mathrm{s}}^{\alpha\beta}$ are defined in Eqs. (23), (27), and (28), respectively. The $d_{\sigma\sigma'}$ function, defined in Eq. (45), is parametrized as follows:

$$d_{\alpha\beta} = \frac{2.1070}{r_{\mathrm{s}}^{\alpha\beta}} + \frac{0.096240}{r_{\mathrm{s}}} \frac{\nabla\rho \cdot \nabla\rho}{\rho^{8/3}}, \tag{53}$$

$$d_{\alpha\alpha} = \frac{2.6422}{r_{\mathrm{s}}^{\alpha\alpha}} + \frac{0.096240}{r_{\mathrm{s}}} \frac{\nabla\rho \cdot \nabla\rho}{\rho^{8/3}}. \tag{54}$$

The parameters appearing in DFT-D3 correction[10] are $s_{r,6} = 1.1882$ and $s_8 = 0.65228$. Fortran code for numerical evaluation of the correlation energy and its derivatives, together with the corresponding Mathematica[68] notebook, can be obtained from the authors by e-mail or from their webpage. The calculations presented in this work were done using GAMESS program.[69,70]

IV. DISCUSSION

Similar strategy for designing a correlation functional, i.e., constructing a real-space model for a spin-resolved correlation hole, was originally proposed by Rajagopal, Kimball, and Banerjee[54] with the first application by Becke,[55] followed by the works of Proynov and Salahub[71] and Tsuneda, Suzumura, and Hirao.[72] A central role in those methods is played by *correlation length*, a function completely determining both short- and long-range behavior of the correlation holes present in those models. Our approach has more degrees of freedom, as the short-range behavior of $h_{\mathrm{C}\lambda}^{\sigma\sigma'}$ is decoupled from the choice of the $d_{\sigma\sigma'}$ function which controls its decay. This flexibility allows us to adjust $d_{\sigma\sigma'}$ to match a specific NL correction without sacrificing the short-range correlation that can be accurately represented by a SL functional.

TABLE I. *Ab initio* numerical constants appearing in Eqs. (49)–(52).

k	P_k	Q_k	R_k	S_k
0	1.696	3.356	1.775	3.205
1	−0.2763	−2.525	0.01213	−1.784
2	−0.09359	−0.4500	-4.743×10^{-3}	3.613×10^{-3}
3	3.837×10^{-3}	−0.1060	0.5566	-4.743×10^{-3}
4	-2.471×10^{-3}	5.532×10^{-4}		0.5566
5	0.7524	-2.471×10^{-3}		
6		0.7524		

The ultimate goal is to develop a general-purpose functional that not only yields satisfactory results for the dispersion interactions, but also performs not worse than the existing approximations in predicting other properties of chemical interest. To do so, the inclusion of the NL constituent and the accompanying adjustment of the SL part should not affect any of the energetically important constraints already satisfied by the meta-GGA rung functionals.[73] Among the formal constraints, the most fundamental one is the non-positivity condition,

$$V_{\mathrm{C}}^{\sigma\sigma',\lambda}[\rho] \leq 0, \tag{55}$$

which is obeyed by our model for every spin-density. Similarly, the scaling conditions formulated by Levy,[61] e.g.,

$$\lim_{\kappa\to 0} \frac{E_{\mathrm{C}}[\rho_\kappa]}{\kappa} = \sum_{\sigma\sigma'} \lim_{\lambda\to\infty} V_{\mathrm{C}}^{\sigma\sigma',\lambda}[\rho] > -\infty, \tag{56}$$

$$\frac{\partial V_{\mathrm{C}}^{\sigma\sigma',\lambda}[\rho]}{\partial\lambda} \leq 0, \tag{57}$$

together with the high-density limit of the correlation functional,[74]

$$\lim_{\kappa\to\infty} E_{\mathrm{C}}[\rho_\kappa] > -\infty, \tag{58}$$

are satisfied. A failure to satisfy condition (58) may contribute to overbinding of molecules.[61]

In addition to conditions (55)–(58), our approximation satisfies a constraint which has a direct connection to the prediction of interaction energies. It was observed by Kamiya, Tsuneda, and Hirao[20] that if a SL functional yields nonzero contributions to the correlation in the tail of the density, then adding a NL correction may lead to a severe overbinding.[20] In the tail of electronic density, where the reduced gradient is

large, the $d_{\sigma\sigma'}$ function of Eq. (45) goes to infinity, thus our SL correlation correctly vanishes.

The correlation self-interaction error is corrected using τ_σ variable (the kinetic energy density), see Eq. (31), similarly to other meta-GGA correlation functionals.[55,75,76] As a result, in our model the parallel-spin correlation vanishes for single-orbital spin-compensated densities, and the total correlation energy is zero for hydrogen atom.

The above-mentioned constraints are merely formal prerequisites for a high-quality approximation to E_C. A decent approximate model should also capture the physics of molecular systems. Our model reflects the following physical properties:

1. Short-range electronic correlation is modeled by an expression borrowed from the homogeneous electron gas, which is also appropriate for real systems.[51,77–79] (See Eqs. (25), (26), and (31).) To the best of our knowledge, we present the first beyond-LDA functional which incorporates analytic representation of the short-range correlation function of the HEG developed by Gori-Giorgi and Perdew.[58]
2. Long-range behavior of the correlation hole is governed by $d_{\sigma\sigma'}$ function (see Eqs. (16), (17), and (45)), which depends on both density and its gradient at a reference point. This function accounts for damping effect of density inhomogeneity ($\nabla\rho_\sigma$) on the correlation hole. Furthermore, the $d_{\sigma\sigma'}$ function contains a free parameter, G. It is used in tuning the spatial range separation of the correlation hole to properly blend with the long-range correlation correction.
3. Our model closely approximates the exact correlation in the HEG regime at metallic densities. (See also the discussion below Eq. (45).)

To make our concept of stitching SL and NL correlation more transparent, we briefly discuss it in the context of range-separated approach of Kohn, Meir, and Makarov.[80] It is possible to solve the dispersion problem within DFT by partitioning the interelectron repulsion, $1/r$, into short-range part, $\exp(-\mu r)/r$, and its long-range complement.[80] (μ is a constant.) Both short-range exchange and correlation are then treated at (semi)local level, and the contributions originating from the long-range interaction are approximated by a formula that is consistent with the Casimir-Polder expression in the asymptotic region. Our treatment follows the same general idea. The difference is as follows: the exponential factor that damps the interelectronic interaction, $\exp(-\mu r)$, is replaced by the $\exp(-d_{\sigma\sigma'}r)$ function of Eqs. (16) and (17) which damps the short range expansion of the approximate correlation holes. Thus, the μ constant is generalized into $d_{\sigma\sigma'}$ function, which depends on density and its gradient at a reference point.

V. NUMERICAL RESULTS

Our aim was to validate the correlation functional presented in this work, preferably without the interference from the errors of an exchange approximation. Therefore, we decided to perform calculations using our correlation combined with full HF-like exchange, and to compare it with other DFAs involving full HF-like exchange. Although a general-purpose approximation cannot be formed by combining semilocal DFT correlation with full exact exchange, it is

TABLE II. Interaction energies in S22 set (kcal/mol).

Dimer	E_{ref}	E_{int}	$E_{dispfree}$
Hydrogen-bonded			
$(NH_3)_2$	− 3.145	− 2.75	− 2.17
$(H_2O)_2$	− 5.004	− 4.86	− 4.41
Formic acid dimer	− 18.751	− 20.17	− 18.75
Formamide dimer	− 16.063	− 16.46	− 14.86
Uracil dimer planar (C_{2h})	− 20.643	− 21.30	− 19.10
2-pyridone · 2-aminopyridine	− 16.938	− 16.33	− 13.67
Adenine · thymine WC	− 16.554	− 16.15	− 13.24
MSE	− 0.13		
MUE	0.58		
MAPE	5.0		
Predominant dispersion			
$(CH_4)_2$	− 0.529	− 0.60	0.14
$(C_2H_4)_2$	− 1.482	− 1.52	− 0.15
Benzene · CH_4	− 1.448	− 1.45	0.10
Benzene dimer parallel-displaced (C_{2h})	− 2.655	− 1.76	2.55
Pyrazine dimer	− 4.256	− 3.36	0.99
Uracil dimer stacked (C_2)	− 9.783	− 9.97	− 3.63
Indole · benzene stacked	− 4.523	− 3.25	2.73
Adenine · thymine stacked	− 11.857	− 11.63	− 3.10
MSE	0.37		
MUE	0.45		
MAPE	13		
Mixed interaction			
Ethene · ethyne	− 1.503	− 1.63	− 0.91
Benzene H_2O	− 3.280	− 3.78	− 2.19
Benzene NH_3	− 2.319	− 2.55	− 0.92
Benzene HCN	− 4.540	− 5.68	− 4.02
Benzene dimer T-shaped (C_{2v})	− 2.717	− 2.72	− 0.18
Indole · benzene T-shaped	− 5.627	− 5.89	− 2.45
Phenol dimer	− 7.097	− 6.87	− 3.96
MSE	− 0.29		
MUE	0.36		
MAPE	9.5		
MSE (total)	0.002		
MUE (total)	0.46		
MAPE (total)	9.3		

TABLE III. Interaction energies in WI7/05 set (kcal/mol).

Dimer	E_{ref}	E_{int}	E_{M06HF}
He · · · Ne	− 0.041	− 0.037	− 0.13
He · · · Ar	− 0.058	− 0.045	− 0.085
Ne · · · Ne	− 0.086	− 0.064	− 0.13
Ne · · · Ar	− 0.13	− 0.07	− 0.15
CH_4 · · · Ne	− 0.18	− 0.18	− 0.20
C_6H_6 · · · Ne	− 0.41	− 0.53	− 0.66
CH_4 · · · CH_4	− 0.53	− 0.59	− 0.12
MSE		− 0.01	− 0.006
MUE		0.04	0.12
MAPE		21	68

TABLE IV. Interaction energies in PPS5/05 set (kcal/mol).

Dimer	E_{ref}	E_{int}	E_{M06HF}
$(C_2H_2)_2$	− 1.36	− 1.47	− 1.06
$(C_2H_4)_2$	− 1.44	− 1.52	− 0.95
Sandwich $(C_6H_6)_2$	− 1.65	− 0.95	0.48
T-shaped $(C_6H_6)_2$	− 2.63	− 2.78	− 1.95
Displaced $(C_6H_6)_2$	− 2.59	− 2.06	− 0.94
MSE		0.18	1.0
MUE		0.31	1.0
MAPE		16	55

a demanding and useful test for a correlation functional. If the correlation functional performs well with large portion of the exact exchange, then there is much room for adjusting the exchange part of a global hybrid or a range-separated hybrid exchange-correlation functional.

All DFT and HF calculations presented below were performed in aug-cc-pVTZ basis. All energies are obtained from self-consistent calculations. Table II contains interaction energies for S22 set of molecules.[66] The reference energies, E_{ref}, are taken from Ref. 67. E_{int} denotes interaction energy calculated using the correlation functional described in this work combined with 100% HF-like exchange and DFT-D3 correction. All energies, as well as mean signed errors (MSE) and mean unsigned errors (MUE) are given in kcal/mol. MAPE are given in percent. Our results (MUE = 0.46 kcal/mol) compare rather favorably to the other methods utilizing full HF-like exchange, VV09 (Ref. 25) (MUE = 0.90 kcal/mol), M06HF[34,81] (MUE = 0.62 kcal/mol), and M06HF-D3[34,81] (MUE = 0.84 kcal/mol). The dispersion-free interaction energies are always significantly below the values that would be obtained if the dispersion term as defined in SAPT was subtracted, see supplementary information in Refs. 18 and 82. This fact suggests that in our model, at equilibrium distances, a large fraction of the dispersion interaction is treated as short-range and accounted for by the SL functional.

We further evaluate the performance of our approximation on the set of systems from nonbonded interaction database of Zhao and Truhlar.[83,84] This database gathers interacting dimers in subsets according to the dominant character of the interaction: dispersion-dominated (WI7/05 and PPS5/05 subsets), dipole interaction (DI6/04 subset), hydrogen-bonded (HB6/04), and charge transfer (CT7/04).

TABLE V. Interaction energies in DI6/04 set (kcal/mol).

Dimer	E_{ref}	E_{int}	E_{M06HF}
$H_2S\cdots H_2S$	− 1.62	− 1.20	− 0.82
$HCl\cdots HCl$	− 1.91	− 1.40	− 0.99
$HCl\cdots H_2S$	− 3.26	− 2.74	− 2.48
$CH_3Cl\cdots HCl$	− 3.39	− 2.77	− 2.72
$CH_3SH\cdots HCN$	− 3.58	− 3.70	− 3.50
$CH_3SH\cdots HCl$	− 4.74	− 4.13	− 4.27
MSE		0.43	0.62
MUE		0.47	0.62
MAPE		17	26

TABLE VI. Interaction energies in HB6/04 set (kcal/mol).

Dimer	E_{ref}	E_{int}	E_{M06HF}
$NH_3\cdots NH_3$	− 3.09	− 2.82	− 2.53
$HF\cdots HF$	− 4.49	− 4.63	− 4.27
$H_2O\cdots H_2O$	− 4.91	− 4.90	− 4.72
$NH_3\cdots H_2O$	− 6.38	− 6.28	− 6.35
$(HCONH_2)_2$	− 15.41	− 16.39	− 15.72
$(HCOOH)_2$	− 17.60	− 19.57	− 19.33
MSE		− 0.45	0.28
MUE		0.58	0.30
MAPE		5.2	4.6

The results are presented in Tables III–VII, respectively. The reference energies (E_{ref}) are calculated at CCSD(T)/mb-aug-cc-pVTZ level, see Ref. 18. We compare our approximation (E_{int}) with M06HF functional[81] (E_{M06HF}) which combines empirically-parametrized meta-GGA correlation with full HF-like exchange. As expected, our model predicts interaction energies more accurately in cases where the dispersion interaction dominates, see Tables III and IV. In case of hydrogen bonded complexes, Table VI, MAPE of either functional is close to 5%. Larger errors are present in DI6/04 and CT7/04 subsets. Although our approximation performs better that M06HF in case of DI6/04 dimers, the error is rather large. In this case, as is seen in Table V, both functionals underestimate the interaction strength and their errors are correlated. This fact suggests that the contribution coming from full HF-like exchange is too repulsive, which cannot be counterbalanced by semilocal DFT correlation. Both functionals display largest errors in charge-transfer complexes. Our approximation underestimates interaction for every CT complex. This behavior to a large degree results from huge errors of the HF theory itself, see E_{HF} column in Table VII. As explained by Cohen, Mori-Sánchez, and Yang[3] this problem can be traced to the localization error of the HF theory, which makes electrons excessively localized on the monomers. This error manifests itself as a concave curve of energy vs. fractional number of electrons, $E(N)$.[3] It is also known that pure semilocal DFT approximations give convex $E(N)$.[3] See Ref. 82 for the relevant discussion of $NH_3\cdots ClF$ dimer. Therefore, adding some amount of semilocal exchange to our approximation should make the $E(N)$ dependence more linear and make the

TABLE VII. Interaction energies CT7/04 (kcal/mol).

Dimer	E_{ref}	E_{int}	E_{M06HF}	E_{HF}
$C_2H_4\cdots F_2$	− 1.06	− 0.33	− 0.67	0.71
$NH_3\cdots F_2$	− 1.80	− 0.74	− 0.90	0.19
$C_2H_2\cdots ClF$	− 3.79	− 2.98	− 4.18	− 0.16
$HCN\cdots ClF$	− 4.80	− 3.70	− 4.02	− 2.10
$NH_3\cdots Cl_2$	− 4.85	− 3.50	− 4.00	− 1.12
$H_2O\cdots ClF$	− 5.20	− 4.69	− 5.26	− 2.91
$NH_3\cdots ClF$	− 11.17	− 10.53	− 11.92	− 5.49
MSE		0.89	0.24	
MUE		0.89	0.59	
MAPE		31	20	

exchange contribution in CT interactions less repulsive, the step which will be undertaken in the future.

VI. CONCLUSIONS

This paper presents a novel form of a SL correlation functional belonging to the meta-GGA rung that may be combined in an optimal way with the dispersion interaction component, either in the DFT+D manner or by incorporating a nonlocal potential. The important feature is that it is based on the first principles, in the form of a number of physical constraints imposed during the derivation. With minimal empiricism, our approximation is adjusted to a desired long-range dispersion correction by optimizing only a single empirical parameter. The parameter has a clear physical meaning: it governs the decay of the approximate correlation hole. Consequently, the correlation hole vanishes exponentially at large inter-electronic distances, which prevents double counting of the electron correlation effect that is already included when adding the long-range dispersion correction. An important and unique facet of our functional is that the adjustment of the empirical range-separation parameter has *not* relaxed any of the physical constraints on which our model is based. The electron correlation is approximated by utilizing several numerical and analytical results of the HEG model. Most importantly, the HEG approximation to the short-range part of the correlation hole is rigorously conserved for arbitrary systems (only the self-interaction pertinent to the HEG model is removed from the parallel-spin correlation hole).

While our new correlation functional can be combined with any of non-local dispersion models, for preliminary calculations of this paper, we employed the atom pairwise additive DFT-D3 dispersion correction. Given the fact that our correlation functional is combined with 100% HF exchange – far from an optimal choice in general case – the numerical results are very encouraging. For the interaction energies of hydrogen-bonded complexes, the accuracy is on a par with that obtained with the M06HF functional, which is a highly parametrized empirical approximation containing full HF exchange. For dispersion-dominated complexes, the predictions of our model compare favorably with VV09 and M06HF. The results in the subsets of dipole-interaction and charge-transfer complexes are less satisfactory, which is easily explained by the inadequacy of the full HF-like exchange component: indeed, the signed errors correlate with the signed errors of the HF method. Obviously, much improvement may be expected when a more appropriate exchange part will be incorporated. Development of an optimal range-separated hybrid exchange approximation, appropriate for our new correlation functional, as well as implementation of non-local van der Waals correlation functionals are underway in our laboratory.

ACKNOWLEDGMENTS

This work was supported by the Polish Ministry of Science and Higher Education, Grant No. N204 248440, and by the National Science Foundation (US), Grant No. CHE-1152474.

[1] J. Dobson, in *Fundamentals of Time-Dependent Density Functional Theory*, Lecture Notes in Physics, Vol. 837, edited by M. A. Marques, N. T. Maitra, F. M. Nogueira, E. Gross, and A. Rubio (Springer, Berlin/Heidelberg, 2012), p. 417.
[2] J. F. Dobson, J. Wang, B. P. Dinte, K. McLennan, and H. M. Le, Int. J. Quantum Chem. **101**, 579 (2005).
[3] A. J. Cohen, P. Mori-Sánchez, and W. Yang, Chem. Rev. **112**, 289 (2012).
[4] J. Dobson and T. Gould, J. Phys.: Condens. Matter **24**, 073201 (2012).
[5] A. Becke and E. Johnson, J. Chem. Phys. **122**, 154104 (2005).
[6] A. Becke and E. Johnson, J. Chem. Phys. **123**, 154101 (2005).
[7] A. Becke and E. Johnson, J. Chem. Phys. **127**, 124108 (2007).
[8] A. Heßelmann, J. Chem. Phys. **130**, 084104 (2009).
[9] J. Ángyán, J. Chem. Phys. **127**, 024108 (2007).
[10] S. Grimme, J. Antony, S. Ehrlich, and H. Krieg, J. Chem. Phys. **132**, 154104 (2010).
[11] A. Tkatchenko and M. Scheffler, Phys. Rev. Lett. **102**, 073005 (2009).
[12] M. Dion, H. Rydberg, E. Schröder, D. Langreth, and B. Lundqvist, Phys. Rev. Lett. **92**, 246401 (2004).
[13] K. Lee, É. Murray, L. Kong, B. Lundqvist, and D. Langreth, Phys. Rev. B **82**, 081101 (2010).
[14] O. Vydrov and T. Van Voorhis, J. Chem. Phys. **130**, 104105 (2009).
[15] O. Vydrov and T. Van Voorhis, Phys. Rev. Lett. **103**, 63004 (2009).
[16] O. Vydrov and T. Van Voorhis, J. Chem. Phys. **133**, 244103 (2010).
[17] O. Vydrov, and T. Voorhis, in *Fundamentals of Time-Dependent Density Functional Theory*, Lecture Notes in Physics, Vol. 837, edited by M. A. Marques, N. T. Maitra, F. M. Nogueira, E. Gross, and A. Rubio (Springer, Berlin/Heidelberg, 2012), pp. 443–456.
[18] K. Pernal, R. Podeszwa, K. Patkowski, and K. Szalewicz, Phys. Rev. Lett. **103**, 263201 (2009).
[19] Ł. Rajchel, P. Żuchowski, M. M. Szczęśniak, and G. Chałasiński, Chem. Phys. Lett. **486**, 160 (2010).
[20] M. Kamiya, T. Tsuneda, and K. Hirao, J. Chem. Phys. **117**, 6010 (2002).
[21] E. D. Murray, K. Lee, and D. C. Langreth, J. Chem. Theory Comput. **5**, 2754 (2009).
[22] J. Perdew, K. Burke, and M. Ernzerhof, Phys. Rev. Lett. **77**, 3865 (1996).
[23] A. D. Becke, Phys. Rev. A **38**, 3098 (1988).
[24] J. P. Perdew and W. Yue, Phys. Rev. B **33**, 8800 (1986).
[25] O. Vydrov and T. Van Voorhis, J. Chem. Phys. **132**, 164113 (2010).
[26] S. Grimme and S. Ehrlich, J. Comput. Chem. **32**, 1456 (2011).
[27] J. Dobson, K. McLennan, A. Rubio, J. Wang, T. Gould, H. Le, and B. Dinte, Aust. J. Chem. **54**, 513 (2002).
[28] A. Hesselmann and G. Jansen, Chem. Phys. Lett. **367**, 778 (2003).
[29] A. Misquitta, R. Podeszwa, B. Jeziorski, and K. Szalewicz, J. Chem. Phys. **123**, 214103 (2005).
[30] A. Koide, J. Phys. B **9**, 3173 (1976).
[31] R. Burcl, G. Chałasiński, R. Bukowski, and M. M. Szczęśniak, J. Chem. Phys. **103**, 1498 (1995).
[32] A. Koide, W. J. Meath, and A. Allnatt, Chem. Phys. **58**, 105 (1981).
[33] L. A. Burns, A. Vazquez-Mayagoitia, B. G. Sumpter, and C. D. Sherrill, J. Chem. Phys. **134**, 084107 (2011).
[34] L. Goerigk and S. Grimme, Phys. Chem. Chem. Phys. **13**, 6670 (2011).
[35] W. Hujo and S. Grimme, J. Chem. Theory Comput. **7**, 3866 (2011).
[36] A. Vazquez-Mayagoitia, C. D. Sherrill, E. Apra, and B. G. Sumpter, J. Chem. Theory Comput. **6**, 727 (2010).
[37] K. S. Thanthiriwatte, E. G. Hohenstein, L. A. Burns, and C. D. Sherrill, J. Chem. Theory Comput. **7**, 88 (2011).
[38] S. Grimme, J. Comput. Chem. **27**, 1787 (2006).
[39] J. Chai and M. Head-Gordon, Phys. Chem. Chem. Phys. **10**, 6615 (2008).
[40] J. Chai and M. Head-Gordon, J. Chem. Phys. **128**, 084106 (2008).
[41] E. Ruiz, D. Salahub, and A. Vela, J. Phys. Chem. **100**, 12265 (1996).
[42] G. Sini, J. S. Sears, and J.-L. Bredas, J. Chem. Theory Comput. **7**, 602 (2011).
[43] R. Podeszwa, K. Pernal, K. Patkowski, and K. Szalewicz, J. Phys. Chem. Lett. **1**, 550 (2010).
[44] M. Swart, M. Solà, and F. Bickelhaupt, J. Chem. Phys. **131**, 094103 (2009).
[45] A. D. Becke, J. Chem. Phys. **107**, 8554 (1997).
[46] M. Levy, Proc. Natl. Acad. Sci. U.S.A. **76**, 6062 (1979).
[47] P. Hohenberg and W. Kohn, Phys. Rev. **136**, B864 (1964).
[48] W. Kohn and L. J. Sham, Phys. Rev. **140**, A1133 (1965).
[49] M. Levy, in *Theoretical and Computational Chemistry*, edited by J. Seminario (Elsevier, 1996), Vol. 4.
[50] E. Baerends and O. Gritsenko, J. Phys. Chem. A **101**, 5383 (1997).
[51] K. Burke, J. Perdew, and M. Ernzerhof, J. Chem. Phys. **109**, 3760 (1998).
[52] A. Sarsa, F. Gálvez, and E. Buendia, J. Chem. Phys. **109**, 7075 (1998).

[53]J. Hollett, L. McKemmish, and P. Gill, J. Chem. Phys. **134**, 224103 (2011).
[54]A. Rajagopal, J. Kimball, and M. Banerjee, Phys. Rev. B **18**, 2339 (1978).
[55]A. Becke, J. Chem. Phys. **88**, 1053 (1988).
[56]C. Lee and R. Parr, Phys. Rev. A **35**, 2377 (1987).
[57]A. Becke, Can. J. Chem. **74**, 995 (1996).
[58]P. Gori-Giorgi and J. Perdew, Phys. Rev. B **64**, 155102 (2001).
[59]A. Overhauser, Can. J. Phys. **73**, 683 (1995).
[60]V. Rassolov, J. Pople, and M. Ratner, Phys. Rev. B **62**, 2232 (2000).
[61]M. Levy, Phys. Rev. A **43**, 4637 (1991).
[62]M. Levy and J. Perdew, Phys. Rev. A **32**, 2010 (1985).
[63]P. Gori-Giorgi, F. Sacchetti, and G. Bachelet, Phys. Rev. B **61**, 7353 (2000).
[64]G. Ortiz, M. Harris, and P. Ballone, Phys. Rev. Lett. **82**, 5317 (1999).
[65]M. Gell-Mann and K. A. Brueckner, Phys. Rev. **106**, 364 (1957).
[66]P. Jurecka, J. Sponer, J. Cerny, and P. Hobza, Phys. Chem. Chem. Phys. **8**, 1985 (2006).
[67]R. Podeszwa, K. Patkowski, and K. Szalewicz, Phys. Chem. Chem. Phys. **12**, 5974 (2010).
[68]*Mathematica*, Wolfram Research, Inc., Champaign, Illinois, 7th ed. (2008).
[69]M. W. Schmidt, K. K. Baldridge, J. A. Boatz, S. T. Elbert, M. S. Gordon, J. H. Jensen, S. Koseki, N. Matsunaga, K. A. Nguyen, S. Su, T. L. Windus, M. Dupuis, and J. A. Montgomery, J. Comput. Chem. **14**, 1347 (1993).
[70]M. S. Gordon, and M. W. Schmidt, "Advances in electronic structure theory: GAMESS a decade later," in *Theory and Applications of Computational Chemistry: The First Forty Years*, edited by C. E. Dykstra, G. Frenking, K. S. Kim, and G. E. Scuseria (Elsevier, Amsterdam, 2005), p. 1167.
[71]E. I. Proynov and D. R. Salahub, Phys. Rev. B **49**, 7874 (1994).
[72]T. Tsuneda, T. Suzumura, and K. Hirao, J. Chem. Phys. **110**, 10664 (1999).
[73]J. Perdew, A. Ruzsinszky, J. Tao, V. Staroverov, G. Scuseria, and G. Csonka, J. Chem. Phys. **123**, 062201 (2005).
[74]M. Levy, Int. J. Quantum Chem. **36**, 617 (1989).
[75]J. P. Perdew, S. Kurth, A. Zupan, and P. Blaha, Phys. Rev. Lett. **82**, 2544 (1999).
[76]Y. Zhao, N. Schultz, and D. Truhlar, J. Chem. Theory Comput. **2**, 364 (2006).
[77]K. Burke, J. Perdew, and D. Langreth, Phys. Rev. Lett. **73**, 1283 (1994).
[78]T. Henderson and R. Bartlett, Phys. Rev. A **70**, 22512 (2004).
[79]A. C. Cancio, C. Y. Fong, and J. S. Nelson, Phys. Rev. A **62**, 062507 (2000).
[80]W. Kohn, Y. Meir, and D. E. Makarov, Phys. Rev. Lett. **80**, 4153 (1998).
[81]Y. Zhao and D. Truhlar, Theor. Chem. Acc. **120**, 215 (2008).
[82]M. Modrzejewski, Ł. Rajchel, M. M. Szczęśniak, and G. Chałasiński, J. Chem. Phys. **136**, 204109 (2012).
[83]Y. Zhao and D. Truhlar, J. Phys. Chem. A **109**, 5656 (2005).
[84]Y. Zhao and D. Truhlar, J. Chem. Theory Comput. **1**, 415 (2005).

Appendix B

Paper II: J. Chem. Theory Comput. 10, 4297 (2014)

JCTC Journal of Chemical Theory and Computation

Article

pubs.acs.org/JCTC

Range-Separated meta-GGA Functional Designed for Noncovalent Interactions

Marcin Modrzejewski,*[,†] Grzegorz Chałasiński,[†] and Małgorzata M. Szczęśniak[‡]

[†]Faculty of Chemistry, University of Warsaw, 02-093 Warsaw, Pasteura 1, Poland

[‡]Department of Chemistry, Oakland University, Rochester, Michigan 48309-4477, United States

ABSTRACT: The accuracy of applying density functional theory to noncovalent interactions is hindered by errors arising from low-density regions of interaction-induced change in the density gradient, error compensation between correlation and exchange functionals, and dispersion double counting. A new exchange−correlation functional designed for noncovalent interactions is proposed to address these problems. The functional consists of the range-separated PBEsol exchange considered in two variants, pure and hybrid, and the semilocal correlation functional of Modrzejewski et al. (*J. Chem. Phys.* **2012**, *137*, 204121) designed with the constraint satisfaction technique to smoothly connect with a dispersion term. Two variants of dispersion correction are appended to the correlation functional: the atom−atom pairwise additive DFT-D3 model and the density-dependent many-body dispersion with self-consistent screening (MBD-rsSCS). From these building blocks, a set of four functionals is created to systematically examine the role of pure versus hybrid exchange and the underlying models for dispersion. The new functional is extensively tested on benchmark sets with diverse nature and size. Truly outstanding performance is demonstrated for water clusters of varying size, ionic hydrogen bonds, and thermochemistry of isodesmic *n*-alkane fragmentation reactions. The merits of each component of the new functional are discussed.

1. INTRODUCTION

DFT is one of the few quantum-chemical methods capable of dealing with problems germane to molecular biology and materials science that involve electronic structure, yet on a scale too large for ab initio wave function tools. So far, however, the approximate character of affordable functionals seriously restricts their predictive power in several important areas, the most prominent ones being related to noncovalently bound systems. An approximate functional focused on performance for noncovalent interactions is the subject of this work.

During the past decade, a large effort has been devoted to resolve the deficiencies in the description of noncovalent interactions. The progress has been indicated by steady improvement of statistical errors in databases of noncovalent interactions.[1,2] Still, part of this apparent advancement is a result of error cancellation between the dispersion-free part of a functional and its a posteriori dispersion correction. Consequently, even for the best performing methods, there exist systems for which the cancellation does not occur and error spikes beyond the average levels. Examples of such problematic systems are water clusters studied in this work.

A practical chemist copes with the issue of large unpredictable errors by cross-checking her calculations with several independent approximate functionals. Thus, to make DFT a dependable tool, we still need new functionals developed independently from the currently existing ones and built from well-defined components, which do not exploit obscure error cancellation.

This work introduces a set of new DFT exchange−correlation functionals intended primarily for noncovalent interactions. They are composed of the recent meta-GGA correlation developed by Modrzejewski et al.,[3] the range-separated PBEsol exchange[4−6] (ωPBEsol), and a dispersion correction,

$$E_{XC} = E_C + E_X(\omega\text{PBEsol}) + E_{disp} \quad (1)$$

The two variants of the dispersion correction employed in this work are DFT-D3 by Grimme et al.[7] (abbreviated as D3) and MBD-rsSCS by Ambrosetti el al.[8] (abbreviated as MBD). There are other possible ways of including dispersion not explored here.[9−12] Furthermore, we assess two variants of short-range exchange: pure PBEsol and a hybrid with an addition of the short-range HF exchange. For brevity, the full exchange will be called either *pure* or *hybrid* depending on the fraction of the short-range exact exchange. In total, there are four combinations of the exchange and dispersion components: MCS-D3, MCS-MBD, MCSh-D3, and MCSh-MBD, where the first part of the label denotes the exchange approximation (MCS for the pure exchange and MCSh for the hybrid) and the

Received: April 23, 2014
Published: September 3, 2014

second part specifies the dispersion correction. This set of functionals will be collectively referred to as MCS.

The MCS functionals are designed to overcome several issues of the currently available exchange−correlation approximations.

First, a part of the difficulties in the description of noncovalent systems can be pinpointed to the poor behavior of approximate exchange functionals in the low-density regions where the density gradient changes substantially upon bond formation.[13,14] The emergence of such regions is the signature of noncovalent bonding[15] and is the source of major contributions to the interaction energy.[13,14] For example, depending on the limit of an exchange enhancement factor for large reduced gradients, the exchange-only interaction curve of a noble gas dimer can be either attractive (as in PBE) or much more repulsive than the Hartree−Fock limit (as in B88).[16] Although the behavior of the exchange is not decisive for the performance of the full exchange−correlation functional due to the possible error cancellation, it may obscure the interpretation of interaction energies and eventually worsen the compatibility with dispersion corrections. One way of ensuring that DFT exchange-only interaction curves resemble the Hartree−Fock ones is by employing range-separated exchange functionals.[17] Also, inclusion of the exact second-order gradient expansion of the exchange functional improves description of the regions relevant for noncovalent systems.[5,18] The ωPBEsol exchange included in the MCS functionals combines both of these remedies.

The second problem with the existing DFT treatments of noncovalent interactions is that a dispersion correction, such as D3, tends to disguise the shortcomings of the base semilocal functional. This may lead to an inconsistency that the *long-range* dispersion correction calibrated for an underbinding semilocal functional becomes larger than the reference value of the *total* dispersion as obtained from the SAPT approach.[19] A BLYP-D3 treatment of complexes from the S22 database serves as an example of such an inconsistency. We discuss this issue later in the text.

The third possible source of errors is double counting of short-range correlation by a semilocal correlation functional and a dispersion correction. The semilocal correlation model employed here is designed to avoid this issue via the design of the corresponding correlation hole. The hole is equipped with a single empirical parameter to control its range. To eliminate the overlap with the dispersion correction, the damping of the hole for large r_{12} is adjusted through empirical optimization.[3]

Some of the features of a density functional deemed here important for noncovalent systems have been recognized and built into the ωB97X-D[20] and ωB97X-D3[21] functionals. Both of these models employ range-separated exchange and have 15 empirical parameters in their energy expressions optimized simultaneously with the dispersion corrections. (A systematic analysis of the B97-type functionals has demonstrated, however, that the number of empirical parameters should be reduced to improve the performance outside the training sets.[22]) The dispersionless density functional of Pernal et al.[23] is also an example of a heavily parametrized functional designed to be used in combination with a dispersion term.

2. THEORY

2.1. Semilocal Correlation. The first term of eq 1, E_C, stands for the recently proposed correlation functional of Modrzejewski et al.[3] The functional has been derived starting from a meta-GGA model for the spin-resolved correlation hole,

$$h_{C\lambda}^{\alpha\beta}(\mathbf{r}_1, r_{12}) = (a_{\alpha\beta} + b_{\alpha\beta}r_{12} + c_{\alpha\beta}r_{12}^2)\exp(-d_{\alpha\beta}r_{12}) \tag{2}$$

$$h_{C\lambda}^{\alpha\alpha}(\mathbf{r}_1, r_{12}) = r_{12}^2(a_{\alpha\alpha} + b_{\alpha\alpha}r_{12} + c_{\alpha\alpha}r_{12}^2)\exp(-d_{\alpha\alpha}r_{12}) \tag{3}$$

where $a_{\sigma\sigma'}$, $b_{\sigma\sigma'}$, and $c_{\sigma\sigma'}$ are functions of density at a given point, obtained from analytic formulas for the short-range (small r_{12}) part of the pair correlation function in the homogeneous electron gas.[24,25] These formulas were modified to include dependence on the kinetic energy density to eliminate the spurious self-interaction in the parallel-spin part.[3] The only empirical parameter of the correlation model, G, governs the exponential damping,

$$d_{\alpha\beta} = \frac{2.1070}{r_s^{\alpha\beta}} + d_{\mathrm{grad}} \tag{4}$$

$$d_{\alpha\alpha} = \frac{2.6422}{r_s^{\alpha\alpha}} + d_{\mathrm{grad}} \tag{5}$$

$$d_{\mathrm{grad}} = \frac{G}{r_s}\frac{\nabla\rho \times \nabla\rho}{\rho^{8/3}} \tag{6}$$

The larger the numerical value of G, the more short-ranged is the character of $h_{C\lambda}^{\sigma\sigma'}(\mathbf{r}_1, r_{12})$. Thus, G can be optimized to adjust the range of the approximate correlation hole to complement, in the manner that avoids double counting, the long-range correlation contributed by the selected variant of a dispersion correction. It should be emphasized that all the exact constraints that are built into our correlation model are obeyed when varying the value of G.[3] In particular, the short-range Taylor expansion of $h_{C\lambda}^{\sigma\sigma'}(\mathbf{r}_1, r_{12})$, which has been accurately modeled after the homogeneous electron gas,[24] remains unchanged when tuning the correlation functional to a specific dispersion correction and an exchange functional. Put differently, the empirical adjustment applied to merge the long-range dispersion with the semilocal correlation does not adversely affect the features that are reliable already at the semilocal level.[26]

For reader's convenience, we present E_C in a form ready for implementation. Following ref 3, E_C is represented as a sum of spin-parallel and antiparallel components

$$E_C = E_C^{\alpha\beta} + E_C^{\beta\alpha} + E_C^{\alpha\alpha} + E_C^{\beta\beta} \tag{7}$$

As for any semilocal functional, E_C is evaluated by numerically integrating the density of the correlation energy on a molecular grid

$$E_C^{\alpha\beta} = \frac{1}{2}\int \mathrm{d}^3\mathbf{r}_1 \int_0^1 \mathrm{d}\lambda \int_0^\infty \frac{\rho_\alpha(\mathbf{r}_1)h_{C\lambda}^{\alpha\beta}(\mathbf{r}_1, r_{12})}{r_{12}} 4\pi r_{12}^2 \mathrm{d}r_{12} = \int \mathrm{d}^3\mathbf{r}_1 \rho_\alpha \pi \frac{\mathcal{B}_{\alpha\beta} + \mathcal{A}_{\alpha\beta}d_{\alpha\beta}}{d_{\alpha\beta}^3} \tag{8}$$

$$E_C^{\alpha\alpha} = \frac{1}{2}\int \mathrm{d}^3\mathbf{r}_1 \int_0^1 \mathrm{d}\lambda \int_0^\infty \frac{\rho_\alpha(\mathbf{r}_1)h_{C\lambda}^{\alpha\alpha}(\mathbf{r}_1, r_{12})}{r_{12}} 4\pi r_{12}^2 \mathrm{d}r_{12} = \int \mathrm{d}^3\mathbf{r}_1 \rho_\alpha \pi \frac{8\mathcal{B}_{\alpha\alpha} + 4\mathcal{A}_{\alpha\alpha}d_{\alpha\alpha}}{d_{\alpha\alpha}^5} \tag{9}$$

The integral over the coupling constant λ is done analytically. $\mathcal{A}_{\alpha\beta}$, $\mathcal{B}_{\alpha\beta}$, $\mathcal{A}_{\alpha\alpha}$, $\mathcal{B}_{\alpha\alpha}$, $d_{\alpha\beta}$, and $d_{\alpha\alpha}$ are functions evaluated at each grid point

$$\mathcal{A}_{\alpha\beta} = \frac{\rho_\beta}{r_s^{\alpha\beta}}[(-P_0 + \sum_{k=1}^{4} P_k (r_s^{\alpha\beta})^k)\exp(-P_5 r_s^{\alpha\beta}) + P_0] - \rho_\beta \tag{10}$$

$$\mathcal{B}_{\alpha\beta} = \frac{\rho_\beta}{(r_s^{\alpha\beta})^2}[(-Q_0 + \sum_{k=1}^{5} Q_k (r_s^{\alpha\beta})^k)\exp(-Q_6 r_s^{\alpha\beta}) + Q_0] + d_{\alpha\beta}\mathcal{A}_{\alpha\beta} \tag{11}$$

$$\mathcal{A}_{\alpha\alpha} = \frac{D_\alpha}{3r_s^{\alpha\alpha}}[(-R_0 + \sum_{k=1}^{2} R_k (r_s^{\alpha\alpha})^k)\exp(-R_3 r_s^{\alpha\alpha}) + R_0] - \frac{D_\alpha}{3} \tag{12}$$

$$\mathcal{B}_{\alpha\alpha} = \frac{D_\alpha}{6(r_s^{\alpha\alpha})^2}[(-S_0 + \sum_{k=1}^{3} S_k (r_s^{\alpha\alpha})^k)\exp(-S_4 r_s^{\alpha\alpha}) + S_0] + d_{\alpha\alpha}\mathcal{A}_{\alpha\alpha} \tag{13}$$

The symbols in eqs 4−6 and eqs 8−13 are defined as follows: ρ_α and ρ_β are electronic spin-densities; ρ is the total electronic density, and τ_α is the kinetic energy density

$$\tau_\alpha = \sum_{i}^{N_\alpha} |\nabla \psi_{i\alpha}|^2 \tag{14}$$

The variable D_α appearing in the parallel-spin part depends on the electron density, its gradient, and τ_α

$$D_\alpha = \tau_\alpha - \frac{|\nabla \rho_\alpha|^2}{4\rho_\alpha} \tag{15}$$

$r_s^{\alpha\alpha}$, $r_s^{\alpha\beta}$, and r_s depend only on electron (spin)-densities

$$r_s^{\alpha\alpha} = \frac{(3/\pi)^{1/3}}{2\rho_\alpha^{1/3}} \tag{16}$$

$$r_s^{\alpha\beta} = \frac{(3/\pi)^{1/3}}{\rho_\alpha^{1/3} + \rho_\beta^{1/3}} \tag{17}$$

$$r_s = \left(\frac{3}{4\pi\rho}\right)^{1/3} \tag{18}$$

$E_C^{\beta\beta}$ is obtained by relabeling the spin indices in $E_C^{\alpha\alpha}$; note also that the equality $E_C^{\alpha\beta} = E_C^{\beta\alpha}$ holds. The only empirical parameter in the correlation functional is G (Table 1). The nonempirical parameters appearing in eqs 10−13 are derived from a short-range model of the correlation hole in the homogeneous electron gas.[3] Their values are defined in Table 2.

2.2. Dispersion Correction. The semilocal exchange−correlation functional is supplemented with a dispersion correction. To confirm the versatility of our approach, we assess two models of the dispersion interaction: D3[7] and MBD.[8]

The dispersion energy in the D3 approximation is defined as

Table 1. Empirical Parameters of the Four Tested MCS Functionals[a]

name	MCS	MCSh	definition
G	0.075	0.100	eq 6
ω	0.300	0.200	eq 24
α	0.000	0.200	eq 23
D3 dispersion			
r_6	1.1822	1.2900	eq 20
s_8	0.7740	1.3996	eq 19
MBD dispersion			
β	0.8033	0.7242	eq 22

[a]The columns labeled "MCS" and "MCSh" correspond to the pure and hybrid variants of the exchange, respectively.

$$E_{\text{disp}}(\text{D3}) = \sum_{AB}\sum_{n=6,8} s_n \frac{C_n^{AB}}{R_{AB}^n} f_n(R_{AB}) \tag{19}$$

$$f_n(R_{AB}) = \frac{1}{1 + 6(R_{AB}/(r_n R_0^{AB}))^{-\alpha_n}} \tag{20}$$

The D3 model contains two empirical functional-dependent parameters:[7] s_8 and r_6. Other parameters appearing in eqs 19 and 20 are common to all functionals and are defined in ref 7. The C_6^{AB} coefficients are interpolated from the ab initio tabulated data obtained for hydrides.[7] The main advantage of D3 is that it is thoroughly tested[1] and available in almost any quantum chemical program. It also offers simple to compute derivatives with respect to nuclear coordinates, which is important for structure optimizations.

The second considered model of the dispersion interaction is MBD.[8] A computation of the MBD energy requires two steps. First, the screening equation[27] is solved for frequency-dependent polarizabilities. Then, the solution of the screening equation is used to set up the Hamiltonian of interacting quantum harmonic oscillators whose correlation energy models the long-range dispersion energy of the real system. While the computational cost of MBD is larger than that of D3, it is still negligible compared to the SCF step. The dipole interaction in the screening equation as well as in the MBD Hamiltonian is range separated with a Fermi-type damping function[8]

$$f_{\text{MBD}}(R_{AB}) = \frac{1}{1 + \exp[-6(R_{AB}/S_{\text{vdW}} - 1)]} \tag{21}$$

$$S_{\text{vdW}} = \beta(R_{\text{vdW}}^A + R_{\text{vdW}}^B) \tag{22}$$

where β is the only functional-dependent parameter of the model. The MBD model is expected to be a good approximation for large molecular systems where an atom-pairwise approximation may no longer capture the many-body contributions to the total interaction energy.[28,29]

2.3. Exchange. The exchange functional is composed of the short-range ωPBEsol exchange, long-range HF exchange, and optionally a fraction α of the short-range HF exchange

$$E_{\text{X,SR}} = (1 - \alpha)E_{\text{X,SR}}(\omega\text{PBEsol}) + \alpha E_{\text{X,SR}}(\text{HF}) \tag{23}$$

The short-range and long-range parts of E_X are defined through the decomposition of the $1/r_{12}$ operator,

$$\frac{1}{r_{12}} = \frac{\text{erfc}(\omega r_{12})}{r_{12}} + \frac{\text{erf}(\omega r_{12})}{r_{12}} \tag{24}$$

Table 2. Ab Initio Numerical Constants Appearing in Eqs 10−13

k	P_k	Q_k	R_k	S_k
0	1.696	3.356	1.775	3.205
1	−0.2763	−2.525	0.01213	−1.784
2	−0.09359	−0.4500	-4.743×10^{-3}	3.613×10^{-3}
3	3.837×10^{-3}	−0.1060	0.5566	-4.743×10^{-3}
4	-2.471×10^{-3}	5.532×10^{-4}		0.5566
5	0.7524	-2.471×10^{-3}		
6		0.7524		

We test two variants of the exchange functional: pure ($\alpha = 0$ and $\omega = 0.3$) and hybrid ($\alpha = 0.2$ and $\omega = 0.2$). The range separation parameter ω for the pure variant is obtained via empirical optimization. The parameters α and ω of the hybrid variant are assumed the same as for the LRC-ωPBEh functional of Rohrdanz et al.[30] It is worthwhile to note that whereas the fixed value of ω is convenient in practical computations, the optimal ω depends on the system size and electronic structure, which is especially important for donor−acceptor systems.[31,32]

The PBEsol exchange,[4] which is the basis for ωPBEsol, has the exact second-order gradient expansion. This feature is important for solids[4] and for large organic molecules.[5] In contrast to PBEsol, the gradient expansion of the PBE exchange is not exact; it is designed to cancel the gradient term of the PBE correlation,[5] which makes it less suitable than PBEsol in conjunction with our correlation functional.

3. TECHNICAL DETAILS

The functionals employed in this study, besides the MCS functionals, are ωPBE,[6,33] B3LYP,[34] BLYP,[35] M06,[36] M06-2X,[36] and ωB97X-D.[20] ωPBE has its range separation parameter fixed at $\omega = 0.4$. The suffix "-D3" denotes functionals with added Grimme's D3 correction.[7] For water 16-mers and for the S22 database the energies are obtained with the LC-ωPBE functional[37] instead of ωPBE. We supply ωPBE and LC-ωPBE with the same D3 correction calibrated by Grimme at al.[7] All DFT computations employ the def2-TZVPPD basis[38,39] unless noted otherwise. The acronyms used to name the types of errors are mean absolute percentage deviation (MAPD), root-mean-square deviation (RMSD), mean absolute deviation (MAD), and mean signed deviation (MSD). Energies are given in kcal/mol.

The training set for the MCS-D3 and MCSh-D3 functionals is composed of the noncovalent interactions database of Zhao and Truhlar.[40,41] The training database is partitioned into subsets according to the nature of the represented interactions. The subsets are as follows: WI7/05 (small dispersion-dominated complexes), PPS5/05 (π-electron dispersion interactions), DI6/04 (dispersion and dipole interactions), HB6/04 (hydrogen bonds), and CT7/04 (ground-state charge-transfer interactions).

The optimization of the MCS-D3 functional consisted of the following steps. First, we generated a grid of parameters (ω,G) satisfying $0.100 \le \omega \le 0.450$ and $0.050 \le G \le 0.150$; for each pair (ω,G), we optimized the D3 correction by finding the pair (r_6, s_8) that minimized the objective function

$$F(r_6, s_8; \omega, G) = 10 \times \mathrm{RMSD(WI7/05)} + \mathrm{RMSD(other)} \quad (25)$$

where RMSD(X) denotes the root-mean-square deviation within the subset X of the training set. Finally, we selected the parameters (ω,G,r_6,s_8) corresponding the smallest MAD and MAPD. Table 3 presents the results for the training set.

Table 3. Training Database for the MCS-D3 and MCSh-D3 Functionals[a]

dimer	CCSD(T)	MCS-D3	MCSh-D3
He ··· Ne	−0.041	−0.020	−0.033
He ··· Ar	−0.058	−0.016	−0.034
Ne ··· Ne	−0.086	−0.015	−0.048
Ne ··· Ar	−0.131	−0.039	−0.061
CH_4 ··· Ne	−0.18	−0.18	−0.18
C_6H_6 ··· Ne	−0.41	−0.41	−0.52
CH_4 ··· CH_4	−0.53	−0.55	−0.47
H_2S ··· H_2S	−1.62	−1.40	−1.52
HCl ··· HCl	−1.91	−1.54	−1.68
HCl ··· H_2S	−3.26	−3.18	−3.32
CH_3Cl ··· HCl	−3.39	−3.08	−3.26
CH_3SH ··· HCN	−3.58	−3.54	−3.70
CH_3SH ··· HCl	−4.74	−4.94	−5.13
C_2H_4 ··· F_2	−1.06	−0.98	−1.06
NH_3 ··· F_2	−1.80	−1.93	−1.95
C_2H_2 ··· ClF	−3.79	−3.74	−3.93
HCN ··· ClF	−4.80	−4.15	−4.03
NH_3 ··· Cl_2	−4.85	−4.86	−5.07
H_2O ··· ClF	−5.20	−5.12	−5.10
NH_3 ··· ClF	−11.17	−13.65	−13.89
NH_3 ··· NH_3	−3.09	−2.78	−2.77
HF ··· HF	−4.49	−4.06	−4.13
H_2O ··· H_2O	−4.91	−4.60	−4.61
NH_3 ··· H_2O	−6.38	−6.35	−6.29
$(HCONH_2)_2$	−15.41	−15.02	−15.14
$(HCOOH)_2$	−17.60	−18.10	−17.94
$(C_2H_2)_2$	−1.36	−1.24	−1.29
$(C_2H_4)_2$	−1.44	−1.59	−1.54
sandwich $(C_6H_6)_2$	−1.65	−1.58	−1.51
T-shaped $(C_6H_6)_2$	−2.63	−2.79	−2.86
displaced $(C_6H_6)_2$	−2.59	−2.80	−2.49

[a]The interaction energies are grouped into five subsets: WI7/05, DI6/04, CT7/04, HB6/04, and PPS5/05. The reference CCSD(T) energies are taken from Ref 23. The monomer geometries are held rigid at their dimer values. The units are kcal/mol.

For the MCS-MBD functional, we kept the same values of ω and G as for MCS-D3. The only difference is that the parameter β of the MBD dispersion was obtained by minimization of RMSD for the S22 set.[42] The different choice of the training sets for the D3 and MBD corrections was due to the poor behavior of the latter for small dispersion-bound dimers.

For the hybrid MCS functionals, MCSh-D3 and MCSh-MBD, we did not optimize α and ω but fixed these parameters at the same values as in the LRC-ωPBEh functional.[30] The

parameter G in the semilocal correlation and the dispersion corrections were optimized in the same way as for MCS-D3 and MCS-MBD.

To determine the stabilization energy upon complex formation, two definitions are employed: the interaction energy and the binding energy. The interaction energy is defined as

$$E_{\text{int}} = E(\text{dimer AB}) - E(\text{isolated A}) - E(\text{isolated B}) \quad (26)$$

where the monomer geometries are held rigid at their dimer values, and the counterpoise correction is employed. In the case of water clusters, we use the binding energy instead of E_{int}

$$E_{\text{bind}} = E((\text{H}_2\text{O})_n) - nE((\text{H}_2\text{O})_{\text{isolated}}) \quad (27)$$

where the coordinates of water molecules relax upon dissociation from the cluster. E_{bind} does not include the energy of zero-point vibrations. The basis set employed for the isolated H_2O monomers does not include any functions centered on the ghost centers.

The reference binding energies of water 16-mers were obtained by combining $\Delta E_{\text{CCSD(T)}}$ with the extrapolated binding energies at the MP2 level, as proposed by Rezac et al.,[43]

$$E_{\text{bind,CCSD(T)}}^{CBS(AVTZ\rightarrow AVQZ)} = E_{\text{HF}}^{AVQZ} + E_{\text{MP2}}^{CBS(AVTZ\rightarrow AVQZ)} + \underbrace{\left(E_{\text{CCSD(T)}}^{AVTZ} - E_{\text{MP2}}^{AVTZ}\right)}_{\Delta E_{\text{CCSD(T)}}}, \quad (28)$$

where AVTZ and AVQZ stand for the aug-cc-pVTZ and aug-cc-pVQZ bases.[39] We employed the extrapolation scheme of Halkier et al.[44]

$$E_{\text{MP2}}^{\text{CBS}(X\rightarrow X+1)} = \frac{(X+1)^3 E_{\text{MP2}}^{X+1} - X^3 E_{\text{MP2}}^{X}}{(X+1)^3 - X^3} \quad (29)$$

with the aug-cc-pVTZ and aug-cc-pVQZ basis sets (X = 3). $E_{\text{MP2}}^{\text{CBS(AVTZ}\rightarrow\text{AVQZ)}}$ was computed with NWChem[45] within the resolution-of-identity approximation (RI-MP2) and with the oxygen 1s orbitals frozen. $E_{\text{CCSD(T)}}^{\text{AVTZ}}$ and $E_{\text{MP2}}^{\text{AVTZ}}$ were taken from Yoo et al.[46] These contributions do not employ the RI approximation.

4. NUMERICAL RESULTS AND DISCUSSION

This section is split into four parts covering a broad spectrum of possible applications. (i) We begin with two databases of noncovalent systems (S22 and A24) that are typical tests for methods focused on noncovalent interactions.[1,47] (ii) Next, we turn to water clusters of increasing size to test how the accuracy of our method changes when going from small dimers to clusters with a large number of distant-neighbor interactions. (iii) We assess the performance of the MCS functionals for ionic hydrogen-bonded interactions, which is a common motif in biological systems. (iv) Finally, we focus on the isodesmic reaction of *n*-alkanes, which is a well-known case where approximate functionals fail to fully account for the effect of intramolecular noncovalent interactions.

4.1. S22 and A24 Databases. S22 and A24 are two databases of noncovalent dimers that facilitate comparisons of density-functional approximations.[42,48] The molecules contained in these databases are listed in Figures 1 and 2. We compare the MCS functionals against the leading functionals in the field of noncovalent interactions:[1,47] Minnesota-family functionals M06-2X and M06-2X-D3, dispersion-corrected range-separated hybrid ωB97X-D, and two functionals based on the B88 exchange[49] (B3LYP-D3 and BLYP-D3).

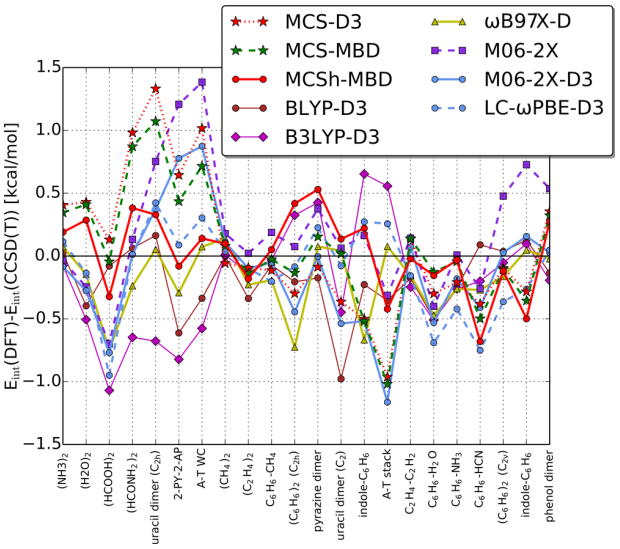

Figure 1. Detailed results for the S22 database. The deviations are with respect to the CCSD(T) results of Podeszwa et al.[50] The energies for the functionals other than MCS are taken from Goerigk and Grimme.[51] 2-PY-2-AP denotes 2-pyridone···2-aminopyridine.

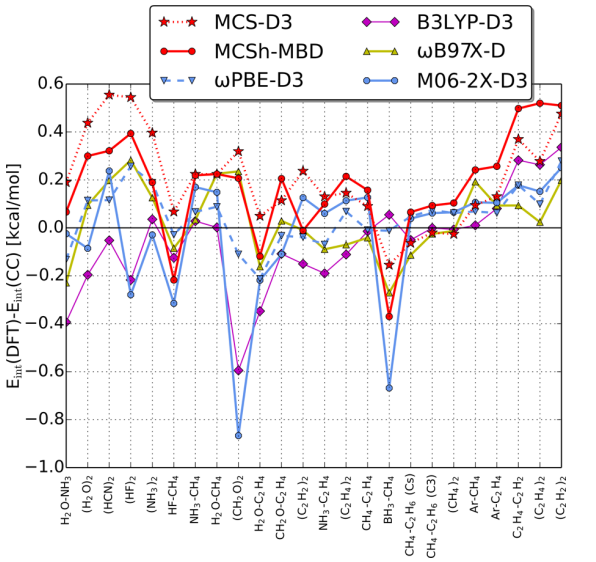

Figure 2. Detailed results for the A24 database. The deviations are with respect to the nonrelativistic interaction energies at the CCSD(T)/CBS level plus CCSDT(Q) corrections.[48] The energies for the functionals other than MCS are taken from Li et al.[47]

An inspection of Table 4 shows that all the MCS functionals afford small percentage errors within the S22 database. Notably, the two hybrids, MCSh-D3 and MCSh-MBD, have errors below 6%. The pure variants, MCS-D3 and MCS-MBD, tend to underbind the dimers from the hydrogen-bonded subset of S22 (Figure 1). For the formamide and uracil dimers, the error is the most pronounced and reaches about 1 kcal mol. The underbinding is eliminated completely only when both the hybrid exchange and MBD correction are employed simulta-

Table 4. Statistical Errors for the S22 and A24 Databases.[42,48a]

	MAPD	RMSD	MAD	MSD
S22				
MCS-D3	7.05	0.54	0.42	0.08
MCS-MBD	6.05	0.47	0.34	0.07
MCSh-D3	5.44	0.44	0.34	0.15
MCSh-MBD	5.94	0.31	0.25	0.03
ωPBE-D3	6.65	0.36	0.27	−0.11
M06-2X	7.38	0.53	0.38	0.20
M06-2X-D3	6.39	0.47	0.34	−0.12
B3LYP	86.4	4.91	3.76	3.76
B3LYP-D3	6.68	0.48	0.39	−0.20
BLYP-D3	5.41	0.33	0.24	−0.20
ωB97X-D	7.37	0.32	0.23	−0.18
A24				
MCS-D3	16.38	0.27	0.22	0.20
MCS-MBD	23.67	0.30	0.27	0.24
MCSh-D3	16.45	0.27	0.21	0.21
MCSh-MBD	22.82	0.27	0.23	0.17
ωPBE-D3	8.06	0.12	0.10	0.05
M06-2X	20.51	0.29	0.23	0.04
M06-2X-D3	14.47	0.27	0.19	−0.03
B3LYP	99.6	1.10	1.00	1.00
B3LYP-D3	9.58	0.21	0.15	−0.06
ωB97X-D	10.05	0.15	0.12	0.03

[a]The units are kcal/mol.

neously. The resulting functional, MCSh-MBD, has exceptionally small absolute as well as relative errors.

Contrary to the results for the S22 database, for A24 we observe that substituting MBD for D3 worsens the percentage errors. This is observed especially for small systems weakly bound by dispersion: $(CH_4)_2$, Ar···CH_4, and Ar···C_2H_4. We stress, however, that these are the only cases where MBD is systematically inferior to D3.

Although the functionals based on the B88 exchange,[49] B3LYP-D3 and BLYP-D3, yield excellent total interaction energies for the S22 database, the physical content of these energies is troubling. It has been known since the work of Lacks and Gordon[13] that B88 is a much more repulsive exchange component than the exact HF exchange. To cancel this contribution, a massive attractive term must be added to the interaction energy. Indeed, the D3 correction for the B88-based functionals tends to be tens of percents larger than E_{disp} for the MCS-D3 functional (Table 5).

While it is impossible to ascertain the precise, physically sound amount of the D3 correction, we argue that a large part of the dispersion contribution for the B88-based functionals serves only to cancel the overrepulsive exchange. D3 is based on the asymptotic multipole form of the dispersion term defined in SAPT (eq 19). Thus, it accounts only for the *long-range* part of the dispersion interaction and cannot, for the equilibrium dimers of S22, be as large as the *total* dispersion defined in SAPT, let alone be larger. The D3 corrections for BLYP-D3 presented in Table 5 are therefore unphysical. The spuriously large dispersion contribution is only somewhat reduced for B3LYP-D3.

Table 5. Comparison of the D3 Dispersion Correction and SAPT Dispersion Plus Exchange Dispersion for Selected Complexes from the S22 Database[a]

dimer	SAPT	B3LYP-D3	MCS-D3	BLYP-D3
$(CH_4)_2$	−1.06	−0.92	−0.79	−1.18
$(C_2H_4)_2$	−2.58	−2.12	−1.52	−2.90
uracil dimer stack	−11.08	−9.16	−6.87	−11.52
C_6H_6−H_2O	−2.82	−2.32	−1.73	−2.89
C_6H_6−NH_3	−2.86	−2.36	−1.76	−2.91

[a]The SAPT dispersion energies are taken from Pernal at al.[23] The units are kcal/mol.

4.2. Water Clusters. Water clusters constitute a challenge for approximate DFT methods. Although water molecules are polar, their clusters are bound not only by electrostatics and induction but also largely by the dispersion effects. More importantly, the cluster sample interactions not represented in the standard test databases are interactions with distant neighbors and multiple hydrogen bonds formed by a single water molecule.

Water clusters exemplify the advantage of our approach over the dispersion-corrected functionals based on massive error cancellation. Figure 3 shows the system-size dependence of the errors of various methods. The MCS functionals show no systematic underbinding or overbinding. This is in contrast to the functionals based on the B88 exchange; B3LYP systematically underbinds, while both B3LYP-D3 and BLYP-D3 systematically overbind due to the overcorrection of the B88 exchange by the D3 term. This error cancellation had no adverse effects in the previous test cases.

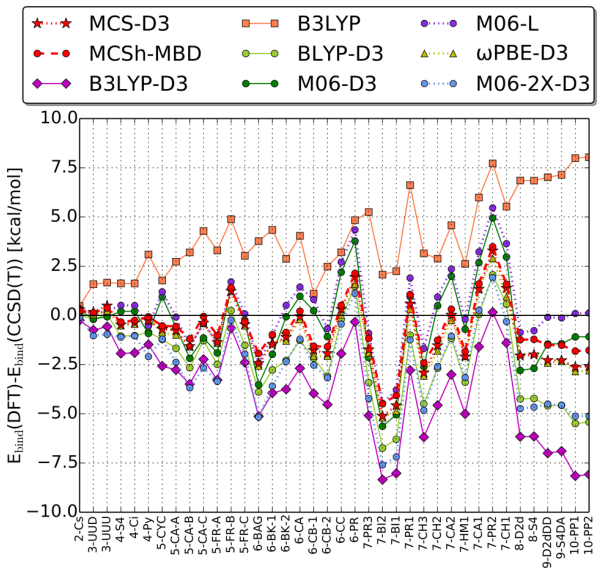

Figure 3. Differences between the CCSD(T)/CBS and DFT binding energies for $(H_2O)_n$ with n = 2,...,10. The coordinates, reference energies, and labels of the water clusters are taken from Temeleso et al.[52]

Table 6 illustrates that all four MCS functionals yield exceptionally small relative and absolute errors for $(H_2O)_n$ with n = 2,...,10. While the choice of the dispersion correction does not influence the average errors, the choice of the exchange functional is more important. The hybrid MCS functionals perform significantly better than the pure counterparts. Of all the tested functionals, MCSh-MBD offers the best performance for the water clusters of Figure 3.

Table 6. Statistical Errors of DFT Methods for $(H_2O)_n$ with n = 2,...,10[a]

functional	MAD	MAPD	MSD	RMSD
MCS-D3	1.53	3.17	−0.94	1.92
MCS-MBD	1.52	3.12	−1.02	1.91
MCSh-D3	**1.25**	2.92	0.87	1.69
MCSh-MBD	1.28	**2.65**	−0.59	**1.64**
M06-D3	1.71	3.58	−0.43	2.22
M06-2X-D3	2.75	5.79	−2.58	3.35
B3LYP	4.01	8.53	4.01	4.52
B3LYP-D3	3.66	7.39	−3.65	4.39
BLYP-D3	2.42	4.68	−2.18	3.04
ωPBE-D3	1.55	3.06	−1.09	1.97
M06-L	1.40	3.13	**0.29**	1.98

[a]The units are kcal/mol.

Figures 4 and 5 focus on the performance of approximate methods for water hexamers and 16-mers. All the MCS

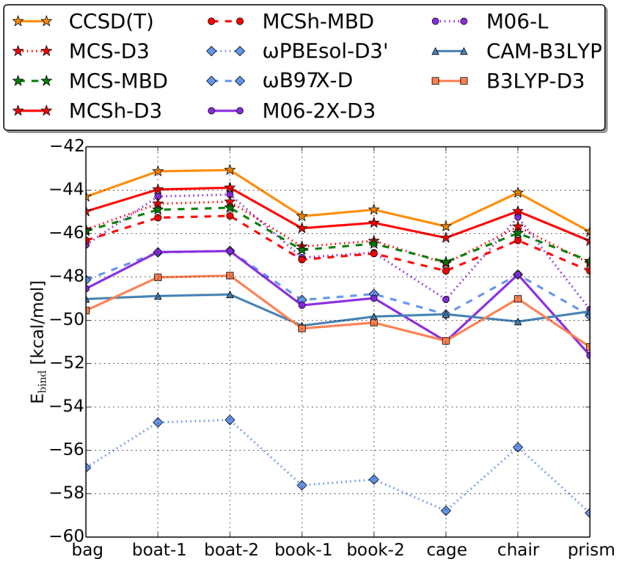

Figure 4. Binding energies of water hexamers. The coordinates and reference CCSD(T)/CBS energies are taken from Bates and Tschumper.[58] The energies for the functionals other than MCS are taken from Leverentz et al.[57]

functionals yield small absolute errors, excellent ordering of the hexamers, and well-reproduced (although not perfectly) tiny energy differences between the 16-mers. The effect of changing the dispersion correction is negligible when the exchange is pure (α = 0). However, there is an appreciable difference between MCSh-D3 and MCSh-MBD for the water 16-mers. While the binding energy for MCSh-MBD agrees almost perfectly with the reference values, MCSh-D3 underbinds by about 4 kcal mol.

The excellent performance of the MCS functionals for the 16-mers is encouraging because these systems exhibit features that are expected in even larger clusters. First, among the systems considered in this study, only the 16-mers contain water molecules participating in four hydrogen bonds. Moreover, the energetics of the 16-mers include significant many-body effects, which are large compared to the energy differences between the isomers. Indeed, Wang et al.[53] have estimated that the 5-body and higher effects in the 4444-a 16-

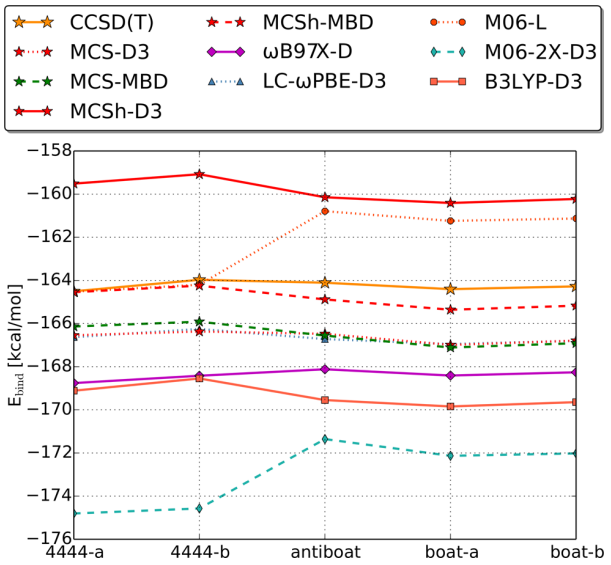

Figure 5. Binding energies of water 16-mers. The coordinates are taken from Yoo et al.[46] The energies for the functionals other than MCS are taken from Leverentz et al.[57]

mer to contribute −2.3 kcal mol to the binding energy at the MP2 level. This is a highly probable estimate because in our computations the MP2 method is shown to approach extremely close the CCSD(T)/CBS limits for all 16-mers (Table 7).

Table 7. Binding Energies of Water 16-mers[a]

system	CCSD(T)	RI-MP2	MCS-D3	MCSh-MBD
4444-a	−164.51	−163.91	−166.54	−164.55
4444-b	−163.97	−163.46	−166.37	−164.24
antiboat	−164.11	−164.07	−166.48	−164.88
boat-a	−164.40	−164.45	−166.99	−165.36
boat-b	−164.28	−164.33	−166.79	−165.17

[a]The CCSD(T) and RI-MP2 energies are extrapolated according to eqs 28 and 29, respectively. The units are kcal/mol.

Many-body effects in the 16-mers are dominated by induction terms, as shown by several studies on trimers of polar molecules.[54−56] This explains why the performance of MP2 is excellent for the 16-mers despite inability of MP2 to recover the third-order triple-dipole dispersion terms. The induction nature of many-body effects justifies the D3 atom-pairwise dispersion correction, which does not comprise any nonadditive three-body dispersion terms.[7] In fact, we have not observed any significant improvement attributable to the MBD dispersion correction that is capable of recovering many-body dispersion.

It should be emphasized that our reference binding energies of the 16-mers are uniformly shifted with respect to those used by Leverentz et al.[57] This is because these authors employed the CCSD(T)/aug-cc-pVTZ energies of Yoo et al.[46] as their final reference values, whereas in our study these energies have been refined in the extrapolation scheme defined in eq 28. The extrapolation has introduced an upward shift of about 6.5 kcal/mol relative to CCSD(T)/aug-cc-pVTZ. A recent quantum Monte Carlo result of Wang et al.[53] for the 4444-a isomer (−165.1(8)kcal mol) is in excellent agreement with our CCSD(T)/CBS extrapolation (−164.51 kcal mol).

dx.doi.org/10.1021/ct500707w | J. Chem. Theory Comput. 2014, 10, 4297−4306

4.3. Ionic Hydrogen Bonds. Hydrogen-bonded systems composed of an ion interacting with a closed-shell molecule provide a simple model of interactions ubiquitous in biochemistry. From the point of view of dispersion corrections, charged dimers belong to the hardest cases; if a dispersion correction does not depend on the density, it will not reflect any alterations of dispersion due to the density change from a neutral to an ion, which is often dramatic. This is the case of the D3 model that has been parametrized within a set of neutral dimers, and its input consists of atomic coordinates only.[59] However, because the total interaction is dominated by electrostatic and induction components, this weakness may not be especially relevant, as dispersion itself is relatively small and thus its accuracy not critical.

Figures 6 and 7 show the performance of MCSh-MBD and compare this functional with the results of popular DFT

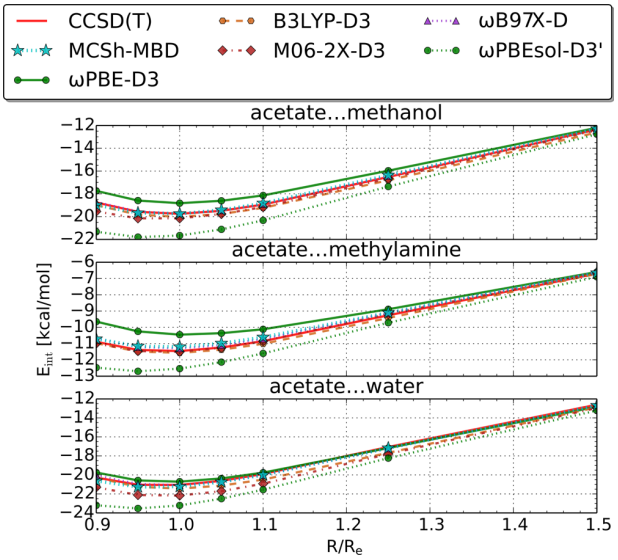

Figure 6. Interaction energy curves for hydrogen-bonded dimers including the acetate anion. The data for B3LYP-D3, M06-2X-D3, and B97X-D are taken from ref 47

methods. The differences between MCSh-MBD, B3LYP-D3, M06-2X-D3, and ωB97X-D are small, and all of the curves are close to the reference ones. The ωPBE-D3 functional is consistently worse than any of the MCS functionals (Table 8) despite its good performance for water clusters.

Table 8 shows that switching from D3 to MBD changes little when applied with the pure MCS functionals. However, the choice the dispersion correction appears more important for the hybrid variants, and the MBD model works better in this case. This observation is consistent with our findings for the hydrogen-bonded dimers of the S22 database and for water clusters.

4.4. Isodesmic Reaction of *n*-Alkanes. The systematic errors of DFT approximations in predicting alkane thermochemistry were discussed by Wodrich et al.,[60] Song et al.,[61] and Grimme et al.[62] They observed that there is a substantial error in reaction energies of isodesmic ethane fragmentation reactions of alkanes, which accumulates as the chain length grows

$$CH_3(CH_2)_mCH_3 + mCH_4 \rightarrow (m+1)C_2H_6 \qquad (30)$$

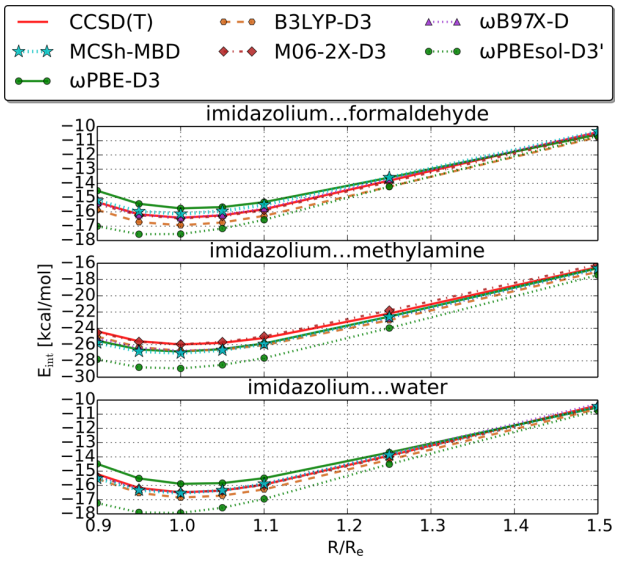

Figure 7. Interaction energy curves for hydrogen-bonded dimers including the imidazolium cation. The data for B3LYP-D3, M06-2X-D3, and B97X-D are taken from ref 47

The performance of approximate functionals for these reactions is connected to the quality of the description of noncovalent interactions. Johnson et al.[18] found that the error in the reactions of eq 30 has its origin in the region of space between 1,3 methylene groups, where the reduced density gradient changes upon fragmentation of an alkane to ethane. This change is a signature of noncovalent bonds.[15]

Previous studies identified the features that a functional should possess to alleviate this problem: (i) range separation of the exchange functional,[61] (ii) restoration of the exact gradient expansion of the exchange[5] (as in PBEsol), (iii) dispersion correction.[61,62] The MCS functionals as well as ωPBEsol-D3′ (discussed in the next section) include all of the above features. As shown in Figure 8, these methods are by far the best performers for reactions in question.

4.5. Merit of the MCS Correlation. The question remains as to whether the correlation functional of our approach is indeed crucial to the quality of the above presented results. One might argue that this accuracy is primarily determined by the exchange and dispersion parts and only weakly dependent on the semilocal correlation. To verify this hypothesis, we have composed a functional that differs from MCS-D3 only by the PBEsol correlation (denoted as ωPBEsol-D3′), that is, both MCS-D3 and ωPBEsol-D3′ share the same ωPBEsol exchange with ω = 0.3 and the same D3 correction. Figure 4 shows that keeping the PBEsol correlation leads to about 25% overbinding in the case of water hexamers. A similar overbinding occurs for the 16-mers (e.g., E_{bind} = −206.1 kcal/mol for the isomer 4444-a). Furthermore, ωPBEsol-D3′ overestimates the interaction energies for every ionic hydrogen-bonded dimer presented in Figures 6 and 7. Evidently, the role of the MCS correlation is essential in these examples, and its replacement by the standard PBEsol correlation leads to serious overestimation of interaction energies.

Nonetheless, it is of note that there exist cases where the choice of a semilocal correlation part matters less. For alkane fragmentation reactions (Figure 8), ωPBEsol-D3′ performs

Table 8. Interaction Energies of Ionic Hydrogen-Bonded Dimers at the Equilibrium Distances[a]

dimer	CCSD(T)	MCS-D3	MCS-MBD	MCSh-D3	MCSh-MBD	ωPBE-D3
acetate... X						
methanol	−19.75	−19.46	−19.57	−19.28	−19.74	−18.82
water	−21.06	−20.97	−21.15	−20.73	−21.22	−20.71
methylamine	−11.46	−10.96	−11.01	−10.85	−11.20	−10.45
imidazolium... X						
formaldehyde	−16.41	−15.84	−15.86	−15.94	−16.14	−15.75
methylamine	−25.98	−26.58	−26.62	−26.69	−27.04	−26.86
water	−16.49	−16.25	−16.30	−16.30	−16.54	−15.89

[a]The units are kcal/mol.

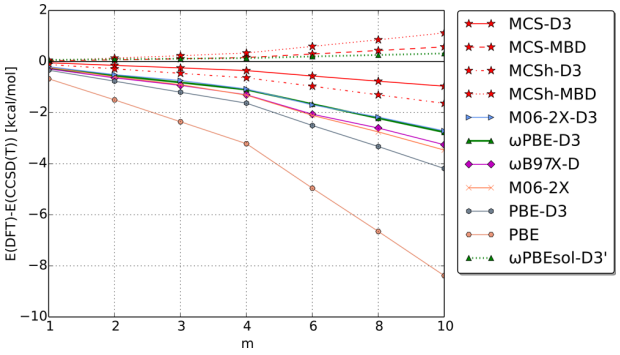

Figure 8. Errors in the energy of the isodesmic reaction. The reference energies and coordinates are taken from Grimme.[62]

even better than the MCS functionals, which suggests the dominant role of the ωPBEsol exchange in this case.

5. SUMMARY AND CONCLUSIONS

We have proposed a new DFT exchange−correlation functional that is specifically optimized for noncovalent interactions. It is composed of well-defined and physically meaningful components, with minimum of empiricism and reduced opportunity for error cancellation. It is built of the meta-GGA correlation functional developed by Modrzejewski et al.[3] and the range-separated PBEsol exchange. The exchange and correlation contain a slight amount of empiricism in a form of parameters defining the scope of various approximations: a single parameter that governs damping of the semilocal correlation hole at large r_{12}, a range-separation parameter controlling the onset of the long-range HF exchange, and in the case of the hybrid exchange, a fraction of the short-range HF exchange.

The novel piece of our functional, the correlation functional, is designed with the constraint satisfaction technique, but with the aid of its single empirical parameter, it may be finely adjusted to any accurate variant of a dispersion correction without compromising any formal or physical constraints that it satisfies.

We have calibrated two long-range dispersion corrections to work with the remaining part of the functional: D3[7] and MBD.[8] Taking into account the two possible variants of exchange and the two variants of dispersion, there is a set of four MCS functionals that are tested in this study.

The test set is composed of popular databases of small noncovalent dimers but includes also the more demanding cases of water clusters, hydrogen-bonded interactions in ion-neutral pairs, and thermochemistry of isodesmic reactions of *n*-alkanes. For the classic S22 database, the MCS functionals perform on a par or better than the leading functionals in the field of noncovalent interactions: B3LYP-D3, M06-2X-D3, and ωB97X-D. More importantly, the MCS functionals perform markedly better than these functionals for large water clusters for which they successfully predict the binding energies from the newly refined CCSD(T)/CBS benchmarks. The good performance for hydrogen bonding extends to ionic hydrogen bonds. Finally, all four MCS functionals display excellent performance in predicting the energetics of isodesmic reactions of *n*-alkanes in direct consequence of the good description of the intramolecular interactions between methylene groups. We find that the PBEsol exchange combined with range separation and a dispersion correction essentially solves the known problems of DFT with isodesmic reactions of alkanes.

In view of the presented results, all four MCS functionals could be recommended for the description of noncovalent systems. The best performer in any case except few-atom dispersion-bound systems is MCSh-MBD.

AUTHOR INFORMATION

Corresponding Author

*E-mail: m.m.modrzejewski@gmail.com.

Notes

The authors declare no competing financial interest.

ACKNOWLEDGMENTS

This work was supported by the National Science Foundation (Grant CHE-1152474) and by the Polish Ministry of Science and Higher Education (Grant N204 248440). M.M. and G.C. gratefully acknowledge additional financial support from the Foundation for Polish Science. Special thanks to Aleksandra Tucholska for creating the TOC graphic for this paper.

REFERENCES

(1) Burns, L. A.; Vazquez-Mayagoitia, A.; Sumpter, B. G.; Sherrill, C. D. *J. Chem. Phys.* **2011**, *134*, 084107.
(2) Podeszwa, R.; Szalewicz, K. *J. Chem. Phys.* **2012**, *136*, 161102.
(3) Modrzejewski, M.; Lesiuk, M.; Rajchel, Ł.; Szczęśniak, M. M.; Chałasiński, G. *J. Chem. Phys.* **2012**, *137*, 204121−204121.
(4) Perdew, J. P.; Ruzsinszky, A.; Csonka, G. I.; Vydrov, O. A.; Scuseria, G. E.; Constantin, L. A.; Zhou, X.; Burke, K. *Phys. Rev. Lett.* **2008**, *100*, 136406.
(5) Csonka, G. I.; Ruzsinszky, A.; Perdew, J. P.; Grimme, S. *J. Chem. Theory Comput.* **2008**, *4*, 888−891.
(6) Henderson, T. M.; Janesko, B. G.; Scuseria, G. E. *J. Chem. Phys.* **2008**, *128*, 194105.
(7) Grimme, S.; Antony, J.; Ehrlich, S.; Krieg, H. *J. Chem. Phys.* **2010**, *132*, 154104.
(8) Ambrosetti, A.; Reilly, A. M.; DiStasio, R. A., Jr.; Tkatchenko, A. *J. Chem. Phys.* **2014**, *140*, 18A508.
(9) Lee, K.; Murray, É.; Kong, L.; Lundqvist, B.; Langreth, D. *Phys. Rev. B* **2010**, *82*, 081101.

(10) Vydrov, O.; Van Voorhis, T. *J. Chem. Phys.* **2010**, *133*, 244103.
(11) Sato, T.; Nakai, H. *J. Chem. Phys.* **2010**, *133*, 194101.
(12) Becke, A.; Johnson, E. *J. Chem. Phys.* **2005**, *122*, 154104.
(13) Lacks, D. J.; Gordon, R. G. *Phys. Rev. A* **1993**, *47*, 4681.
(14) Murray, E. D.; Lee, K.; Langreth, D. C. *J. Chem. Theory Comput.* **2009**, *5*, 2754−2762.
(15) Johnson, E. R.; Keinan, S.; Mori-Sanchez, P.; Contreras-Garcia, J.; Cohen, A. J.; Yang, W. *J. Am. Chem. Soc.* **2010**, *132*, 6498−6506.
(16) Kannemann, F. O.; Becke, A. D. *J. Chem. Theory Comput.* **2009**, *5*, 719−727.
(17) Kamiya, M.; Tsuneda, T.; Hirao, K. *J. Chem. Phys.* **2002**, *117*, 6010.
(18) Johnson, E. R.; Contreras-Garca, J.; Yang, W. *J. Chem. Theory Comput.* **2012**, *8*, 2676−2681.
(19) Misquitta, A.; Podeszwa, R.; Jeziorski, B.; Szalewicz, K. *J. Chem. Phys.* **2005**, *123*, 214103.
(20) Chai, J.-D.; Head-Gordon, M. *Phys. Chem. Chem. Phys.* **2008**, *10*, 6615−6620.
(21) Lin, Y.-S.; Li, G.-D.; Mao, S.-P.; Chai, J.-D. *J. Chem. Theory Comput.* **2013**, *9*, 263−272.
(22) Mardirossian, N.; Head-Gordon, M. *J. Chem. Phys.* **2014**, *140*, 18A527.
(23) Pernal, K.; Podeszwa, R.; Patkowski, K.; Szalewicz, K. *Phys. Rev. Lett.* **2009**, *103*, 263201.
(24) Gori-Giorgi, P.; Perdew, J. *Phys. Rev. B* **2001**, *64*, 155102.
(25) Rassolov, V.; Pople, J.; Ratner, M. *Phys. Rev. B* **2000**, *62*, 2232.
(26) Burke, K.; Perdew, J.; Ernzerhof, M. *J. Chem. Phys.* **1998**, *109*, 3760.
(27) Tkatchenko, A.; DiStasio, R. A., Jr.; Car, R.; Scheffler, M. *Phys. Rev. Lett.* **2012**, *108*, 236402.
(28) Ruzsinszky, A.; Perdew, J. P.; Tao, J.; Csonka, G. I.; Pitarke, J. *Phys. Rev. Lett.* **2012**, *109*, 233203.
(29) Gobre, V. V.; Tkatchenko, A. *Nat. Commun.* **2013**, *4*, 2341.
(30) Rohrdanz, M. A.; Martins, K. M.; Herbert, J. M. *J. Chem. Phys.* **2009**, *130*, 054112.
(31) Modrzejewski, M.; Rajchel, Ł.; Chałasiński, G.; Szczęśniak, M. M. *J. Phys. Chem. A* **2013**, *117*, 11580−11586.
(32) Koppen, J. V.; Hapka, M.; Modrzejewski, M.; Szczęśniak, M. M.; Chałasiński, G. *J. Chem. Phys.* **2014**, *140*, 244313.
(33) Perdew, J.; Burke, K.; Ernzerhof, M. *Phys. Rev. Lett.* **1996**, *77*, 3865−3868.
(34) Stephens, P. J.; Devlin, F. J.; Chabalowski, C. F.; Frisch, M. J. *J. Phys. Chem.* **1994**, *98*, 11623−11627.
(35) Gill, P. M.; Johnson, B. G.; Pople, J. A.; Frisch, M. J. *Chem. Phys. Lett.* **1992**, *197*, 499−505.
(36) Zhao, Y.; Truhlar, D. *Theor. Chem. Acc.* **2008**, *120*, 215−241.
(37) Vydrov, O. A.; Heyd, J.; Krukau, A. V.; Scuseria, G. E. *J. Chem. Phys.* **2006**, *125*, 074106.
(38) Weigend, F.; Ahlrichs, R. *Phys. Chem. Chem. Phys.* **2005**, *7*, 3297−3305.
(39) Schuchardt, K. L.; Didier, B. T.; Elsethagen, T.; Sun, L.; Gurumoorthi, V.; Chase, J.; Li, J.; Windus, T. L. *J. Chem. Inf. Model.* **2007**, *47*, 1045−1052.
(40) Zhao, Y.; Truhlar, D. *J. Phys. Chem. A* **2005**, *109*, 5656−5667.
(41) Zhao, Y.; Truhlar, D. *J. Chem. Theory Comput.* **2005**, *1*, 415−432.
(42) Jurecka, P.; Sponer, J.; Cerny, J.; Hobza, P. *Phys. Chem. Chem. Phys.* **2006**, *8*, 1985−1993.
(43) Rezac, J.; Riley, K. E.; Hobza, P. *J. Chem. Theory Comput.* **2011**, *7*, 2427−2438.
(44) Halkier, A.; Klopper, W.; Helgaker, T.; Jorgensen, P.; Taylor, P. R. *J. Chem. Phys.* **1999**, *111*, 9157−9167.
(45) Valiev, M.; Bylaska, E. J.; Govind, N.; Kowalski, K.; Straatsma, T. P.; Van Dam, H. J.; Wang, D.; Nieplocha, J.; Apra, E.; Windus, T. L.; de Jong, W. *Comput. Phys. Commun.* **2010**, *181*, 1477−1489.
(46) Yoo, S.; Apra, E.; Zeng, X. C.; Xantheas, S. S. *J. Phys. Chem. Lett.* **2010**, *1*, 3122−3127.
(47) Li, A.; Muddana, H. S.; Gilson, M. K. *J. Chem. Theory Comput.* **2014**, *10*, 1563−1575.
(48) Rezac, J.; Hobza, P. *J. Chem. Theory Comput.* **2013**, *9*, 2151−2155.
(49) Becke, A. D. *Phys. Rev. A* **1988**, *38*, 3098−3100.
(50) Podeszwa, R.; Patkowski, K.; Szalewicz, K. *Phys. Chem. Chem. Phys.* **2010**, *12*, 5974.
(51) Goerigk, L.; Grimme, S. *Phys. Chem. Chem. Phys.* **2011**, *13*, 6670−6688.
(52) Temelso, B.; Archer, K. A.; Shields, G. C. *J. Phys. Chem. A* **2011**, *115*, 12034.
(53) Wang, F.-F.; Deible, M. J.; Jordan, K. D. *J. Phys. Chem. A* **2013**, *117*, 7606−7611.
(54) Szczęśniak, M. M.; Chałasiński, G. *J. Mol. Struct.: THEOCHEM* **1992**, *261*, 37−54.
(55) Szczęśniak, M. M.; Kendall, R. A.; Chałasiński, G. *J. Chem. Phys.* **1991**, *95*, 5169−5178.
(56) Chałasiński, G.; Szczęśniak, M. M.; Cieplak, P.; Scheiner, S. *J. Chem. Phys.* **1991**, *94*, 2873−2883.
(57) Leverentz, H. R.; Qi, H. W.; Truhlar, D. G. *J. Chem. Theory Comput.* **2013**, *9*, 995−1006.
(58) Bates, D. M.; Tschumper, G. S. *J. Phys. Chem. A* **2009**, *113*, 3555−3559.
(59) Grimme, S.; Hujo, W.; Kirchner, B. *Phys. Chem. Chem. Phys.* **2012**, *14*, 4875−4883.
(60) Wodrich, M. D.; Corminboeuf, C.; von Ragué Schleyer, P. *Org. Lett.* **2006**, *8*, 3631.
(61) Song, J.-W.; Tsuneda, T.; Sato, T.; Hirao, K. *Org. Lett.* **2010**, *12*, 1440−1443.
(62) Grimme, S. *Org. Lett.* **2010**, *12*, 4670−4673.

Appendix C

Paper III: J. Chem. Theory Comput. 12, 3662 (2016)

JCTC Journal of Chemical Theory and Computation

Article

pubs.acs.org/JCTC

Employing Range Separation on the meta-GGA Rung: New Functional Suitable for Both Covalent and Noncovalent Interactions

Marcin Modrzejewski,*[,†] Michal Hapka,[†] Grzegorz Chalasinski,[†] and Malgorzata M. Szczesniak[‡]

[†]Faculty of Chemistry, University of Warsaw, 02-093 Warsaw, Pasteura 1, Poland

[‡]Department of Chemistry, Oakland University, Rochester, Michigan 48309-4477, United States

Supporting Information

ABSTRACT: We devise a scheme for converting an existing exchange functional into its range-separated hybrid variant. The underlying exchange hole of the Becke-Roussel type has the exact second-order expansion in the interelectron distance. The short-range part of the resulting range-separated exchange energy depends on the kinetic energy density and the Laplacian even if the base functional lacks the dependence on these variables. The most successful practical realization of the scheme, named LC-PBETPSS, combines the range-separated Perdew–Burke–Ernzerhof (PBE) exchange lifted to the hybrid meta-generalized gradient approximation rung and the Tao–Perdew–Staroverov–Scuseria (TPSS) correlation. The value of the range-separation parameter is estimated theoretically and confirmed by empirical optimization. The D3 dispersion correction is recommended for all energy computations employing the presented functional. Numerical tests show remarkably robust performance of the method for noncovalent interaction energies, barrier heights, main-group thermochemistry, and excitation energies.

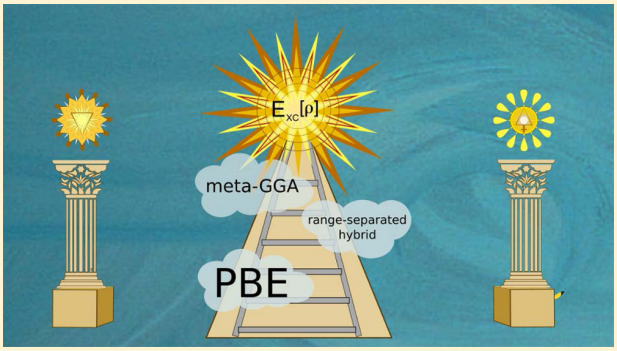

1. INTRODUCTION

Since the seminal works of Becke,[1,2] it is known that the inclusion of the Hartree–Fock (HF) exchange in density-functional models not only moves practical density functional theory (DFT) toward the goal of chemical accuracy in thermochemistry, but also has a theoretical justification rooted in the analysis of the exchange holes in molecular systems.[3] There are currently two prevalent ways of including the exact exchange in approximate DFT: as a fraction of the full HF exchange or as a long-range exact exchange component enabled only at long interelectron distances. The functionals built using the former approach, global hybrids, have become a staple of computational chemistry owing to their favorable trade-off between accuracy and cost.[1,2,4] However, the inclusion of only a fraction of the orbital exchange results in merely a slight correction of the self-interaction error inherited from the pure semilocal predecessors of global hybrids. To correct this deficiency, in range-separated (long-range corrected) hybrids the 100% HF exchange is introduced at long range. This way, the exact $-1/R$ behavior of the exchange potential is forced upon approximate potentials.[5,6] At the same time, range separation avoids the use of the full orbital exchange at all distances, which would be incompatible with an approximate semilocal correlation.

Range-separated hybrids are free from a number of shortcomings arising as a consequence of the self-interaction error. The correct long-range potential of a range-separated hybrid exchange makes the highest occupied molecular orbital (HOMO) energy close to the vertical ionization energy,[7,8] approximately satisfying Janak's theorem.[9] The spurious propensity to transfer electrons is reduced, which improves the description of donor–acceptor systems with partial charge transfer in ground and excited states. The inclusion of the long-range exact exchange also corrects the underestimation of Rydberg excitation energies and oscillator strengths,[10] and corrects the overestimation of longitudinal (hyper)-polarizabilities of polyenes.[11]

The majority of the available range-separated functionals are hybrids based on the generalized gradient approximation (GGA).[10,12−19] Notably, a systematic search spanning the vast space of possible mathematical forms have been conducted to find range-separated GGAs with the best general performance.[20] In contrast, only a few attempts have been made to develop a range-separated meta-GGA functional, that is, a hybrid model in which the semilocal part depends not only on the density and density gradient, but also on the kinetic energy density and in some cases the Laplacian. Empirical functionals of this kind have been proposed by Lin et al.[21,22] (ωM05-D and ωM06-D3) and by Peverati et al.[23] (M11). While these methods are heavily parametrized, for example, M11 contains 40 empirical parameters, the available tests show that the improvement over the best range-separated GGAs is nonuniform and minor.[22,24] A nonempirical range-separated meta-

Received: April 21, 2016
Published: July 18, 2016

DOI: 10.1021/acs.jctc.6b00406
J. Chem. Theory Comput. 2016, 12, 3662−3673

GGA based on the Tao−Perdew−Staroverov−Scuseria (TPSS) functional was tested by Vydrov et al.,[5] but for thermochemistry this method showed no improvement over the pure TPSS functional.

The purpose of this work is to construct a reliable range-separated functional in which the short-range exchange part is a meta-GGA derived from an existing nonempirical semilocal model.

The range-separated exchange energy consists of two components, short-range and long-range, defined according to the range split of the electron interaction,

$$\frac{1}{s} = \frac{\mathrm{erfc}(\omega s)}{s} + \frac{\mathrm{erf}(\omega s)}{s} \tag{1}$$

where ω is the range separation parameter and $s = |\mathbf{r}_1 - \mathbf{r}_2|$. Inserting eq 1 into the definition of the exchange energy yields the formulas for the short-range and long-range components:

$$E_{\mathrm{X,approx}}^{\mathrm{SR}} = \frac{1}{2}\sum_{\sigma}\iint \frac{\rho_\sigma(\mathbf{r}_1)h_{\mathrm{X,approx}}^{\sigma}(\mathbf{r}_1, \mathbf{r}_2)\mathrm{erfc}(\omega s)}{s}\,\mathrm{d}^3\mathbf{r}_1\,\mathrm{d}^3\mathbf{r}_2 \tag{2}$$

$$E_{\mathrm{X,exact}}^{\mathrm{LR}} = \frac{1}{2}\sum_{\sigma}\iint \frac{\rho_\sigma(\mathbf{r}_1)h_{\mathrm{X,exact}}^{\sigma}(\mathbf{r}_1, \mathbf{r}_2)\mathrm{erf}(\omega s)}{s}\,\mathrm{d}^3\mathbf{r}_1\,\mathrm{d}^3\mathbf{r}_2 \tag{3}$$

The long-range exchange energy $E_{\mathrm{X,exact}}^{\mathrm{LR}}$ is based on the exact, orbital-dependent HF exchange hole

$$h_{\mathrm{X,exact}}^{\sigma}(\mathbf{r}_1, \mathbf{r}_2) = -\frac{\left|\sum_i^{N_\sigma}\psi_{i\sigma}^*(\mathbf{r}_1)\psi_{i\sigma}(\mathbf{r}_2)\right|^2}{\rho_\sigma(\mathbf{r}_1)} \tag{4}$$

In the definition of the short-range exchange energy $E_{\mathrm{X,approx}}^{\mathrm{SR}}$, one has to assume a specific form of the approximate exchange hole $h_{\mathrm{X,approx}}^{\sigma}$. As in the case of the exchange energy density, the local definition of the exchange hole is not unique. However, the ambiguity disappears in the system average of the hole.[25]

In what follows, we present equations for closed-shell systems with $\rho_\alpha = \rho_\beta = \rho/2$. There is no loss of generality because the exchange functional for arbitrary spin polarizations is simply related to its spin-compensated counterpart by the formula[26]

$$E_{\mathrm{X}}[\rho_\alpha, \rho_\beta] = \frac{1}{2}E_{\mathrm{X}}[2\rho_\alpha] + \frac{1}{2}E_{\mathrm{X}}[2\rho_\beta] \tag{5}$$

For clarity, hereafter we skip the spin index in the exchange hole symbol.

There exists a series of range-separated GGAs which employ various levels of exact constraints in the model exchange hole inserted into the definition of $E_{\mathrm{X}}^{\mathrm{SR}}$.

One of the earliest range-separated functionals are those of Iikura, Tsuneda, Yanai, and Hirao (ITYH),[27] who devised a general technique of converting existing GGAs into range-separated hybrids. The ITYH scheme was employed in several functionals, including LC-BLYP, LC-BOP, LC-PBEOP, and CAM-B3LYP.[10,12,13]

The ITYH exchange hole is based on a simple modification of the local density approximation (LDA) exchange hole.[27] It has the correct value at $s = 0$,

$$h_{\mathrm{X,ITYH}}(\mathbf{r}_1, s = 0) = h_{\mathrm{X,exact}}(\mathbf{r}_1, s = 0) = -\frac{\rho(\mathbf{r}_1)}{2} \tag{6}$$

and satisfies the energy integral

$$\frac{1}{2}\int \frac{h_{\mathrm{X,ITYH}}(\mathbf{r}_1, s)}{s} 4\pi s^2\,\mathrm{d}s = \epsilon_{\mathrm{X,approx}}(\mathbf{r}_1) \tag{7}$$

where $\epsilon_{\mathrm{X,approx}}$ is the exchange energy density of a given base functional. The ITYH hole fails to fulfill two other exact conditions appropriate to a semilocal functional: the hole normalization[14]

$$\int h_{\mathrm{X,exact}}(\mathbf{r}_1, s) 4\pi s^2\,\mathrm{d}s = -1 \tag{8}$$

and the correct second-order short-range expansion of the spherically averaged exchange hole at zero current density,[28−30]

$$h_{\mathrm{X,exact}}(\mathbf{r}_1, s) = -\frac{\rho}{2} - Qs^2 + \ldots \tag{9}$$

$$Q = \frac{1}{12}\nabla^2\rho - \frac{1}{6}\tau + \frac{1}{24}\frac{(\nabla\rho)^2}{\rho} \tag{10}$$

where τ is the kinetic energy density

$$\tau = 2\sum_{i=1}^{N_{\mathrm{orb}}}|\nabla\psi_i|^2 \tag{11}$$

It should be stressed that eq 10 cannot be satisfied at the GGA level.

Several GGAs have been developed in which the exchange hole obeys more exact conditions than the ITYH model. The range-separated Perdew−Burke−Ernzerhof (PBE) functionals of Henderson et al.[14] and of Vydrov et al.[15] satisfy eq 6, eq 7, eq 8, and only approximately eq 10. Both methods are an improvement over the ITYH model in atomization energies and barrier heights.[14]

Still, there is a possibility for going one rung higher than the existing range-separated GGAs. This work presents a scheme for construction of meta-GGA range-separated exchange functionals which employ the kinetic energy density and the Laplacian to exactly include the second-order coefficient of eq 10. The method allows one to transform an existing GGA or a meta-GGA model into its range separated variant. The resulting functional depends on the kinetic energy density and the Laplacian even if the base functional does not.

In the following, we begin by deriving the working equations of the new range-separation scheme. Next, we search for a preferred combination of the base exchange functional and the accompanying correlation model. Finally, we test the performance of the selected functional on a test set including thermochemical energy differences, barrier heights, noncovalent interaction energies, and excitation energies.

2. THEORY

2.1. Exchange Hole Model. Our range-separation scheme requires an exchange hole model which integrates to $\epsilon_{\mathrm{X,approx}}$ and has enough degrees of freedom to satisfy two further conditions: the exact value of $h_{\mathrm{X,approx}}$ at $s = 0$ and the exact coefficient of s^2. These prerequisites are satisfied by the generalized Becke−Roussel (BR) exchange hole.[31,32] The spherically averaged generalized BR hole,

$$h_{\mathrm{X,BR}}(a, b, \mathcal{N}; s) = -\mathcal{N}\frac{a}{16\pi bs}[(a|b - s| + 1)\mathrm{e}^{-a|b-s|} - (a|b + s| + 1)\mathrm{e}^{-a|b+s|}] \tag{12}$$

includes three parameters, a, b, and $\mathcal{N}$, which we will define by selecting a subset of three equations from a wider set of

DOI: 10.1021/acs.jctc.6b00406
J. Chem. Theory Comput. 2016, 12, 3662−3673

possible conditions. For any $a > 0$ and $b > 0$, the normalization integral of $h_{X,BR}$ is

$$\int h_{X,BR}(a, b, \mathcal{N}; s) 4\pi s^2 \, ds = -\mathcal{N} \tag{13}$$

In the original BR model, the parameters a and b are fixed by enforcing the zeroth- and second-order coefficients of eq 9, and the normalization is set to -1, that is, $\mathcal{N} = 1$. With these definitions satisfied, the original $h_{X,BR}$ reduces to the exact exchange hole when applied to the hydrogen atom.[31]

The original definitions of the BR model have to be modified so that the electrostatic potential generated by $h_{X,BR}$ corresponds to the assumed base exchange energy density:

$$\frac{1}{2}\int_0^\infty \frac{h_{X,BR}(a, b, \mathcal{N}; s)}{s} 4\pi s^2 \, ds = \epsilon_{X,approx} \tag{14}$$

The formula for the short-range component of $\epsilon_{X,approx}$ will be given in section 2.2. Following Becke[32] and Precechtelova et al.,[33] we enforce eq 14 at the cost of relaxing the normalization condition. The set of equations defining the parameters of $h_{X,BR}$,

$$\frac{x-2}{x^2}\left(e^x - 1 - \frac{x}{2}\right) = -\frac{6Q}{\pi\rho^2}\epsilon_{X,approx} \tag{15}$$

$$a = \sqrt{\pi\rho\frac{(2 - 2e^x + x)}{x\epsilon_{X,approx}}} \tag{16}$$

$$b = x/a \tag{17}$$

$$\mathcal{N} = 4\pi\rho \, e^x/a^3 \tag{18}$$

is to be solved at each point of space. (For the derivation of eqs 15−18 see the Appendix of ref 32.) For any physically allowed right-hand side, a unique $x > 0$ solves eq 15. The solution can be obtained with a numerical solver or interpolation.

The resulting exchange hole integrates to the given $\epsilon_{X,approx}$ (eq 14), has the exact value at the origin (eq 6), and recovers the exact coefficient of s^2 (eq 10). However, its normalization integral differs in general from the exact value of -1.

2.2. Short-Range Exchange Energy. The short-range exchange energy density $\epsilon^{SR}_{X,approx}$ is the difference between the full-range semilocal exchange and its long-range part:

$$\epsilon^{SR}_{X,approx} = \epsilon_{X,approx} - \epsilon^{LR}_{X,approx} \tag{19}$$

We define $\epsilon^{LR}_{X,approx}$ using the potential generated by $h_{X,BR}$:

$$\epsilon^{LR}_{X,approx} = \frac{1}{2}\int_0^\infty \frac{h_{X,BR}(s)\mathrm{erf}(\omega s)}{s} 4\pi s^2 \, ds = \frac{1}{2}U^{LR}_{X,approx} \tag{20}$$

The integration in eq 20 can be done analytically, giving

$$\begin{aligned} U^{LR}_{X,approx} = &-\frac{\mathcal{N}\omega}{\nu}\,\mathrm{erf}(\nu) \\ &+ \frac{\mathcal{N}\omega}{2\nu}(1 - \mu^2 + \mu\nu)\,\mathrm{erfc}(\mu - \nu)\exp(\mu^2 - 2\mu\nu) \\ &+ \frac{\mathcal{N}\omega}{2\nu}(-1 + \mu^2 + \mu\nu)\,\mathrm{erfc}(\mu + \nu)\exp(\mu^2 + 2\mu\nu) \end{aligned} \tag{21}$$

$$\mu = \frac{a}{2\omega} \tag{22}$$

$$\nu = b\omega \tag{23}$$

For small values of ν, the right-hand side of eq 21 should be evaluated using a Taylor series expansion to avoid numerical errors. Finally, the short-range exchange energy is obtained by integrating $\epsilon^{SR}_{X,approx}$ over the whole space:

$$E^{SR}_{X,approx} = \int \epsilon^{SR}_{X,approx}(\mathbf{r}_1)\rho(\mathbf{r}_1) \, d\mathbf{r}_1 \tag{24}$$

The complete range-separated exchange energy is the sum of $E^{SR}_{X,approx}$ and the long-range HF exchange,

$$E_{X,approx} = E^{SR}_{X,approx} + E^{LR}_{X,exact} \tag{25}$$

2.3. One-Electron Self-Interaction Error. We use the example of the self-interaction error in the ground state of the hydrogen atom to illustrate the difference between our meta-GGA range-separation scheme and the existing GGA approaches.

The ground state of the hydrogen atom is a difficult limiting case for conventional DFT approximations. Using only local variables $\rho(\mathbf{r}_1)$ and $\nabla\rho(\mathbf{r}_1)$, GGAs have no way of knowing that the density under consideration belongs to a single-particle system. Therefore, the one-electron self-interaction error arises as a residual value left by an imperfect cancellation between an approximate exchange energy and the Coulomb repulsion.[31,36] A single-electron density can be detected using the kinetic energy density τ, thus meta-GGA functionals can, at least partially, reduce the self-interaction error.

The large-ω behavior of the exact short-range exchange energy of the hydrogen atom is given by the expansion[37]

$$E^{SR}_{X,exact}(\omega \to \infty) = -\frac{1}{16\omega^2} + \frac{1}{32\omega^4} + \ldots \tag{26}$$

Equation 26 assumes the exact density. Gill et al. have shown that the first term on the right-hand side is recovered already by the local density approximation, but the term of order $1/\omega^4$ requires $h_{X,approx}$ with the correct second-order expansion for small s.[37] Indeed, the short-range meta-GGA functionals derived in this work, which satisfy eq 10, approach $E^{SR}_{X,exact}(\omega \to \infty)$ visibly faster than the existing GGAs (Figure 1). The reduction of errors for large ω is seen for all tested base functionals: PBE,[38] B88,[39] and TPSS.[40]

Figure 2 shows why, in our scheme, TPSS is not a preferred candidate for the base exchange functional, and PBE should be used instead. Let $\langle h_X\rangle(s)$ denote the system and spherical average of the exchange hole for the hydrogen atom,

$$\langle h_X\rangle(s) = \int \rho(\mathbf{r}_1)\, h_X(\mathbf{r}_1, s) \, d\mathbf{r}_1 \tag{27}$$

The real-space analysis of the total exchange energy is then expressed as

$$E_X = \int_0^\infty H^{TOT}_X(s) \, ds \tag{28}$$

where

$$H^{TOT}_X(s) = 2\pi s\langle h_X\rangle(s) \tag{29}$$

and the short-range exchange energy is

$$E^{SR}_X(\omega) = \int_0^\infty H^{SR}_X(s) \, ds \tag{30}$$

where

$$H^{SR}_X(s) = 2\pi s\langle h_X\rangle(s)\,\mathrm{erfc}(\omega s) \tag{31}$$

DOI: 10.1021/acs.jctc.6b00406
J. Chem. Theory Comput. 2016, 12, 3662−3673

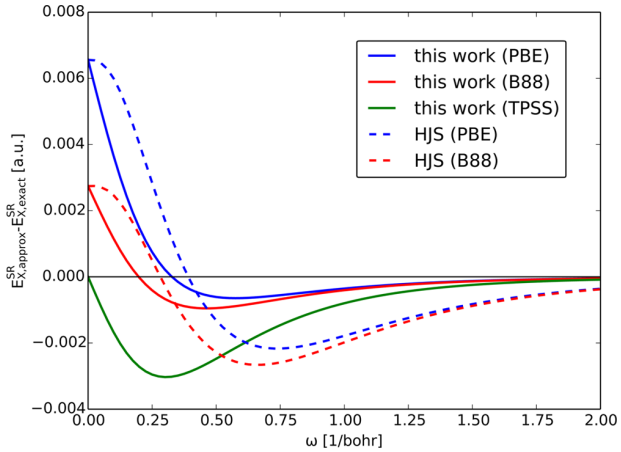

Figure 1. Differences between approximate and exact short-range exchange energies of the ground state of the hydrogen atom. All computations employ the aug-cc-pV5Z basis set[34] and HF orbitals. The short-range GGA models of Henderson et al.[14,35] are denoted as HJS. Correlation energies are not included.

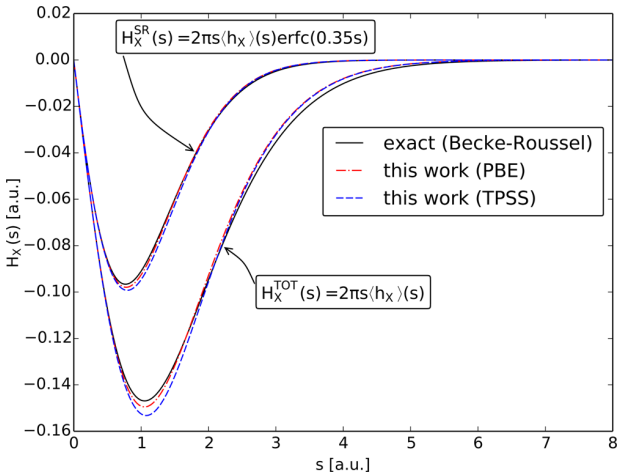

Figure 2. Real-space analysis of the contributions to the (short-range) exchange energy of the hydrogen atom. All computations employ the aug-cc-pV5Z basis set[34] and HF orbitals.

For the TPSS exchange, $H_X^{TOT}(s)$ is too deep around $s = 1$ bohr and too shallow in the tail, but these two errors perfectly cancel each other to yield the exact E_X enforced by the construction of the TPSS exchange. However, the factor $\mathrm{erfc}(\omega s)$ included in the short-range energy cuts off the tail of $H_X^{TOT}(x)$, thus leaving the relatively large short-range error uncompensated in E_X^{SR}. By contrast, in the PBE energy, the short-range and long-range errors in $H_X^{TOT}(s)$ do not cancel perfectly, but the error at short range is small, and the factor $\mathrm{erfc}(\omega s)$ enhances the error cancellation in E_X^{SR}.

The single-electron density of the hydrogen atom was previously utilized as a constraint in the design of several functionals. The TPSS exchange of Tao et al.[40] and the MVS exchange of Sun et al.[41] are parametrized to recover the exact exchange energy in this limit. The hydrogen atom energy is also included in the training set of the empirical M05-2X functional.[42] Here, we use the single-electron limit to estimate the value of ω which is most appropriate for the range-separated exchange energy obtained using our scheme. According to Figure 1, our model of the short-range PBE exchange energy recovers the exact energy at $\omega = 0.33$. Later in the text we will show that this value is nearly optimal for the atomization energies and barrier heights of small molecules.

Apart from its manifestation in approximate exchange energy functionals, the self-interaction error arises as a nonvanishing correlation energy of a single-electron system. In the case of the pure PBE exchange-correlation functional, the total energy of the hydrogen atom is only 0.0006 au lower than the exact energy, but at the same time the correlation contribution amounts to −0.006 au (−3.8 kcal/mol). This error can be eliminated only at the meta-GGA level. The desired improvement over the PBE correlation is provided by TPSS.[40,43] The TPSS correlation is built on the PBE formula, but with one-electron self-interaction terms subtracted.[43] As a result, TPSS yields exactly zero correlation energy for the hydrogen atom, which we regard as a feature compatible with our exchange model. We will test the advantage of using the TPSS correlation over PBE for general systems in the following section.

2.4. Complete Exchange-Correlation Model. To fully define our exchange-correlation functional, we have to specify the base exchange functional together with the accompanying model for correlation. We restrict our search to two exchange-correlation models only: PBE and TPSS. The choice of these two functionals reflects our preferrence for methods with a small number of empirical parameters. Still, it remains possible to pair our range-separation scheme with formulas including multiple adjustable parameters and to perform a comprehensive empirical optimization.

Let LC-*XY* denote a range-separated functional where *X* is the base model for exchange ($\epsilon_{X,approx}$ in eq 15), and *Y* is the accompanying correlation. Our search comprises three candidate functionals, LC-PBETPSS, LC-PBEPBE, and LC-TPSSTPSS, applied on a set of atomization energies (AE6[44]) and barrier heights (BH6[44]). Each functional is employed with a varying value of ω. The best method is selected for further tests described in the remainder of this paper. The AE6 and BH6 benchmarks are representative of 109 atomization energies and 44 barrier heights, respectively, in the Database/3 collection.[44]

LC-TPSSTPSS is the poorest performing functional, which cannot fully benefit from the addition of the long-range exact exchange. For this functional, a single value of ω cannot work well for both AE6 and BH6: the optimal value for the former set is $\omega = 0.0$, that is, the limit of the pure TPSS functional, whereas for the latter set $\omega = 0.35$ minimizes the mean absolute error (MAE). A similar behavior of the TPSS range-separated hybrid has been observed by Vydrov et al.[5] The numerical data for LC-TPSSTPSS are available in the Supporting Information.

The problem of choosing a universally applicable value of ω arises again in the case of the candidate based entirely on the PBE model, LC-PBEPBE, albeit it is not as severe as for LC-TPSSTPSS. At $\omega = 0.30$, the average error in the barrier heights is only 1.6 kcal/mol, but at the same time the error for the atomization energies is as high as 10.5 kcal/mol, which is large compared to the existing range-separated functionals.[14]

The best overall accuracy is achieved by LC-PBETPSS (Figure 3). The optimal range-separation parameter for this functional is in the interval $0.30 \leq \omega \leq 0.35$, depending on the weight of the BH6 set relative to AE6. (The percentage errors on the BH6 set are much larger than on AE6, see the Supporting Information.) This result matches our theoretical estimate, $\omega = 0.33$, based on the minimization of the self-

DOI: 10.1021/acs.jctc.6b00406
J. Chem. Theory Comput. 2016, 12, 3662−3673

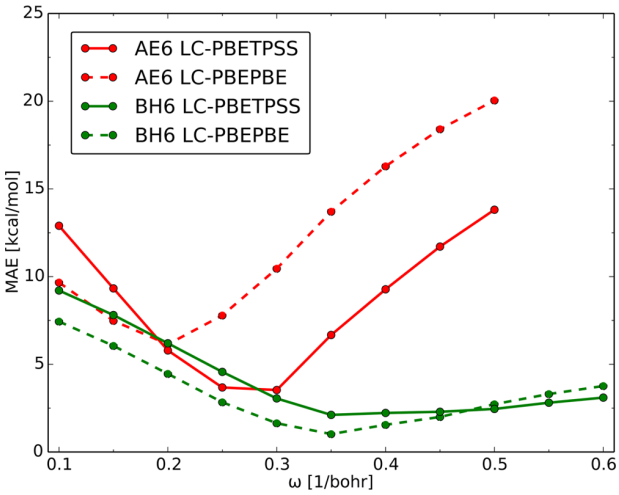

Figure 3. Mean absolute errors on the AE6 and BH6 sets.[44] All DFT computations employ the def2-QZVPP basis set.[34,45] The reference values are taken from ref 4 (AE6) and ref 46 (BH6).

interaction error for the hydrogen atom. Taking into account the relatively large errors in the barrier heights, we choose ω = 0.35 for the final version of LC-PBETPSS recommended for general use. The MAEs at this value of the range-separation parameter are 6.7 kcal/mol for AE6 and 2.1 kcal/mol for BH6. LC-PBETPSS is the final, recommended functional which we will employ in the full test set.

The long-range correction proposed here should not be confused with the correction based on the ITYH scheme, which can be applied, for example, in the Gaussian program, to any pure functional. Let us denote by LC-PBETPSS(ITYH) a functional which employs the ITYH-based range-separated PBE exchange.[27] Using the above-described procedure for optimizing the range-separation parameter, we find that ω = 0.7 is optimal simultaneously for AE6 (MAE = 14.7 kcal/mol) and BH6 (MAE = 2.6 kcal/mol). For both sets, LC-PBETPSS-(ITYH) is inferior to LC-PBETPSS, but the difference is especially large for the atomization energies. On the AE6 set, LC-PBETPSS(ITYH) is only slightly more accurate than the pure PBETPSS functional without any addition of the HF exchange. For $0.20 \leq \omega \leq 0.35$, where LC-PBETPSS performs well for AE6, LC-PBETPSS(ITYH) yields extremely large MAEs above 30 kcal/mol. Alternatively, one could combine the range-separated PBE exchange of Henderson et al.[14] and the TPSS correlation to obtain LC-PBETPSS(HJS). While this method performs generally better than LC-PBETPSS(ITYH), for its optimal value of ω = 0.45, the errors for AE6 (MAE = 9.9 kcal/mol) and BH6 (MAE = 2.4 kcal/mol) are both larger than for LC-PBETPSS. The numerical data for LC-PBETPSS-(ITYH) and LC-PBETPSS(HJS) are available in the Supporting Information.

2.5. Dispersion Correction. A dispersion correction compensates for the deficiencies of a semilocal DFT approximation in the modeling of long-range correlation contributions to noncovalent interaction energies. We test the performance of LC-PBETPSS with the D3 correction of Grimme et al.[47] The general form of the atom-pairwise D3 correction is[47]

$$E_{\mathrm{disp}}(\mathrm{D3}) = -\sum_{A>B}\sum_{n=6,8} s_n \frac{C_n^{AB}}{R_{AB}^n} f_{\mathrm{damp}}^{(n)}(R_{AB}) \tag{32}$$

$$f_{\mathrm{damp}}^{(n)}(R_{AB}) = \frac{1}{1 + 6(R_{AB}/(r_n R_0^{AB}))^{-\alpha_n}} \tag{33}$$

where $f_{\mathrm{damp}}^{(n)}$ is the damping function. The only functional-dependent parameters are r_6 and s_8. The C_6^{AB} dipole−dipole coefficients are obtained ab initio, tabulated, and interpolated for the effective coordination numbers in the system of interest. The minimization of the MAE for LC-PBETPSS-D3 on the S22 set of noncovalent systems[48,49] for LC-PBETPSS yields r_6 = 0.88971. The $1/R^8$ term is not included because it does not decrease the MAE for the training set (s_8 = 0). We employ the original damping function $f_{\mathrm{damp}}^{(n)}(R_{AB})$,[47] which vanishes for $R_{AB} \to 0$, instead of the newer Becke−Johnson damping[50] to avoid double counting of the interaction energy at short range. Optionally, a 3-body term can be added to model the Axilrod−Teller−Muto contribution to the dispersion energy:[47]

$$E_{\mathrm{disp}}^{3-\mathrm{body}}(\mathrm{D3}) = -\sum_{A>B>C} C_9^{ABC} \frac{(3\cos\theta_a \cos\theta_b \cos\theta_c + 1)}{(R_{AB}R_{BC}R_{CA})^3} f_{\mathrm{damp}}^{(9)}(\bar{R}_{\mathrm{ABC}}) \tag{34}$$

where θ_a, θ_b, and θ_c are angles between the three interacting atoms, and $\bar{R}_{\mathrm{ABC}}$ is the geometric mean of the interatomic distances. The triple-dipole coefficient C_9^{ABC} is approximated as

$$C_9^{ABC} = -\sqrt{C_6^{AB}C_6^{AC}C_6^{BC}} \tag{35}$$

The nonadditive three-body term is known to be important for large systems.[51]

3. RESULTS AND DISCUSSION

3.1. Electronic-Structure Methods. The functional developed in this work is denoted as LC-PBETPSS. For the clarity of presentation, let us list its main characteristics which were discussed in the previous sections. The range-separated exchange combines the meta-GGA short-range PBE exchange and the 100% HF exchange at long range. The range-separation parameter of the exchange is fixed at ω = 0.35. The TPSS model is used for the correlation term. The LC-PBETPSS functional is applied with the D3 dispersion correction (LC-PBETPSS-D3) and for some systems without the dispersion term (LC-PBETPSS). The LC-PBETPSS functional is implemented in the developer version of the Molpro program.[52]

To make a fair presentation of the performance of the new method, we have assembled a test set of well-established functionals for comparison. The LC-ωPBE functional of Vydrov and Scuseria[15] is a GGA range-separated functional based on the PBE exchange and PBE correlation. The numerical comparison between LC-PBETPSS-D3 and LC-ωPBE-D3 probes the cumulative effect of upgrading the short-range exchange to meta-GGA and removing the one-electron self-interaction error from the correlation. The M06-2X empirical meta-GGA functional of Zhao and Truhlar[53] is a workhorse of modern computational chemistry. Even though this functional reproduces a large part of the dispersion energy in the vicinity of equilibrium separations, adding the D3 correction slightly improves the results in general. M06-2X-D3 is the best dispersion-corrected meta-GGA hybrid on the

DOI: 10.1021/acs.jctc.6b00406
J. Chem. Theory Comput. 2016, 12, 3662−3673

GMTKN30 database.[54] ωB97XD is an empirical, dispersion-corrected, range-separated GGA functional of Chai and Head-Gordon.[18] It is designed for thermochemistry, kinetics, and energies of noncovalent systems. ωB97X[17] is a predecessor of ωB97XD, which is not optimized for use with a dispersion correction. Still, its design makes it suitable for spectroscopic properties.[55] We employ ωB97X in the part of our tests devoted to excitation energies. M06-L is an empirical meta-GGA functional which does not contain any HF exchange.[53] It is known for the reliable description of hydrogen-bonded systems.[56] Finally, B3LYP-D3 is an example of a hybrid functional[57] developed in the 1990s, supplemented with the modern D3 correction.

In addition to DFT methods, for ground-state charge-transfer dimers we use the DLPNO−CCSD(T) method,[58] which is a low-scaling approximation within the coupled-cluster wave function formalism including connected triples. The numerical thresholds for DLPNO−CCSD(T) are set at the "tight" level defined in Table 1 of ref 59, as recommended for noncovalent interactions.[59] The DLPNO−CCSD(T) computations are performed with the ORCA 3.0.3 program.[60]

3.2. Hydrogen-Bonded Systems. Modeling of hydrogen-bonded clusters is still challenging for modern DFT procedures. Common hybrid GGAs and the M06-type functionals accurately describe the binding energies but unexpectedly fail for the proton-exchange barriers on the CEPX33 set of NH_3, H_2O, and HF clusters.[56,61] In our tests on the CEPX33 set, LC-PBETPSS-D3 performs consistently well for both properties (Figures 4 and 5). It is the best method for the binding energies and only slightly less accurate than the best functional (M06-L) for the barriers. The D3 correction added to LC-PBETPSS improves the results for both binding energies and barrier heights (Table 1). This is in contrast to LC-ωPBE, for which the effect of supplying the dispersion term is inconsistent.

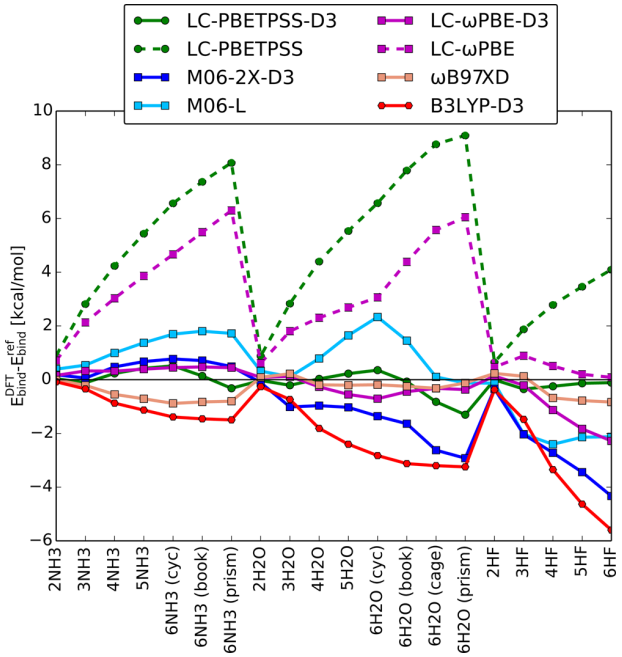

Figure 4. Errors for the binding energies of the CEPX33 set. The computational details are provided in Table 1.

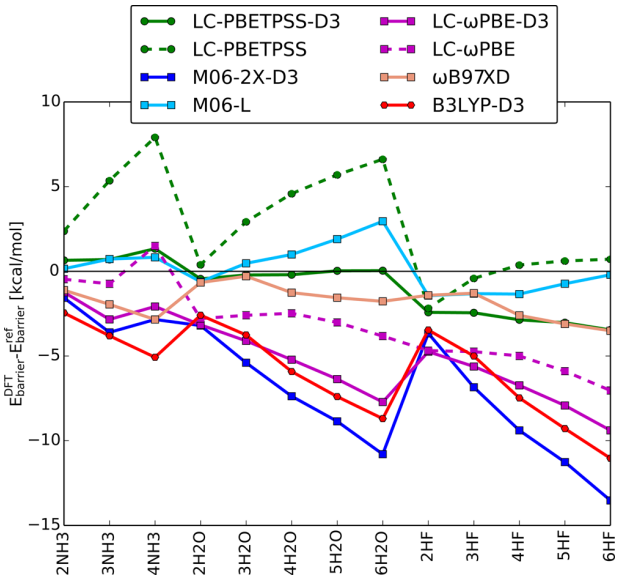

Figure 5. Errors for the proton-exchange barriers of the CEPX33 set. The computational details are provided in Table 1.

Table 1. Mean Absolute Errors (kcal/mol) for the Binding Energies (BE) and Proton-Exchange Barriers (PX) of the CEPX33 Set[a]

method	BE	PX
LC-PBETPSS-D3	0.28	1.37
LC-PBETPSS	4.71	3.09
M06-L	1.21	1.05
ωB97XD	0.41	1.80
M06-2X-D3	1.40	6.79
LC-ωPBE	2.74	3.44
LC-ωPBE-D3	0.55	5.16
B3LYP-D3	1.99	5.84

[a]Energies are computed with the aug-cc-pVQZ basis.[34] The geometries and reference energies are taken from ref 61.

To test if the high accuracy of LC-PBETPSS-D3 persists for systems larger than those of the CEPX33 set, we apply this functional on the set of water 16-mers studied by Yoo et al.[62] Here, some of the water molecules are connected through hydrogen bonds to four nearest neighbors. The structures of kind I (4444-a and 4444-b) include eight such nodes, whereas the structures of kind II (antiboat, boat-a, and boat-b) include four water molecules with such high connectivity.[62] As illustrated in Figure 6, LC-PBETPSS-D3 represents reliably the absolute binding energies, but it predicts that the clusters of kind I are slightly too stable relative to the clusters of kind II. A similar, yet more pronounced error in the relative energies is present for the M06-type functionals: M06-L and M06-2X-D3.

3.3. Noncovalent Charge-Transfer Dimers. Since the 1990s, it is known that pure and global hybrid functionals severely overestimate binding energies of noncovalent charge-transfer dimers.[65,66] Range-separated functionals achieve qualitative improvement by removing the main cause of the overbinding, which is an unrealistic propensity to transfer electrons between the donor and acceptor. The distinction between range-separated functionals and more traditional DFT approximations is apparent for the interaction energy curve of the NH_3...ClF dimer (Figure 7). The two deepest, most

DOI: 10.1021/acs.jctc.6b00406
J. Chem. Theory Comput. 2016, 12, 3662−3673

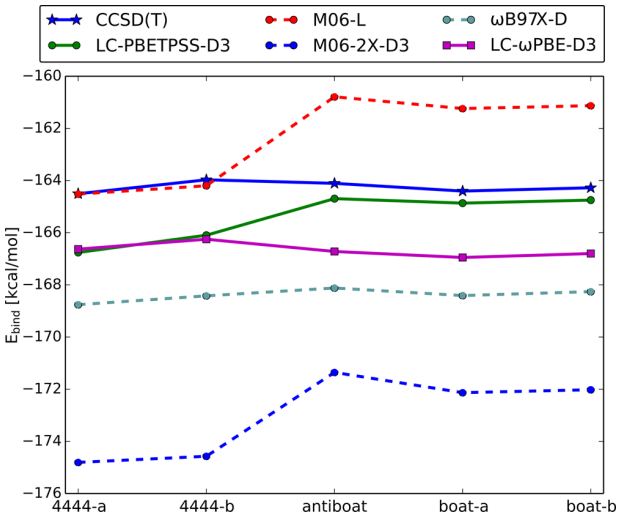

Figure 6. Binding energies of water 16-mers. The def2-TZVPPD basis[34,45] is employed for LC-PBETPSS-D3. The basis-set extrapolated CCSD(T) energies are taken from ref 63. The energies for the existing DFT methods are taken from ref 64.

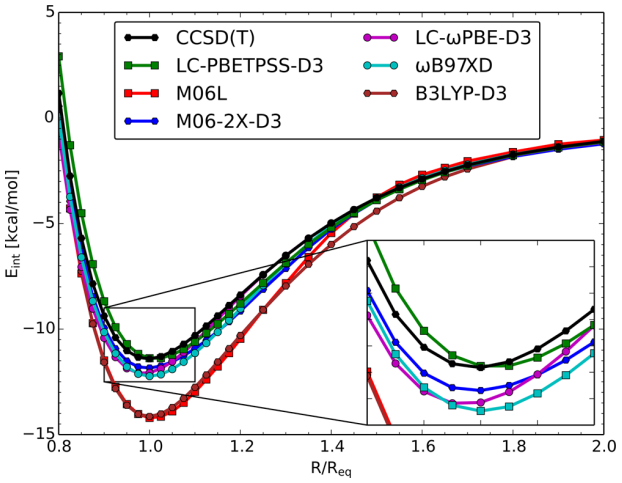

Figure 7. Interaction energy curves for the NH_3...ClF dimer.

overbinding curves belong to M06-L and B3LYP-D3, a pure functional and a global hybrid, respectively. The range-separated methods, LC-PBETPSS-D3 in particular, yield a distinct group of energies close to the reference CCSD(T) curve. The only functional which performs well but is not range-separated, M06-2X-D3, includes a relatively large fraction of the HF exchange (54%).

The LC-PBETPSS-D3 curve is extremely close to the reference curve in the vicinity of the equilibrium separation of NH_3...ClF, but its repulsive part is overestimated. For the compressed dimer at R/R_{eq} = 0.8, the interaction energy of LC-PBETPSS-D3 (E_{int} = +2.92 kcal/mol) is qualitatively different from that of LC-ωPBE-D3 (E_{int} = −0.72 kcal/mol), but in accordance with the reference coupled-cluster result (E_{int} = +1.17 kcal/mol).

Similar behavior of approximate DFT methods is observed for the CT9 set of relatively weakly bound donor−acceptor equilibrium dimers (Table 2). The CT9 set gathers the dimers of the CT7/04 set Zhao and Truhlar[67] (C_2H_2...ClF, C_2H_4...F_2, H_2O···ClF, HCN···ClF, NH_3...Cl_2, NH_3...F_2) and a subset of the complexes studied by Yourdkhani et al.[68] (CF_3CN···BF_3, GeF_3CN···BF_3, SiF_3CN···BF_3). The MAEs for CT9 are similar for all range-separated functionals and for M06-2X-D3, but the range-separated hybrids tend to underbind, while M06-2X-D3 predicts excessive binding. Compared with the uncorrected variants, both LC-PBETPSS and LC-ωPBE benefit from the D3 dispersion correction.

Table 2. Mean Absolute Errors (kcal/mol) for the Interaction Energies of the CT9 Set of Charge-Transfer Dimers[a]

method	MAE
DLPNO−CCSD(T)	0.18
M06-2X-D3	0.37
LC-PBETPSS-D3	0.39
LC-PBETPSS	1.44
LC-ωPBE-D3	0.41
LC-ωPBE	1.14
ωB97XD	0.41
B3LYP-D3	0.73
M06-L	0.81

[a]DFT computations are performed with the def2-QZVPP basis. The reference energies at the CCSD(T) level and the DLPNO−CCSD(T) energies are extrapolated to the basis-set limit (aug-cc-pVTZ → aug-cc-pVQZ) with the automated extrapolation scheme available in ORCA.[60] The same computational procedure is employed for the interaction energy curves of the NH_3...ClF dimer.

For additional comparison, we also employ the low-scaling DLPNO−CCSD(T) wave function method. With the MAE of 0.18 kcal/mol on the CT9 set, DLPNO−CCSD(T) is more accurate than any tested DFT method. However, it is still computationally more expensive than single-determinantal DFT approaches owing to the relatively strong dependence on the basis set quality.

3.4. Main-Group Thermochemistry. To test the performance of LC-PBETPSS-D3 for main-group thermochemistry, we use the sets of isodesmic reaction energies,[69] Diels−Alder reaction energies (DARC),[54] and reaction energies with a large contribution of the intramolecular dispersion energy (IDISP).[54]

A general-purpose functional has to describe the energy differences between covalently bound structures while including the contributions from intramolecular noncovalent interactions. A model case of this kind involves the reaction energies of *n*-alkane isodesmic fragmentation

$$CH_3(CH_2)_mCH_3 + mCH_4 \rightarrow (m+1)C_2H_6 \quad (36)$$

Several authors have enumerated the factors which affect the accuracy of approximate DFT for these reactions. Grimme[69] noted that a dispersion correction is crucial, but even a dispersion-corrected semilocal DFT lacks a proper description of middle-range correlation. Johnson et al.[70] ascribed the size-dependent errors in the reaction energies to the deficient description of regions where the reduced density gradient changes upon the reaction. An appropriate description of these regions is provided by the PBEsol exchange energy which obeys the exact second-order expansion for small density gradients.[70,71] Song et al.[72] stressed the importance of correcting the exchange functional via range separation. Finally, Modrzejewski et al.[63] demonstrated a remarkable improvement in the isodesmic reaction energies when using the MCS functional, which combines the range-separated PBEsol

DOI: 10.1021/acs.jctc.6b00406
J. Chem. Theory Comput. 2016, 12, 3662−3673

exchange and our meta-GGA correlation optimized to work with a dispersion correction.[73]

In our tests, all functionals underestimate alkane stability with the error proportional to the alkane size (Figure 8). The

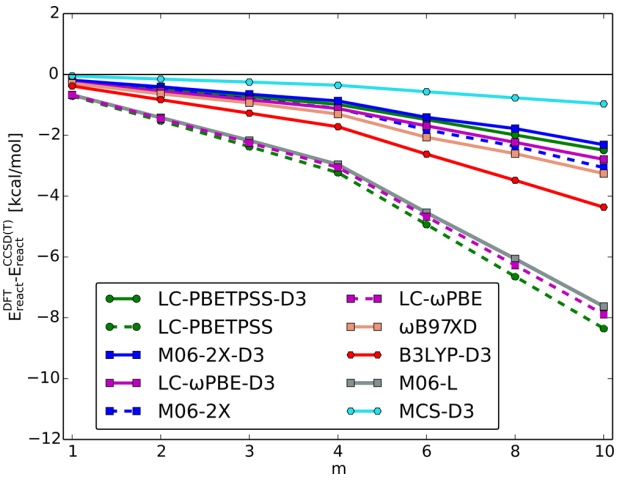

Figure 8. Errors in isodesmic reaction energies of *n*-alkane fragmentation. The geometries and reference energies at the CCSD(T) level are taken from ref 69. The def2-QZVP basis is employed for all DFT computations except for MCS-D3. MCS-D3 is a range-separated functional based on the PBEsol exchange.[63] The energies for MCS-D3 are computed using the def2-TZVPP basis.

two error curves with the lowest slope belong to LC-PBETPSS-D3 and M06-2X-D3. Without the D3 correction, LC-PBETPSS and LC-ωPBE form a group of outliers together with the pure M06-L functional. The dispersion term has only a limited effect on M06-2X, which appears to account for the essential part of the intramolecular dispersion energy via its extensive empirical parametrization.

The DARC subset of the GMTKN30 database[54] comprises 14 Diels–Alder reaction energies in which the reactants containing multiple conjugated bonds react to form cyclic and bicyclic products (see Figure 1 in ref 74). Most of the existing DFT approximations underestimate the reaction energies in this set.[74] The reasons for that have general implications for the application of approximate DFT for main group thermochemistry. Johnson et al.[74] have argued that the reactants of the Diels–Alder reaction have delocalized electron densities, therefore these structures are artificially stabilized due to the self-interaction (delocalization) error. On the products side, the bicyclic molecules have bridgehead carbons whose noncovalent repulsion tends to be overestimated by approximate DFT.[74] Because of these two systematic effects, the energetic gain of going from the reactants to the products is underestimated.

LC-PBETPSS-D3 achieves the lowest mean absolute error of all functionals tested on the DARC set (Table 3). The addition of the dispersion correction to LC-PBETPSS reduces the MAE by a factor of 4. In contrast, supplying the D3 term to LC-ωPBE increases the MAE from 6.3 to 10 kcal/mol. The effect of the three-body dispersion term included in LC-PBETPSS-D3 + 3body is negligible due to the small size of the systems.

The IDISP subset of the GMTKN30 database is composed of six reaction energies in which alkanes undergo transformations between structures with different amounts of the intramolecular dispersion energy.[54] A typical reaction included

Table 3. Mean Absolute Errors (kcal/mol) for the Reaction Energies of the IDISP and DARC Sets[a]

method	IDISP	DARC
LC-PBETPSS-D3	2.35[b]	1.38[c]
LC-PBETPSS-D3 + 3body	2.27[b]	1.37[c]
LC-PBETPSS	11.38[b]	6.07[c]
M06-L[d]	6.55	8.04
M06-2X-D3[d]	1.71	2.28
LC-ωPBE-D3[d]	4.13	10.04
LC-ωPBE[d]	8.03	6.30
B3LYP-D3[d]	6.63	10.23
ωB97XD[d]	2.63	1.98

[a]Reference energies and geometries are obtained from the companion Web site of ref 54. [b]Computed with the def2-QZVP basis. [c]Computed with the def2-QZVPP basis. [d]Reference 54.

in IDISP is presented in Figure 9. LC-PBETPSS-D3, M06-2X-D3, and ωB97XD are the best methods tested on this set

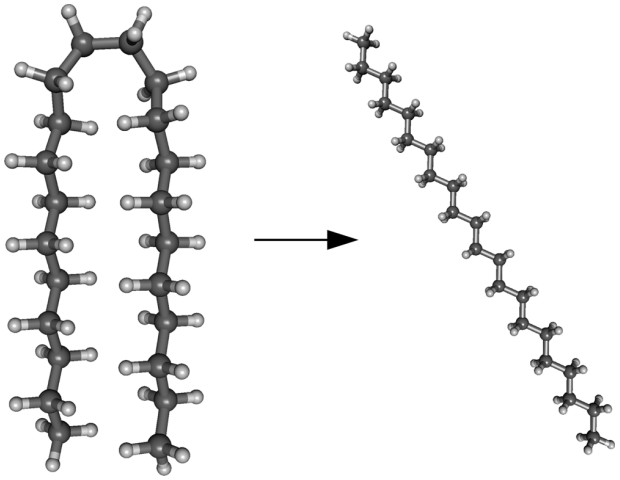

Figure 9. Example of a reaction included in the test set for intramolecular dispersion interactions (IDISP).[54]

(Table 3). The D3 correction is important and beneficial for both LC-PBETPSS and LC-ωPBE. The addition of the three-body D3 term has a noticeable beneficial effect on the reaction energies predicted by LC-PBETPSS-D3 + 3body.

3.5. Excitation Energies. Numerous authors have reported evidence that there exists a marked advantage of using range-separated functionals over more traditional DFT approximations for excitation energies of donor–acceptor systems and for Rydberg transitions, without compromising on valence excitations.[10,13] To test the performance of LC-PBETPSS, we apply it to the lowest charge-transfer excitations of aromatic donor-tetracyanoethylene (Ar-TCNE) pairs (Table 4) as well as valence and Rydberg excitations of CO, N_2, H_2CO, C_2H_4, and C_4H_6 (Table 5).

Due to the limitations of the software suite in which LC-PBETPSS has been initially implemented, the excitation energies for this functional are obtained using real-time time-dependent DFT (RT-TDDFT) instead of the usual linear response equations.[75,76] The propagation of the density matrix was carried out for 2500 au (60 fs) for all molecules except for the TCNE–xylene dimer and ethylene, which were propagated for 3000 au and 10000 au, respectively. The time step in each

DOI: 10.1021/acs.jctc.6b00406
J. Chem. Theory Comput. 2016, 12, 3662–3673

Table 4. Energies (eV) of the Lowest CT Transitions in Gas-Phase Ar−TCNE Complexes[a]

Ar	benzene	toluene	*o*-xylene
ref[77]	3.59	3.36	3.15
ωB97X[17]	3.67	3.34	3.37
LC-ωPBE	4.00	3.65	3.68
LC-PBETPSS	3.87	3.50	3.49
B3LYP	2.06	1.81	1.88
M06-L	1.65	1.46	1.56
M06-2X	3.03	2.93	2.78
GW[78]	3.58	3.27	2.89
BNL[b]	3.8	3.4	3.0

[a]DFT calculations employ the cc-pVDZ basis set.[34] [b]The range-separated BNL functional[79] includes a system-dependent parameter ω. The energies are taken from ref 80.

case was Δt = 0.1 au (0.0024 fs). Each time a dc pulse with a duration of 0.24 fs and field strength of E_{max} = 0.0001 au was applied. All RT-TDDFT calculations were carried out in the Molpro program.[52]

LC-PBETPSS achieves about the same level of accuracy for Rydberg, valence, and charge-transfer excitations (Tables 4 and 5). While the best DFT method for the charge-transfer transitions is ωB97X,[17] there is only an insignificant difference between ωB97X, LC-PBETPSS, and LC-ωPBE for valence and Rydberg excitations.

3.6. Symmetry-Adapted Perturbation Theory. Symmetry-adapted perturbation theory provides a framework for computation and intepretation of noncovalent interaction energies.[86] The energy contributions defined in SAPT can be computed using approximate functionals, provided that orbital coefficients, orbital energies, and density response functions are available.

The accuracy of the total interaction energy as well as of the individual SAPT contributions is contingent on the realistic description of the density tail, therefore traditional pure and global hybrid functionals must employ asymptotic corrections of the exchange-correlation potential.[87] Range-separated functionals do not require the corrections which change the decay rate of the potential, but they need a procedure that levels the HOMO energy with negative of the vertical ionization potential (IP).[88] The adjustment of the orbital energy involves tuning of the range-separation parameter for each molecule of interest to satisfy Koopmans' theorem:[80]

$$\epsilon_{HOMO}(\omega) = -IP(\omega) \quad (37)$$

The procedure of solving eq 37 is repeated for each interacting monomer,[88] therefore each monomer is assigned its unique value of ω.

To illustrate the importance of using the monomer-dependent range-separation parameters, we employ LC-PBETPSS and the range-separated PBE functional of Henderson et al.[14] (HJS-ωPBE) to compute the total SAPT interaction energies on the A24 set of noncovalent dimers.[89] Here, the total interaction energy is a sum of the first- and second-order SAPT contributions plus a so-called delta-HF term. Each functional is used to compute the orbital coefficients and energies provided to the SAPT program, but the exchange-

Table 5. Energies (eV) of Valence and Rydberg Transitions in CO, N_2, Formaldehyde, Ethylene, and *trans*-1,3-Butadiene

transition	ref	B3LYP	M06-L	M06-2X	ωB97X[17]	LC-ωPBE	LC-PBETPSS
CO[a]							
$\sigma \rightarrow \pi^*$	8.51[d]	8.40	8.58	8.22	8.53	8.55	8.66
$\sigma \rightarrow 3s$	10.78[d]	9.83	9.35	10.86	10.77	10.84	10.76
$\sigma \rightarrow 3p\sigma$	11.40[d]	10.21	9.61	10.86	11.22	11.34	11.15
$\sigma \rightarrow 3p\pi$	11.53[d]	10.27	9.87	10.90	11.31	11.42	11.28
N_2[a]							
$\sigma_g \rightarrow 3p\pi_u$	12.90[d]	11.78	10.85	12.47	12.57	12.68	12.50
$\sigma_g \rightarrow 3p\sigma_u$	12.98[d]	11.62	10.53	12.53	12.59	12.70	12.52
$\pi_u \rightarrow 3s\sigma_g$	13.24[f]	12.04	11.76	12.49	12.88	13.01	12.86
H_2CO[a]							
$n \rightarrow 3sa_1$	7.09[d]	6.43	6.14	7.09	7.28	7.26	7.11
$n \rightarrow 3pb_2$	7.97[d]	7.15	6.49	7.90	8.12	8.11	7.98
$n \rightarrow 3pa_1$	8.12[d]	7.16	6.57	7.78	8.00	8.00	7.84
$\sigma \rightarrow \pi^*$	8.68[d]	9.01	7.01	8.81	8.99	9.11	8.92
C_2H_4[b]							
$\pi \rightarrow 3s$	7.11[e]	6.56	6.60	6.85	7.38	7.52	7.44
$\pi \rightarrow \pi^*$	7.96[c]	7.32	7.18	7.47	7.57	7.63	7.69
$\pi \rightarrow 3d\delta$	8.90[e]	7.61	7.22	8.42	8.98	9.23	9.13
$\pi \rightarrow 3d\delta$	9.08[e]	7.77	7.47	8.52	9.08	9.33	9.21
$\pi \rightarrow 3d\pi$	9.33[e]	7.69	7.52	8.58	9.09	9.38	9.28
$\pi \rightarrow 3d\pi$	9.51[e]	8.09	7.92	8.82	9.46	9.79	9.68
C_4H_6[b]							
$\pi \rightarrow \pi^*$	6.32[c]	5.54	5.62	5.76	5.88	5.97	5.98
Ryd ($2A_u$)	6.66[e]	5.88	5.87	6.15	6.84	6.94	6.86
Ryd ($2B_u$)	7.07[e]	6.36	6.09	6.75	7.29	7.40	7.29
Ryd ($3B_u$)	8.00[e]	6.74	6.39	7.46	8.04	8.30	8.18
MAE		0.97	1.36	0.42	0.20	0.23	0.22

[a]Energies are computed with the augmented Sadlej basis.[81] [b]Energies are computed with the 6-311(3+,3+)G** basis.[82] [c]Theoretical energy at the FCIQMC level, ref 83. [d]Experimental energy, ref 10. [e]Experimental energy, ref 84. [f]Experimental energy, ref 85.

DOI: 10.1021/acs.jctc.6b00406
J. Chem. Theory Comput. 2016, 12, 3662−3673

correlation kernel is in every case at the adiabatic local density approximation level.

The improvement of LC-PBETPSS upon using eq 37 is clear, with over 3-fold reduction of the MAE for the total interaction energies (Table 6). The errors are reduced by a similar factor for HJS-ωPBE. With the monomer-dependent parameter ω, LC-PBETPSS achieves slightly better accuracy than the common PBE0AC approach, that is, the PBE0 functional[90] employed with the asymptotic correction of Gruning et al.[87]

Table 6. Mean Absolute Errors (kcal/mol) for the Total SAPT Interaction Energies of the A24 Set[a]

method	MAE
HJS-ωPBE(ω = 0.40)	0.19
HJS-ωPBE(ω = *)[b]	0.07
LC-PBETPSS(ω = 0.35)	0.30
LC-PBETPSS(ω = *)[b]	0.09
PBE0AC	0.12

[a]SAPT calculations employ the aug-cc-pVTZ basis set. [b]Range-separation parameters are adjusted to satisfy eq 37.

4. SUMMARY AND CONCLUSIONS

We have proposed a method of creating meta-GGA range-separated exchange functionals from existing semilocal approximations. Owing to the use of the kinetic energy density and the Laplacian, the underlying exchange hole has the exact second-order expansion in the interelectron distance. The importance of this condition is demonstrated for the hydrogenic density, for which the functionals derived using the new approach show a clear reduction of the self-interaction errors compared to existing range-separated GGAs.

While the method is general, its performance strongly depends on the selected pair of the base exchange functional and the accompanying correlation. The initial numerical tests on small sets of atomization energies and barrier heights have shown that the preferred pair of the semilocal models is the PBE exchange and the TPSS correlation. Therefore, the only functional considered in the full suite of tests and the method which we recommend for general use is LC-PBETPSS.

The onset of the long-range HF exchange is controlled by the range-separation parameter which is estimated theoretically and confirmed by empirical optimization to be ω = 0.35. For applications in SAPT, we recommend to adjust ω to enforce Koopmans' theorem for the interacting monomers.

Supplementing LC-PBETPSS with the D3 dispersion correction (comprising only the $1/R^6$ term) generally improves the accuracy of the method for all test sets considered in this work. We observe additional slight improvement when a three-body dispersion term is included for large systems.

As Figure 10 illustrates, the accuracy of LC-PBETPSS-D3 is remarkably consistent across the whole range of tests which probe the performance for noncovalent interaction energies, barrier heights, and thermochemical energy differences. The errors corresponding to LC-PBETPSS-D3 are in most cases either the smallest or close to the best functionals. The only other functional achieving a similar level of consistent accuracy is ωB97XD. When applied to excited states of small systems, LC-PBETPSS describes charge-transfer and Rydberg excitations with a similar level of accuracy as valence excitations.

Compared to LC-ωPBE-D3, the new method offers improved accuracy for the reaction energies of the IDISP set,

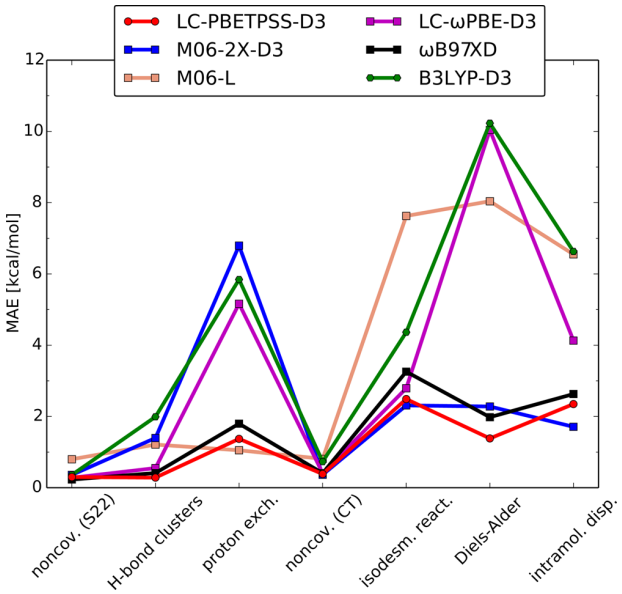

Figure 10. General view of the performance of DFT methods on the benchmark sets considered in this work. The data points for the isodesmic reaction are the absolute errors for dodecane.

Diels–Alder reaction energies, and proton-exchange barriers. While LC-PBETPSS-D3 works better for covalent bonds, it does not compromise on the accuracy for noncovalent interaction energies. Moreover, the dispersion correction is more compatible with LC-PBETPSS than with LC-ωPBE. The D3 term is beneficial for LC-ωPBE when applied to the interaction energies of noncovalent dimers and clusters, but it degrades the accuracy for proton-exchange barriers and Diels–Alder reaction energies. The performance of LC-PBETPSS-D3 is free from such irregularities.

Compared to M06-2X-D3, the new method is more reliable for the binding energies and barrier heights of hydrogen-bonded systems while providing a similar level of accuracy in alkane thermochemistry.

To conclude, the tests presented in this work show that LC-PBETPSS-D3 combines reliability with low empiricism. Further work is needed to assess the performance of the new functional for systems with more complicated electronic structure.

■ ASSOCIATED CONTENT

Supporting Information

The Supporting Information is available free of charge on the ACS Publications website at DOI: 10.1021/acs.jctc.6b00406.

Spreadsheets containing detailed numerical data and computational details, geometries for the CT9 set and the NH_3...ClF dimer (ZIP)

■ AUTHOR INFORMATION

Corresponding Author

*E-mail: m.m.modrzejewski@gmail.com.

Funding

M.M. and M.H. were supported by the Polish Ministry of Science and Higher Education (Grants No. 2014/15/N/ST4/02170 and No. 2014/15/N/ST4/02179). M.M.S. and G.C. were supported by the National Science Foundation (Grant No. CHE-1152474). M.M., M.H., and G.C. gratefully acknowl-

edge additional financial support from the Foundation for Polish Science. Special thanks to Aleksandra Tucholska for creating the TOC graphic.

Notes

The authors declare no competing financial interest.

REFERENCES

(1) Becke, A. D. *J. Chem. Phys.* **1993**, *98*, 5648−5652.
(2) Becke, A. D. *J. Chem. Phys.* **1993**, *98*, 1372−1377.
(3) Becke, A. D. *J. Chem. Phys.* **2014**, *140*, 18A301.
(4) Peverati, R.; Truhlar, D. G. *Philos. Trans. R. Soc., A* **2014**, *372*, 20120476.
(5) Vydrov, O. A.; Heyd, J.; Krukau, A. V.; Scuseria, G. E. *J. Chem. Phys.* **2006**, *125*, 074106.
(6) Baer, R.; Livshits, E.; Salzner, U. *Annu. Rev. Phys. Chem.* **2010**, *61*, 85−109.
(7) Refaely-Abramson, S.; Sharifzadeh, S.; Govind, N.; Autschbach, J.; Neaton, J. B.; Baer, R.; Kronik, L. *Phys. Rev. Lett.* **2012**, *109*, 226405.
(8) Kronik, L.; Stein, T.; Refaely-Abramson, S.; Baer, R. *J. Chem. Theory Comput.* **2012**, *8*, 1515−1531.
(9) Janak, J. F. *Phys. Rev. B: Condens. Matter Mater. Phys.* **1978**, *18*, 7165−7168.
(10) Tawada, Y.; Tsuneda, T.; Yanagisawa, S.; Yanai, T.; Hirao, K. *J. Chem. Phys.* **2004**, *120*, 8425.
(11) Kamiya, M.; Sekino, H.; Tsuneda, T.; Hirao, K. *J. Chem. Phys.* **2005**, *122*, 234111.
(12) Song, J.-W.; Hirosawa, T.; Tsuneda, T.; Hirao, K. *J. Chem. Phys.* **2007**, *126*, 154105.
(13) Yanai, T.; Tew, D. P.; Handy, N. C. *Chem. Phys. Lett.* **2004**, *393*, 51−57.
(14) Henderson, T. M.; Janesko, B. G.; Scuseria, G. E. *J. Chem. Phys.* **2008**, *128*, 194105.
(15) Vydrov, O. A.; Scuseria, G. E. *J. Chem. Phys.* **2006**, *125*, 234109.
(16) Rohrdanz, M. A.; Martins, K. M.; Herbert, J. M. *J. Chem. Phys.* **2009**, *130*, 054112.
(17) Chai, J.; Head-Gordon, M. *J. Chem. Phys.* **2008**, *128*, 084106.
(18) Chai, J.-D.; Head-Gordon, M. *Phys. Chem. Chem. Phys.* **2008**, *10*, 6615−6620.
(19) Lin, Y.-S.; Li, G.-D.; Mao, S.-P.; Chai, J.-D. *J. Chem. Theory Comput.* **2013**, *9*, 263−272.
(20) Mardirossian, N.; Head-Gordon, M. *J. Chem. Phys.* **2014**, *140*, 18A527.
(21) Lin, Y.-S.; Tsai, C.-W.; Chai, J.-D. *J. Chem. Phys.* **2012**, *136*, 154109.
(22) Lin, Y.-S.; Li, G.-D.; Mao, S.-P.; Chai, J.-D. *J. Chem. Theory Comput.* **2012**, *9*, 263−272.
(23) Peverati, R.; Truhlar, D. G. *J. Phys. Chem. Lett.* **2011**, *2*, 2810−2817.
(24) Mardirossian, N.; Head-Gordon, M. *J. Chem. Phys.* **2015**, *142*, 074111.
(25) Ernzerhof, M.; Perdew, J. P. *J. Chem. Phys.* **1998**, *109*, 3313−3320.
(26) Oliver, G.; Perdew, J. *Phys. Rev. A: At., Mol., Opt. Phys.* **1979**, *20*, 397−403.
(27) Iikura, H.; Tsuneda, T.; Yanai, T.; Hirao, K. *J. Chem. Phys.* **2001**, *115*, 3540−3544.
(28) Becke, A. *J. Chem. Phys.* **1988**, *88*, 1053.
(29) Becke, A. *Can. J. Chem.* **1996**, *74*, 995.
(30) Lee, C.; Parr, R. *Phys. Rev. A: At., Mol., Opt. Phys.* **1987**, *35*, 2377.
(31) Becke, A.; Roussel, M. *Phys. Rev. A: At., Mol., Opt. Phys.* **1989**, *39*, 3761.
(32) Becke, A. D. *J. Chem. Phys.* **2003**, *119*, 2972−2977.
(33) Precechtelova, J. P.; Bahmann, H.; Kaupp, M.; Ernzerhof, M. *J. Chem. Phys.* **2015**, *143*, 144102.
(34) Schuchardt, K. L.; Didier, B. T.; Elsethagen, T.; Sun, L.; Gurumoorthi, V.; Chase, J.; Li, J.; Windus, T. L. *J. Chem. Inf. Model.* **2007**, *47*, 1045−1052.
(35) Weintraub, E.; Henderson, T. M.; Scuseria, G. E. *J. Chem. Theory Comput.* **2009**, *5*, 754−762.
(36) Perdew, J. P.; Zunger, A. *Phys. Rev. B: Condens. Matter Mater. Phys.* **1981**, *23*, 5048.
(37) Gill, P. M.; Adamson, R. D.; Pople, J. A. *Mol. Phys.* **1996**, *88*, 1005−1009.
(38) Perdew, J.; Burke, K.; Ernzerhof, M. *Phys. Rev. Lett.* **1996**, *77*, 3865−3868.
(39) Becke, A. D. *Phys. Rev. A: At., Mol., Opt. Phys.* **1988**, *38*, 3098−3100.
(40) Tao, J.; Perdew, J. P.; Staroverov, V. N.; Scuseria, G. E. *Phys. Rev. Lett.* **2003**, *91*, 146401.
(41) Sun, J.; Perdew, J. P.; Ruzsinszky, A. *Proc. Natl. Acad. Sci. U. S. A.* **2015**, *112*, 685−689.
(42) Zhao, Y.; Schultz, N.; Truhlar, D. *J. Chem. Theory Comput.* **2006**, *2*, 364−382.
(43) Perdew, J. P.; Tao, J.; Staroverov, V. N.; Scuseria, G. E. *J. Chem. Phys.* **2004**, *120*, 6898−6911.
(44) Lynch, B. J.; Truhlar, D. G. *J. Phys. Chem. A* **2003**, *107*, 8996−8999.
(45) Weigend, F.; Ahlrichs, R. *Phys. Chem. Chem. Phys.* **2005**, *7*, 3297−3305.
(46) Karton, A.; Tarnopolsky, A.; Lamere, J.-F.; Schatz, G. C.; Martin, J. M. *J. Phys. Chem. A* **2008**, *112*, 12868−12886.
(47) Grimme, S.; Antony, J.; Ehrlich, S.; Krieg, H. *J. Chem. Phys.* **2010**, *132*, 154104.
(48) Jurecka, P.; Sponer, J.; Cerny, J.; Hobza, P. *Phys. Chem. Chem. Phys.* **2006**, *8*, 1985−1993.
(49) Podeszwa, R.; Patkowski, K.; Szalewicz, K. *Phys. Chem. Chem. Phys.* **2010**, *12*, 5974.
(50) Grimme, S.; Ehrlich, S. *J. Comput. Chem.* **2011**, *32*, 1456.
(51) Grimme, S. *Chem. - Eur. J.* **2012**, *18*, 9955−9964.
(52) Werner, H.-J.; Knowles, P. J.; Knizia, G.; Manby, F. R.; Schütz, M. *WIREs Comput. Mol. Sci.* **2012**, *2*, 242−253.
(53) Zhao, Y.; Truhlar, D. *Theor. Chem. Acc.* **2008**, *120*, 215−241.
(54) Goerigk, L.; Grimme, S. *Phys. Chem. Chem. Phys.* **2011**, *13*, 6670−6688.
(55) Tsai, C.-W.; Su, Y.-C.; Chai, J.-D.; Li, G.-D. *Phys. Chem. Chem. Phys.* **2013**, *15*, 8352−8361.
(56) Chan, B.; Gilbert, A. T.; Gill, P. M.; Radom, L. *J. Chem. Theory Comput.* **2014**, *10*, 3777−3783.
(57) Stephens, P. J.; Devlin, F. J.; Chabalowski, C. F.; Frisch, M. J. *J. Phys. Chem.* **1994**, *98*, 11623−11627.
(58) Riplinger, C.; Sandhoefer, B.; Hansen, A.; Neese, F. *J. Chem. Phys.* **2013**, *139*, 134101.
(59) Liakos, D. G.; Sparta, M.; Kesharwani, M. K.; Martin, J. M.; Neese, F. *J. Chem. Theory Comput.* **2015**, *11*, 1525−1539.
(60) Neese, F. *WIREs Comput. Mol. Sci.* **2012**, *2*, 73−78.
(61) Karton, A.; O'Reilly, R. J.; Chan, B.; Radom, L. *J. Chem. Theory Comput.* **2012**, *8*, 3128−3136.
(62) Yoo, S.; Apra, E.; Zeng, X. C.; Xantheas, S. S. *J. Phys. Chem. Lett.* **2010**, *1*, 3122−3127.
(63) Modrzejewski, M.; Chalasinski, G.; Szczesniak, M. M. *J. Chem. Theory Comput.* **2014**, *10*, 4297−4306.
(64) Leverentz, H. R.; Qi, H. W.; Truhlar, D. G. *J. Chem. Theory Comput.* **2013**, *9*, 995−1006.
(65) Ruiz, E.; Salahub, D. R.; Vela, A. *J. Am. Chem. Soc.* **1995**, *117*, 1141−1142.
(66) Ruiz, E.; Salahub, D. R.; Vela, A. *J. Phys. Chem.* **1996**, *100*, 12265−12276.
(67) Zhao, Y.; Truhlar, D. *J. Chem. Theory Comput.* **2005**, *1*, 415−432.
(68) Yourdkhani, S.; Korona, T.; Hadipour, N. L. *J. Comput. Chem.* **2015**, *36*, 2412−2428.
(69) Grimme, S. *Org. Lett.* **2010**, *12*, 4670−4673.
(70) Johnson, E. R.; Contreras-García, J.; Yang, W. *J. Chem. Theory Comput.* **2012**, *8*, 2676−2681.
(71) Csonka, G. I.; Ruzsinszky, A.; Perdew, J. P.; Grimme, S. *J. Chem. Theory Comput.* **2008**, *4*, 888−891.

DOI: 10.1021/acs.jctc.6b00406
J. Chem. Theory Comput. 2016, 12, 3662−3673

(72) Song, J.-W.; Tsuneda, T.; Sato, T.; Hirao, K. *Org. Lett.* **2010**, *12*, 1440−1443.
(73) Modrzejewski, M.; Lesiuk, M.; Rajchel, L.; Szczesniak, M. M.; Chalasinski, G. *J. Chem. Phys.* **2012**, *137*, 204121.
(74) Johnson, E. R.; Mori-Sanchez, P.; Cohen, A. J.; Yang, W. *J. Chem. Phys.* **2008**, *129*, 204112.
(75) Lopata, K.; Govind, N. *J. Chem. Theory Comput.* **2011**, *7*, 1344−1355.
(76) Eshuis, H.; Balint-Kurti, G. G.; Manby, F. R. *J. Chem. Phys.* **2008**, *128*, 114113.
(77) Hanazaki, I. *J. Phys. Chem.* **1972**, *76*, 1982−1989.
(78) Blase, X.; Attaccalite, C. *Appl. Phys. Lett.* **2011**, *99*, 171909.
(79) Livshits, E.; Baer, R. *Phys. Chem. Chem. Phys.* **2007**, *9*, 2932.
(80) Stein, T.; Kronik, L.; Baer, R. *J. Am. Chem. Soc.* **2009**, *131*, 2818−2820.
(81) Casida, M. E.; Jamorski, C.; Casida, K. C.; Salahub, D. R. *J. Chem. Phys.* **1998**, *108*, 4439−4449.
(82) Caricato, M.; Trucks, G. W.; Frisch, M. J.; Wiberg, K. B. *J. Chem. Theory Comput.* **2011**, *7*, 456−466.
(83) Daday, C.; Smart, S.; Booth, G. H.; Alavi, A.; Filippi, C. *J. Chem. Theory Comput.* **2012**, *8*, 4441−4451.
(84) Caricato, M.; Trucks, G. W.; Frisch, M. J.; Wiberg, K. B. *J. Chem. Theory Comput.* **2010**, *6*, 370−383.
(85) Zhao, Y.; Truhlar, D. G. *J. Phys. Chem. A* **2006**, *110*, 13126−13130.
(86) Misquitta, A.; Podeszwa, R.; Jeziorski, B.; Szalewicz, K. *J. Chem. Phys.* **2005**, *123*, 214103.
(87) Gruning, M.; Gritsenko, O. V.; van Gisbergen, S. J. A.; Baerends, E. J. *J. Chem. Phys.* **2001**, *114*, 652−660.
(88) Hapka, M.; Rajchel, L.; Modrzejewski, M.; Chalasinski, G.; Szczesniak, M. M. *J. Chem. Phys.* **2014**, *141*, 134120.
(89) Rezac, J.; Hobza, P. *J. Chem. Theory Comput.* **2013**, *9*, 2151−2155.
(90) Adamo, C.; Barone, V. *J. Chem. Phys.* **1999**, *110*, 6158−6170.

DOI: 10.1021/acs.jctc.6b00406
J. Chem. Theory Comput. 2016, 12, 3662−3673